NASA/TM-2003-212415

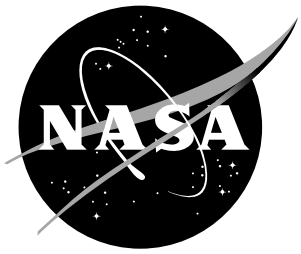


# A Study of the Mechanical Properties of Modern Radial Aircraft Tires

*Robert H. Daugherty*
*Langley Research Center, Hampton, Virginia*

May 2003

# The NASA STI Program Office . . . in Profile

Since its founding, NASA has been dedicated to the advancement of aeronautics and space science. The NASA Scientific and Technical Information (STI) Program Office plays a key part in helping NASA maintain this important role.

The NASA STI Program Office is operated by Langley Research Center, the lead center for NASA's scientific and technical information. The NASA STI Program Office provides access to the NASA STI Database, the largest collection of aeronautical and space science STI in the world. The Program Office is also NASA's institutional mechanism for disseminating the results of its research and development activities. These results are published by NASA in the NASA STI Report Series, which includes the following report types:

- TECHNICAL PUBLICATION. Reports of completed research or a major significant phase of research that present the results of NASA programs and include extensive data or theoretical analysis. Includes compilations of significant scientific and technical data and information deemed to be of continuing reference value. NASA counterpart of peer-reviewed formal professional papers, but having less stringent limitations on manuscript length and extent of graphic presentations.

- TECHNICAL MEMORANDUM. Scientific and technical findings that are preliminary or of specialized interest, e.g., quick release reports, working papers, and bibliographies that contain minimal annotation. Does not contain extensive analysis.

- CONTRACTOR REPORT. Scientific and technical findings by NASA-sponsored contractors and grantees.

- CONFERENCE PUBLICATION. Collected papers from scientific and technical conferences, symposia, seminars, or other meetings sponsored or co-sponsored by NASA.

- SPECIAL PUBLICATION. Scientific, technical, or historical information from NASA programs, projects, and missions, often concerned with subjects having substantial public interest.

- TECHNICAL TRANSLATION. English-language translations of foreign scientific and technical material pertinent to NASA's mission.

Specialized services that complement the STI Program Office's diverse offerings include creating custom thesauri, building customized databases, organizing and publishing research results ... even providing videos.

For more information about the NASA STI Program Office, see the following:

- Access the NASA STI Program Home Page at ***http://www.sti.nasa.gov***

- E-mail your question via the Internet to help@sti.nasa.gov

- Fax your question to the NASA STI Help Desk at (301) 621-0134

- Phone the NASA STI Help Desk at (301) 621-0390

- Write to:
  NASA STI Help Desk
  NASA Center for AeroSpace Information
  7121 Standard Drive
  Hanover, MD 21076-1320

NASA/TM-2003-212415

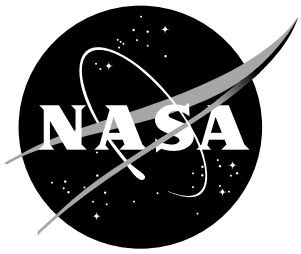

# A Study of the Mechanical Properties of Modern Radial Aircraft Tires

*Robert H. Daugherty*
*Langley Research Center, Hampton, Virginia*

National Aeronautics and
Space Administration

Langley Research Center
Hampton, Virginia 23681-2199

May 2003

Available from:

NASA Center for AeroSpace Information (CASI)
7121 Standard Drive
Hanover, MD 21076-1320
(301) 621-0390

National Technical Information Service (NTIS)
5285 Port Royal Road
Springfield, VA 22161-2171
(703) 605-6000

# Contents

## Abstract

An experimental investigation was conducted at the NASA Langley Research Center to study the effects of various parameters on the mechanical properties of a number of modern radial aircraft tires such as would be found in the present commercial transport aircraft fleet. The range of tire sizes encompasses most of the tires that would be observed on both nose- and main - landing gear installations. The investigation presented herein represents the first phase of a multi-year, multi-phase effort to characterize modern radial aircraft tires in an attempt to provide guidance for the engineer when seeking a way to design, model, or otherwise determine the likely behavior of a radial tire in a particular aircraft application. The mechanical properties under investigation for this testing phase included static load-deflection behavior, footprint area, footprint aspect ratio, contact pressure ratio, footprint half-width, rolling radius and axle height, rolling drag coefficient, conicity, side force response, drag force response, aligning torque, overturning torque, lateral center of pressure shift, and friction force moment arm. The parameters that were varied to evaluate these mechanical properties included vertical load, tire inflation pressure, forward speed, yaw angle, and surface wetness condition.

Three radial tire sizes were tested and found to behave similarly in terms of static load-deflection when the results were non-dimensionalized. Footprint areas were found to be insensitive to variations in inflation pressure within a large range of pressures designed to simulate 80 Fahrenheit degrees of temperature change from origin to destination for a flight. Uniformly, the footprint contact area was less than that which could be ascribed to inflation pressure alone and thus the actual contact pressures in the footprint are higher than the inflation pressure. A single model to describe this was found for all tires. Footprint aspect ratios were evaluated and found not to vary with inflation pressure in the range tested but to vary with the vertical load. A single model to describe this was found for all tires. Tire footprint half-width was evaluated and found to be nearly stable for all tires and speeds. A single model to describe this was found for all tires. The radial aircraft tires were found to behave, in a general sense, as a bias-ply aircraft tire in that the rolling radius was substantially less than the axle height measurement. However, the rule of thumb that is typically used for a bias-ply tire rolling radius does not apply and an appropriate rule of thumb for the radial aircraft tires is presented. The radial aircraft tires were found to behave similarly in terms of rolling friction and a single model is also presented to describe this. The tires all appeared to exhibit a tendency to provide uncommanded side force while rolling at zero yaw angle and these data are presented.

The radial aircraft tires were found to behave like most other tires in response to variations in vertical load and yaw angle. The side-force coefficient, which is a measure of cornering efficiency, was found to increase with increases in yaw angle and decrease with increases in vertical load. A single model to provide a predictive capability for the side force coefficient, regardless of tire size, is presented. Drag force was found to slightly increase with increases in yaw angles at constant vertical load. Aligning torque was found to be restorative for all conditions and tires tested, a result indicating that the tires are stable in yaw within the limits of testing. A single model to provide a predictive capability for the aligning torque, regardless of tire size, is presented. Overturning torque was found generally to increase with increases in vertical load or yaw angle. A single model to provide a predictive capability for the overturning torque, regardless of tire size, is presented. Lateral center of pressure shift was found to be relatively constant in both magnitude and response to variations in yaw angle for all three tires tested. A single model for this behavior is presented. Friction force moment arm was found to vary with yaw angle, however, this highly non-linear behavior was not described in model form.

## Introduction

In 1960, the National Aeronautics and Space Administration (NASA) published a reference report entitled "Mechanical Properties of Pneumatic Tires With Special Reference to Modern Aircraft Tires" (ref 1.). This report intended to present a study "which has as its primary aims the determination of the most important variables which influence the various tire properties and the establishment of some simple quantitative equations for most of these properties". The comprehensive report discussed pneumatic tires in general, including automotive tires, and aircraft tires as well. At that time, the state of the art in aircraft tire design was the bias-ply tire, and virtually all aircraft tires were based on a fairly limited number of variations of this basic design. The report was based largely on existing, previously published experimental data. In generalized descriptions of the behavior of classes of tires for individual parameters, the authors frequently used empirical relationships rather than rigorous theoretical derivations, as they believed the proper goal was to reach a "fair correspondence to reality". Due in part to this practical and useful approach, the report gained wide distribution and was used by many communities over the course of the next 40 years and became the standard of practical tire behavior modeling. Not the least of these communities was the aircraft landing gear and wheel and tire community. The report, referred to now simply as "R-64", is still being used but is recognized as lacking in applicability since the advent of radial aircraft tires.

In partial response to discussions that have arisen in the Society of Automotive Engineers (SAE) A-5 Committee (Aerospace Landing Gear Systems), NASA has taken on the role of attempting to update this reference document by experimentally determining some mechanical properties of modern radial aircraft tires. The R-64 document attempted to quantify the behavior of more than 60 parameters known to be measurable for a tire. This breadth of scope cannot be repeated in either the present phase of testing reported herein, nor in later phases. Some of the information presented in the R-64 document could be classified as being of $2^{nd}$ or $3^{rd}$ order in the sense that though effects of certain parameters can be measured, those effects are of such small magnitude as to not appreciably change the overall behavior of the tire. And certainly as the information user desires to step back and more globally-represent the effect of the tire on the larger vehicle, more parameters become classifiable as $2^{nd}$ and $3^{rd}$ order. Thus, based in part on discussions within SAE A-5 Committees, the community has suggested that only a reasonable subset of the original R-64 document need be updated to reflect the majority of needs in the tire community. One of the areas that is of concern to the community is that of shimmy analysis. Shimmy analysis modeling is fairly well developed. However, one of the features not well defined is the accuracy of the tire behavior input into such models. It is known that relatively small changes in the known or modeled behavior of certain tire parameters can cause a mathematical model or an actual piece of hardware to migrate from the stable into the unstable region regarding shimmy and other types of dynamic events. A list of parameters common to several types of shimmy models and other dynamic vibration models was developed and the testing reported herein attempts to begin to address the measurement of some of the desired parameters.

The purpose of this paper is to present the results of tests conducted at the NASA Langley Research Center's Aircraft Landing Dynamics Facility (ALDF) to determine the effects of various parameters on some of the mechanical properties of three modern radial aircraft tires designed to represent the range of sizes likely to be encountered on typical modern commercial jet transport aircraft. The mechanical properties under investigation for this testing phase included static load-deflection behavior, footprint area, footprint aspect ratio, contact pressure ratio, footprint half-width, rolling radius and axle height, rolling drag coefficient, conicity, side force response, drag force response, aligning torque, overturning torque, lateral center of pressure shift, and friction force moment arm. The

parameters that were varied to evaluate these mechanical properties included vertical load, tire inflation pressure, forward speed, yaw angle, and surface wetness condition. The ranges of load, speed, pressure, yaw angle, and surface wetness were designed to represent the likely variations one would encounter in actual aircraft operations. Data were generated for vertical loads up to at least the rated load for each tire and sometimes as high as twice the rated load, pressures representing a tire 40 Fahrenheit degrees cooler and warmer than the rated pressure, speeds up to 200 kts, yaw angles ranging from about +/- 8 degrees, and dry and wet surfaces where appropriate.

This report represents the first phase of testing in what is hoped to be a program of multiple phases. Testing in the present report focused on measuring parameters very commonly used in a variety of analyses and simulations. Many of the measurements reported on herein are ones that are typically obtained in static laboratory testing while a few have been obtained on drum-type dynamometers. More infrequently, the measurements are obtained in some type of flat-track testing. Subsequent phases of testing will seek to measure parameters less frequently or never-before measured on a flat track at forward speeds and will include parameters more classically needed for dynamic analyses such as shimmy, etc.

## Symbols

All values for parameters in this report are presented in U.S. Customary Units except where otherwise noted.

Af footprint area, in^2

Ah axle height, inches

AR footprint aspect ratio

Avert vertical acceleration at the test axle, g

Alat lateral acceleration at the test axle, g

Along longitudinal acceleration at the test axle, g

Cp lateral center of pressure shift, inches

D nominal tire diameter, in

Dn distance from tire center to north load beam, in

Ds distance from tire center to south load beam, in

Fd total drag force parallel to wheel plane, lb.

Fd,n drag force measured on north side of tire, lb.

Fd,s drag force measured on south side of tire, lb.

| | |
|---|---|
| FFma | friction force moment arm, in |
| Fs | side force perpendicular to wheel plane, lb. |
| Fz | total vertical force on tire, lb. |
| Fz,n | vertical force measured on north side of tire, lb. |
| Fz,s | vertical force measured on south side of tire, lb. |
| Lf | footprint length, in |
| Lr | rated load, lb. |
| Mx | overturning torque, in-lb. |
| Mz | aligning torque, in-lb. |
| P | inflation pressure, psi |
| Pc | contact pressure, psi |
| Pr | rated tire inflation pressure, psi |
| R | ratio of vertical force to rated load |
| Rcp | contact pressure ratio |
| re | rolling radius, in |
| t | tire temperature, deg C |
| to | initial tire temperature, deg C |
| Wh | footprint half-width, in |
| Ws | section width of tire as reported by manufacturer, in |
| Wt | weight of the lower mass supported by the load beams, lb. |
| %δ | percent deflection |
| $\beta_x$ | coefficients of curve-fitting equations |
| δ | tire deflection, in |

$\mu$ generalized friction coefficient

$\mu d$ drag force coefficient parallel to wheel plane

$\mu s$ side force coefficient perpendicular to wheel plane

$\Psi$ tire yaw angle, deg

Abbreviations:

psi pounds per square inch

## Apparatus

### Test Tires and Wheels

The tires used in this study were standard, off-the-shelf commercially available modern radial aircraft tires. Three tires were used to provide a representative range of tire sizes that span the expected range in the commercial jet transport fleet. While these tires may be used on more than the application referred to here, a convenient method to describe each tire is by way of the aircraft it is commonly used on. The smallest tire was a 27 X 7.75 R15 tire with a 12-ply rating. This tire is referred to as a "737 nose tire". The tire size nomenclature is typical throughout this report, with the "27", for example, in the above name describing the nominal overall tire diameter in inches. The "7.75" describes the nominal overall tire width at its largest section in inches. The "R15" designates this is a radial tire and is to be mounted on a 15–inch diameter wheel designed for radial tires. The 12-ply rating denotes that the "strength" of the carcass is equal to the strength of an old bias-ply design with 12 "first" generation ply layers. The 737 nose tire has a rated load of 9650 lb. and a rated inflation pressure of 200 psi. Typically, the rated load and inflation pressure for a bias-ply tire are such that supporting the rated load at the rated pressure statically will cause the tire to be deflected to approximately 35% of its available deflection prior to bottoming out. While a radial tire's rated load and pressure is not defined in exactly the same way, it is sufficient to expect that the deflection is more approximately 24-33% of the available deflection. Figure 1 presents a photograph of the 737 nose tire for scale reference. Figure 2 presents a photograph of the radial aircraft wheel that was procured and used to mount the test tire. The next largest tire was a 42 X 17.0 R18 tire with a 26-ply rating. This tire has a rated load of 36100 lb. and a rated pressure of 194 psi and is hereafter referred to as a "777 nose tire". The largest of the tires was a 50 X 20.0 R22 tire with a 32-ply rating. This tire has a rated load of 57100 lb. and a rated pressure of 220 psi and is hereafter referred to as a "777 main tire". This tire and wheel can also be seen in figures 1 and 2.

### Test Facility

All forward-speed tests in this investigation were conducted at the NASA Langley Research Center Aircraft Landing Dynamics Facility (ALDF). The facility consists of a set of rails 2800 ft long on

which a 60-ft-long, 117000-lb carriage travels. A photograph of the facility is shown in figure 3. The carriage is propelled at speeds up to 224 knots by a high-pressure water jet and is arrested by a set of water turbines connected by nylon tapes. A photograph of the carriage is shown in figure 4 and the drop carriage, a fixture capable of translating vertically and to which the test tire is ultimately attached is identified. A more detailed description of the facility can be found in reference 2. The test tires were mounted on aircraft wheels and then mounted on one of two test axles, depending on tire size, that allowed them to be installed in a force-measurement dynamometer shown in figure 5. The test runway was a smooth, ungrooved concrete runway with an average texture depth (ATD) of approximately 0.004 inches. The ATD is a means of quantifying the average macrotexture of a surface and is found by spreading a known volume of a substance, oftentimes grease, on the desired surface and then measuring the area it covers. A more detailed description of this methodology can be found in reference 3. The runway has typical expansion joints and is level to less than 1/16-inch variation in 100 feet. Tests to evaluate and measure the static load-deflection of the test tires as well as define the contact footprint characteristics were conducted in a carriage hangar facility. In this facility, a device known as the "frictionless platform" is used to load the tires vertically and allows a minimum of lateral ground-plane forces to be transmitted to the ground. The device consists of a tabletop mounted on oil-fed cylindrical bearings, which allow free movement of the tabletop in a single lateral direction while vertical load is applied. This permits all of the tire lateral ground plane forces to be forced to travel through the dynamometer measurement beams so as not to provide a secondary load path through the ground which allows forces to escape without measurement. A photograph of a test tire on this tabletop is shown in figure 6. This facility was also used to calibrate the data measurement system on board the test carriage.

**Instrumentation**

The parameters measured in this study included tire vertical force, side force, drag force, axle height, carriage position, test wheel revolutions, yaw angle, and footprint width. The forces were measured by using the dynamometer sketched in figure 7. Vertical force was measured by using two separate strain-gauged beams, and variations in their load distribution provided a measure of overturning torque. Likewise, drag force was measured by using two separate instrumented beams, and variations in their load distribution gave a measure of aligning torque. Side force was measured using a single instrumented beam mounted in line with the wheel axle. A three-axis accelerometer package was mounted directly to one end of the wheel axle to permit the acceleration forces of the lower mass to be isolated from the tire contact plane force data in all three axes. The lower mass is the effective mass that the load beams support and includes the mass of the axle, wheel, tire, and part of the dynamometer itself. The acceleration data assure that final calculations of loads data represent the forces generated only by the tire at the ground contact plane. Typically, correcting the data inertially results in a somewhat less noisy time history. Of particular interest is eliminating the fore-aft direction inertial forces as the test carriage is always in a state of non-zero acceleration throughout a test run. Axle height was measured using an infrared sensor designed to reflect a beam of infrared wavelength energy at the ground and is then received and sent through a diffraction grating. Frequency is then converted to speed using this non-contact sensor. The placement of the sensor on the dynamometer is identified in figure 5. Carriage position was also measured using a non-contact sensor designed to pass over metal plates placed every ten feet down the length of the test track. Carriage speed could thus be calculated, on average, every ten feet. Test wheel revolutions were measured with an identical sensor and provided a pulse on the recorded time histories every time the wheel rotated. A metal target was affixed to each test wheel to provide this data. Test tire yaw angle was measured using a linear variable displacement transducer

mounted on a hydraulic cylinder used to actuate the rotation of the entire dynamometer fixture during test runs evaluating the effect of yaw angle. Footprint width measurements are described in the test procedures section of this document.

Analog data from each transducer were converted to digital signals onboard the test carriage by a pulse-code-modulation system and were serially telemetered to a receiving station at microwave frequencies where the data stream was decommutated. This set of data remained in digital form and was fed into a desktop computer. The same set of data was also passed through a digital to-analog converter and fed through a 14-channel oscillograph to give an immediate accounting of carriage and transducer performance during a run. The telemetry system provides 1066 samples per second for each of the desired channels up to a maximum of 28 channels. The 12-bit digital system allows a 10-volt analog range on the test carriage ( -5 volts to +5 volts) to be resolved into 4096 discrete digital levels, or counts. The digital signals transmitted from the carriage thus permitted a data resolution of 1 part in 4096. Normally, full-scale span on each channel was approximately 50 percent of the maximum. This, combined with typical "noise" on each analog channel before digital conversion (equal to approximately 3 counts for most channels), results in an overall resolution of the system of approximately 0.2 percent. In addition to being calibrated in a general sense before the test program began, the five force measurement channels as well as the three accelerometer channels were calibrated before each test run by injecting a known resistance across one leg of the strain-gauged bridges that comprise each of these sensors. By virtue of knowing the sensitivity of each channel relative to the voltage changes resulting from changes in known resistance, it was possible to finely-adjust the sensitivity of each of these channels automatically before each run. This insured that any sensitivity changes due to temperature or other effects were automatically corrected and permitted the highest fidelity measurements possible.

The following list provides the calibration information for the channels used in this study. It should be noted that two different sensitivities were used for the drag force channels. The higher sensitivity (denoted by the lower "K" value, which is the amount of engineering units associated with the magnitude of the calibration delta) was used for each test tire when the testing was planned to involve only rolling straight ahead with no test tire yaw angle. In these types of tests, it was desirable to be able to measure small drag loads as finely as possible. In addition, all of the testing using the 737 nose tire, because of its small size, made use of the higher sensitivity drag channels. For the 777 nose and 777 main tire testing under the presence of yaw angle, lower-sensitivity drag channels were used to allow aligning torque measurements to be made without electrically over-ranging the drag load beams.

| Name | K Engineering units per calibration delta | Calibration delta,counts | Engineering units per count (minimum resolution) |
|---|---|---|---|
| North vertical force | 105575. lbf | 2841 | 37.2 lbf |
| South vertical force | 101520. lbf | 2874 | 35.3 lbf |
| North drag force | 48493.2 lbf | 1289 | 37.6 lbf |
| South drag force | 48321.0 lbf | 1260 | 38.4 lbf |
| Side force | 70094.7 lbf | 1289 | 54.4 lbf |
| Vertical acceleration | -7.44 g's | -1482 | 0.005 g's |
| Longitudinal acceleration | -15.55 g's | -1803 | 0.009 g's |
| Lateral acceleration | -8.27 g's | -1620 | 0.005 g's |
| Test wheel revolutions | N/A | N/A | N/A |
| Carriage position | N/A | N/A | N/A |

| | | | |
|---|---|---|---|
| Yaw angle | 10.20 deg | 1000 | 0.01 deg |
| Axle height | -10.80 in. | 2000 | -0.005 in. |
| High sens. North drag | 7516.9 lbf | 1841 | 4.1 lbf |
| High sens. South drag | 7759.7 lbf | 1844 | 4.2 lbf |

## Test Procedure

Four test procedures were used in the course of this study. The first involved obtaining static load-deflection data for each tire. In this testing, the test tire was inflated to one of the three desired inflation pressures prior to a test series. The telemetered data stream was observed in real time and the test tire was lowered to the tabletop of the frictionless platform. Hydraulic load was slowly applied to the drop carriage fixture in an attempt to deflect the test tire at a rate no higher than 2 inches per minute. The desired peak load prior to reversing the process and reducing load back to zero was either approximately twice the rated load of the tire (about 75000 lb. in the case of the 777 main tire). The real-time data stream was recorded every few seconds during the process so that a plot of the load-deflection could be produced later. The test was repeated for the other two desired pressures. The tire pressures used throughout the test program were the rated tire pressure, the pressure associated with operating tire in a 40 Fahrenheit-degree cooler environment, and the pressure associated with operating tire in a 40 Fahrenheit-degree warmer environment. The value of 40 Fahrenheit-degrees was chosen to represent a realistic deviation of a temperature that might be encountered while conducting a commercial transport flight from a relatively warm environment to a cooler environment or vice versa. The pressure was calculated according to the following gas law:

$$P = Pr * (273 + t)/(273 + to) \qquad \text{(eq. 1)}$$

For the 737 nose tire and the 777 nose tire, the pressure change corresponding to this temperature difference was 15 psi. For the 777 main tire, the pressure change corresponding to this temperature difference was 17 psi.

The second test procedure involved making measurements of the footprint of each test tire at various vertical loads and inflation pressures. For each condition, the tire was inflated to the desired pressure and a sheet of white construction board was placed on the tabletop of the frictionless platform and under the tire. The tire tread ribs were then covered with powdered chalk and then the tire was lowered to the surface. Tire load was increased to the desired value as closely as possible and the actual vertical load on the tabletop was read using a calibration standard device installed in the frictionless platform. The tire vertical load was then removed and the chalk footprint on the construction board along with the inflation pressure and peak load was recorded for later analysis to determine the footprint areas.

The third test procedure involved making measurements of tire mechanical properties at forward speed but zero yaw angle on the ALDF facility described above. A mechanical stop set at zero degrees yaw was used to prevent any movement of the dynamometer and thus the test tire with regard to yaw angle. In this case, the test tire inflation pressure was set before each run to within 1 psi of the desired value. The test carriage was prepared to apply the proper hydraulic force to the drop carriage to produce the desired vertical force on the test tire. During a test run, the carriage was accelerated to the desired speed, the drop carriage was commanded to lower the test tire down to the runway surface, and the

desired vertical force was applied to the test tire. The tire was allowed to spinup to the ground synchronous speed and attain steady-state vertical force levels, and then rolled across a footprint width indicator strip. After this was accomplished, the drop carriage was commanded to unload the tire and raise it off of the runway surface and the test carriage was thereafter arrested to a stop. The footprint width indicator strip consisted of a piece of construction board taped to the runway with its long axis transverse to the direction of tire travel at a spot where it was known that the vertical force and carriage and test wheel speeds would be quasi-steady state. A photograph of such an indicator strip is shown in figure 8. The strip was annotated with the pertinent test run information and then covered with a light coat of general-purpose grease. As the tire traversed the construction board, the elemental slip in the tire footprint would cause a slight difference in the sheen of the grease on the board and it was quite simple to then make a small mark on the board at the lateral extreme edges of where the tire footprint had passed by and thus measure the footprint width at the desired speed and load.

The final test procedure was quite similar to the preceding one, but made use of a variable yaw system capability on board the test carriage. The tire and carriage were prepared as before, but rather than a mechanical stop to hold the yaw at zero degrees, a hydraulic system was prepared to allow the dynamometer to touch down normally on the runway surface at nearly zero yaw. After the tire was loaded vertically and had ground-synchronous speed, the dynamometer was commanded to begin sweeping in yaw from the approximate zero position to a positive yaw stop at about +9 degrees. Shortly thereafter, another command was issued to begin sweeping back towards the negative yaw direction, pass through zero yaw, and then continue to the negative yaw angle stop of approximately –8 degrees. The rate of the yaw sweep was adjusted depending on whether the test run was at towed speeds (approximately 5 kts), 100 kts, 150 kts, or 200 kts. The rate of the yaw sweep needed to be adjusted because if the yaw angle is varied too quickly then as one sweeps up in yaw and then back down through the same range the response in side force or cornering would exhibit hysteresis. Figure 9 presents a plot to demonstrate the lack of such a hysteresis loop, confirming that this test procedure is sufficiently close to obtaining quasi-static yawed-rolling data. After the dynamometer was finished with the yaw sweep, the test would typically end as described in the preceding procedure. For some of these yawed-rolling tests, the runway surface was wetted to simulate the wetness condition that might be found just after a typical rain shower or during a mild rain shower. A series of sprinkler nozzles line the test runway and just prior to a test where a wet runway was desired the sprinklers would be turned on and the surface allowed to become as uniformly wet as possible. The target wetness condition was a water depth on the ungrooved, smooth concrete runway of approximately 0.03 inches. A device to measure this depth was used that provides an optical methodology to indicate water depth. Though the target was approximately 0.03 inches, the range of depths that were encountered during the course of a test run due to uneven drying, wind, and other factors was more likely approximately 0.01 to 0.05 inches.

Test matrices for the majority of the test program relating to the zero-yaw rolling radius and half-width footprint testing as well as the yawed-rolling cornering testing are presented in tables 1, 2, and 3 for the 737 nose tire, 777 nose tire, and 777 main tire respectively. The tables list the date and run number associated with each test conducted. The tables also list values read from the data files as described earlier including footprint width, axle height, carriage distance and speed, test tire revolutions, test carriage distance for those revolutions, rolling radius, vertical force, drag force, side force, and multiple of rated load. Included at the bottom of each table are data recorded for the footprint area testing including the footprint width and length as read from the chalk impressions on the construction board, vertical force, and multiple of rated load. It should be noted that in each table, where a data entry is blank, either the test run itself was not conducted, or the particular value was not readable or reliable and thus not reported. It also should be noted that for the 737 nose tire testing under yawed-rolling

conditions, the clearance between the dynamometer itself and the test runway was of such a small value that as the tire tread was worn away, it made it impossible to gain enough deflection to obtain the highest of the desired vertical forces. Finally, it should also be noted that for the 777 main tire testing, a catastrophic wheel bearing failure occurred on the first of the yawed-rolling tests, damaging the wheel to the extent that no further testing was possible.

## Data Reduction

The following are sign conventions used in this test program. Vertical force is always defined as positive. Drag force is defined as positive in the direction opposite travel. Side force is defined as positive towards the north side of the facility and in other words is positive when the tire provides lateral forces to the left of the direction of travel as seen from the rear of the carriage. Vertical acceleration is defined as positive upwards. Longitudinal acceleration is defined as positive forward. Lateral acceleration is defined as positive left, or northward. Axle height is always defined as positive. Yaw angle is defined as positive when the tire is steered towards the left, or northward, as compared to the direction of travel. To provide insight regarding the meaning and definition of the parameters defined below, figure 10 presents two sketches showing the forces and moments acting on a yawed, rolling tire. The sketches are drawn showing positive sign conventions.

During a run, the digital telemetered data received from the carriage are recorded by the desktop computer at a rate of 1066 samples per second. Typically, force and acceleration data are retrieved from the computer memory at a rate of 150 samples per second and then mathematically filtered to 30 Hz using a $4^{th}$ order low-pass Butterworth filter.

Vertical force was obtained by adding the outputs of the two vertical load beams, and it was then corrected using axle acceleration data to account for lower mass inertial forces due to vertical accelerations according to the following formula:

$$Fz = (Fz,n + Fz,s) + Wt*Avert \qquad \text{(eq. 2)}$$

To non-dimensionalize the vertical force on each of the test tires, a ratio of the vertical force to the rated load was obtained according to the following formula:

$$R = Fz/Lr \qquad \text{(eq. 3)}$$

Drag force was obtained by adding the outputs of the two drag load beams, and it was then corrected using axle acceleration data to account for lower mass inertial forces due to longitudinal accelerations according to the following formula:

$$Fd = (Fd,n + Fd,s) - Wt*Along \qquad \text{(eq. 4)}$$

Drag force coefficients were obtained by dividing the drag force by the vertical force according to the following formula:

$$\mu d = Fd/Fz \qquad \text{(eq. 5)}$$

Side force was obtained by measuring the output of the side load beam, and it was then corrected using axle acceleration data to account for lower mass inertial forces due to lateral accelerations according to the following formula:

$$Fs = (Fs\ measured) + Wt*Alat \quad \text{(eq. 6)}$$

Side force coefficients were obtained by dividing the side force by the vertical force according to the following formula:

$$\mu s = Fs/Fz \quad \text{(eq. 7)}$$

Aligning torque was obtained by summing the moments described by the drag load beams multiplied by their respective distances from the tire centerline according to the following formula:

$$Mz = (Fd,s*Ds) - (Fd,n*Dn) \quad \text{(eq. 8)}$$

Overturning torque was obtained by summing the moments described by the vertical load beams multiplied by their respective distances from the tire centerline according to the following formula:

$$Mx = (Fz,n*Dn) - (Fz,s*Ds) \quad \text{(eq. 9)}$$

Lateral center of pressure shift was obtained by subtracting the moment described by the side force acting at some axle height from the overturning torque moment, and dividing this value by the vertical force according to the following formula:

$$Cp = (Mx-Fs*Ah)/Fz \quad \text{(eq. 10)}$$

Friction force moment arm was obtained by dividing the aligning torque by the side force according to the following formula:

$$FFma = Mz/Fs \quad \text{(eq. 11)}$$

The aligning torque is that torque that typically opposes the tire increasing its yaw angle. In the force measurement dynamometer in this test program, it is manifested by one drag beam being put in more tension than can be accounted for by its share of the rolling drag and likewise the other drag beam is reduced in tension and may even be forced into compression. It is these disparate forces which allows the aligning torque to be calculated. In an automobile, for example, the aligning torque is what is responsible for the tendency for the vehicle to align itself to track straight if one lets go of the steering wheel while in a turn. Dividing the aligning torque by the side force provides a measure of where it appears the side force is acting as compared to the steering axis. Because this is a restorative moment, the placement of the centroid of side forces, referred to as the friction force moment arm, moves aft of the steering axis. The overturning torque is simply the tendency for the wheel to be turned over laterally due mainly to the side force acting well below the axle. However, the overturning torque also has a component that cannot be calculated just by observing the side force. The placement of the centroid of

the vertical forces acting in the footprint actually shifts towards the direction of side force so that there is an additional moment acting to turn the wheel over and it is equal to the lateral center of pressure shift times the vertical force.

Another calculated value of importance in this test program is rolling radius. One of the findings from R-64 was that pneumatic tires have neither the rpm associated with the actual value of the axle height and the synchronous ground speed, nor an rpm associated with the actual circumference of the tire as one might make an analogy with a tank tread. To calculate rolling radius, each pertinent test run was evaluated and a measurement of test carriage distance traveled for some distance before and after the footprint width indicator strip. Due to the nature of the pulses from the carriage position and test wheel revolution sensors, these data were not filtered and were retrieved from the computer at the full 1066 samples per second rate. The time to travel the distance was recorded and test carriage speed was calculated. In addition, the time it took at the same place in the run as carriage speed was calculated for the test tire to rotate a certain number of revolutions at quasi steady-state conditions was also recorded. Figure 11 presents plots of test carriage position and test tire revolutions for a typical run to illustrate this. Thus the distance the test carriage traveled in the time required for a certain number of test tire revolutions was known. Finally, the distance traveled for each tire revolution was calculated and divided by 2 π to provide a measure of the effective rolling radius of the tire. This value is the *apparent* axle height if one wanted to make an rpm calculation based on axle height and ground speed.

For testing at zero yaw angle where rolling radius, footprint half-width, rolling drag, and conicity were being evaluated, in addition to the carriage position and test wheel revolution data, typically the vertical, drag, and side force data were plotted and hand-faired for a period of about ½ second around the placement of the footprint width indicator strip on the runway.

Footprint half-width was calculated simply by dividing full footprint widths as indicated by the strips in half. Footprint aspect ratios were calculated by dividing the width of the chalk footprints on the construction board by the length of the footprints for each load and inflation pressure for each tire. Footprint areas were evaluated by superimposing a 10-inch by 10-inch perpendicular scale on each chalk footprint on the construction board. The footprint was then photographed using a digital camera. A commercially-available software package, originally designed to evaluate digital medical images, was used to digitize and scale each footprint. The program then calculates the area designated by the user after a proper scale calibration has been entered. Footprint contact pressures were calculated by dividing the actual vertical force by the measured footprint area from each footprint test. Finally, contact pressure ratios were calculated by dividing the contact pressures by the tire inflation pressures.

## Results and Discussion

### General

The intention of this initial phase of testing is to determine the mechanical properties of modern radial aircraft tires and to begin to look at generalized effects of parameters such as speed, vertical force, inflation pressure, and yaw angle on the response and behavior of a range of tire sizes likely to be encountered in actual commercial jet transport operations. Some of the mechanical properties have never been observed and measured under controlled conditions (i.e., a flat track facility), and others have never been conducted at forward speed. One of the desired outcomes is to compare measurements made statically in the laboratory and, where possible, measurements made at-speed with the hope that

correlations between the two can be made and eliminate the need for at-speed testing for certain parameters in the future. Many of the mechanical properties described in this report are generalized and simple empirical relationships are offered to describe how one might reach a reasonable estimate of the likely behavior of tires within the size range tested.

## Footprint Characteristics

### *Footprint Area*

As described in the test procedures section, chalk footprints were recorded for all three test tire sizes for a variety of loads at three different inflation pressures. Appendix A presents the results of these footprint area tests with a digital image of each of the chalk impressions. In some cases, the edges of the chalk footprint was quite clear, and in other cases the edge was so faint as to not be readily visible in a digital image so the edge was hand-enhanced before the image was recorded.

The footprint area for each of the footprints presented in Appendix A was plotted along with the peak vertical force recorded during each test. Figures 12, 13, and 14 present the plots for the 737 nose tire, the 777 nose tire, and the 777 main tire respectively. In each plot, the actual test data are represented by solid symbols and additional curves are presented to show what the footprint area versus load relationship would be if the tire behaved as a perfect membrane, i.e. as if there were no carcass structural stiffness and the tire were to behave as a balloon or thin pressurized membrane. In each case, it is seen that the actual amount of contact area is less than that predicted by a membrane model. As the vertical force is increased, the discrepancy between the membrane model and the actual behavior is increased due to the fact that the tire sidewalls and carcass become increasingly involved in the support of the overall load. It is also noted that there is very little difference in the footprint area behavior for each tire as a result of increases in inflation pressure. Though a coherent trend can be seen where footprint area decreases very slightly as the inflation pressure increases, the footprint areas can be considered to be essentially constant within the pressure range tested. It should be noted that this pressure range associated with an 80-Fahrenheit degree temperature change is substantially larger than the 5 psi range typically monitored and adhered to by aircraft maintenance operators.

### *Contact Pressure Ratio*

The area of each footprint was combined with the vertical force for each test and a contact pressure (sometimes referred to as a bearing pressure) was calculated according to the following formula:

$$Pc = Fz/Af \qquad \text{(eq. 12)}$$

The contact pressure was then divided by the actual tire inflation pressure for each test and a contact pressure ratio was calculated according to the following formula:

$$Rcp = Pc/P \qquad \text{(eq. 13)}$$

Figures 15, 16, and 17 present plots of the contact pressure ratio versus multiple of rated load for the 737 nose tire, the 777 nose tire, and the 777 main tire respectively. In each plot, the test data for all pressures are represented by a single data series since it was previously concluded that the inflation pressure plays an insignificant role, within the range tested, in the contact footprint area. Figure 18 presents a plot with all of the non-dimensionalized data represented as a single series. A curve was fit to these data to represent a model for predicting the contact pressure a modern radial aircraft tire imposes on the surface. The contact pressure ratio can be calculated according to the following empirical relationship:

$$Rcp = 0.2991*R + 1.0431 \quad \text{(eq. 14)}$$

The contact pressure itself can be calculated according to the following empirical relationship:

$$Pc = P*(0.2991*R + 1.0431) \quad \text{(eq. 15)}$$

Reference 1 reports contact pressure ratios for bias-ply aircraft tires ranges from approximately .86 at low tire deflections to as high as 1.43 at large tire deflections. The present data for radial aircraft tires suggests that the radial tire behaves similarly but may have increased contact pressure ratios at higher deflections as compared to the bias-ply tire. A further area of study is suggested regarding the effect of this contact pressure ratio on the hydroplaning speed of radial aircraft tires.

***Footprint Aspect Ratio***

In light of the suggestion above that contact pressure ratio may affect the hydroplaning speed of radial aircraft tires, likewise, data exists to suggest that footprint aspect ratio also may play a part in the hydroplaning phenomenon. Reference 4 discusses studies with truck and automotive tires of bias-ply construction and found that the hydroplaning speed was affected by the footprint aspect ratio.

Each of the footprints presented in Appendix A were measured for both overall width and length. A footprint aspect ratio was calculated for each test according to the following formula:

$$AR = Wh*2/Lf \quad \text{(eq. 16)}$$

Figures 19, 20, and 21 present plots of the footprint aspect ratio versus multiple of rated load for the 737 nose tire, the 777 nose tire, and the 777 main tire respectively. In each plot, the test data are initially separated into the three test pressures to determine whether an effect of inflation pressure is present. As was the case for the contact pressure ratio, no significant effect of inflation pressure within the range tested is reportable. Figure 22 presents a plot with all of the non-dimensionalized footprint aspect ratio data represented as a single series without regard to inflation pressure. A curve was fit to these data to represent a model for predicting the footprint aspect ratio for a modern radial aircraft tire. The footprint aspect ratio can be calculated according to the following empirical relationship:

$$AR = 0.1795*R^2 - 0.7127*R + 1.2979 \quad \text{(eq. 17)}$$

### Static Load-Deflection Characteristics

Each of the three tires was tested under static conditions, and at three different inflation pressures, to determine their load-deflection behavior at loads up to approximately twice the rated load for the 737 and 777 nose tires and up to approximately 1.3 times the rated load for the 777 main tire due to facility hardware limitations. The tests were conducted according to accepted standards regarding speed of load application and data points shown are for both increasing and decreasing load. Figures 23, 24, and 25 present plots of the tire deflection versus vertical load for the 737 nose tire, the 777 nose tire, and the 777 main tire respectively. For each tire, the expected trend was observed with deflection increasing at a given vertical load as inflation pressure was decreased. On average, the approximate change in deflection for each tire based on a 7.7% change in pressure (equal to the 40 F degree change) can be estimated to be about 5-6%.

Static load-deflection data are also often presented in non-dimensional form and are presented in figure 26 as percent deflection versus multiple of rated load. Percent deflection is defined as the tire deflection divided by the distance between the wheel flange and the unloaded radius of the tire times 100. Only the rated pressure is presented for each tire in this plot for ease of viewing. The figure shows that as the nominal diameter of the radial tire increases, the percent deflection at a given multiple of rated load also increases slightly. An empirical equation was fit to these data to provide a relationship describing percent deflection as a function of multiple of rated load and nominal tire diameter and can be calculated according to the following:

$$\%\delta = -7.18 + 38.85*R - 5.10*R^2 + 0.20*D \qquad \text{(eq. 18)}$$

A line representing this model evaluated for each of the three radial tires is also plotted in figure 26.

### Zero-Yaw, At-Speed Characteristics

#### *Footprint Half-Width*

One of the parameters used in shimmy analysis models is the half-width of the tire footprint. This parameter is simple to measure in a quasi-static condition in the laboratory but difficult to measure accurately on a drum dynamometer since often the inflation pressure is adjusted to account for the drum curvature and clearly the footprint contact patch must be different from that on a flat track. This test program sought to measure the footprint half-width under a full range of speeds on a flat track to provide the highest fidelity data possible to define the behavior of this parameter. The full footprint width was measured by using the footprint width indicator strips described earlier and the footprint half-width was calculated by dividing the width measurements by 2. Figures 27, 28, and 29 present plots of the tire footprint half-width versus multiple of rated load for the 737 nose tire, the 777 nose tire, and the 777 main tire respectively. This set of plots shows test results under static conditions (no forward speed) and for three inflation pressures. The results indicate no sensitivity of the footprint half-width to tire inflation pressure within the range tested. Figures 30, 31, and 32 present plots of the tire footprint half-width versus multiple of rated load for the 737 nose tire, the 777 nose tire, and the 777 main tire respectively for the entire speed range tested. The speeds are shown as a nominal desired speed of each test and are not meant to represent the actual test speeds at the moment the tire ran over the footprint width indicator strip. Since it was previously determined that inflation pressure has no effect on this parameter within the range tested, these data are presented only for rated tire inflation pressure. The

results indicate no sensitivity of the footprint half-width to forward speed within the range tested and only slight sensitivity to multiple of rated load. There is some discrete non-linearity in the behavior of the 777 nose tire as the vertical force approaches twice the rated load. These data show the effect of the "jump" in tire footprint width due to the next set of tread ribs coming into slight contact with the ground. As the static tire footprints appeared to indicate as well, though the measurable footprint width has this discrete jump, the amount of load on this small contact area is likely very small and thus not necessarily influential on the real torsional behavior of the tire that the measurement seeks to obtain for shimmy analysis. Because neither pressure nor speed appear to have a significant influence on the behavior of the radial aircraft tire footprint half-width, it appears satisfactory to allow flat-plate laboratory measurements to suffice for providing reliable information regarding this parameter into dynamic analyses. Further, an empirical means of calculating the radial aircraft tire footprint half-width was developed by curve-fitting the results from all three tires to allow for estimates of footprint half-width without the need for laboratory testing. The footprint half-width can be calculated according to the following empirical relationship:

$$Wh = Ws/2.8 + 0.7*(R - 1) \qquad \text{(eq. 19)}$$

This relationship was evaluated for each of the tires and is plotted as the single line on figures 30-32 along with the discrete test data.

By way of comparison to bias-ply construction aircraft tires, near rated deflection (that is, the deflection associated with supporting the rated load at the rated inflation pressure), reference 1 reports that the bias-ply aircraft tire exhibits a footprint half-width of approximately 42% of the tire section width. The radial aircraft tire data reported herein for rated load exhibits a relatively constant footprint half-width of 35% of the tire section width.

***Rolling Radius***

The rolling radius of a tire is a parameter that may be used to relate the translational velocity of the vehicle to the angular velocity of the tire/wheel combination. If there was enough slip in the tire footprint the tire might rotate as if the true radius were the geometric value of the axle height. Conversely, if the tread elements acted just as a tank tread does, then the rolling radius for a rotating tire would be equal to the undeflected, or free, radius regardless of axle height. Neither of these cases is true and the generalized pneumatic tire exhibits parts of both of these characteristics. Reference 1 reported that for bias-ply construction tires, a satisfactory empirical relationship to describe the relationship between rolling radius and tire deflection was:

$$re = D/2 - 1/3* \delta \qquad \text{(eq. 20)}$$

where $\delta$ was measured under pure vertical loading. Before evaluating the rolling radius for the radial aircraft tires, the 777 nose tire was used to provide an example of the effect of speed on the axle height as a function of vertical load. Figure 33 presents a plot of axle height versus vertical load for the 777 nose tire at its rated inflation pressure for speeds ranging from static to 200 kts. The solid circular data points denote the static load-deflection behavior which is the standard method of describing vertical stiffness. The figure shows a slight trend of increasing axle height as speed increases, although as the speed rises to approximately 100 kts the coherence of the trend begins to fade. This response in axle height is due to the tire gaining radial stiffness as a result of increasing angular velocity, although just as

for most of the previously reported footprint parameters, the radial aircraft tire appears to be remarkably stable in terms of its response to inflation pressure and speed and can often be regarded as insensitive to these parameters for the most part. Based on this, figures 34, 35, and 36 present plots of rolling radius versus vertical load for the 737 nose tire, the 777 nose tire, and the 777 main tire respectively for the entire speed range tested and without regard to inflation pressure. For reference on each plot, the static load-deflection behavior expressed as axle height versus vertical load is denoted by the circular data points as an example of the lower limit of what the rolling radius could possibly be. The radial aircraft tires generally appear to have a more stable tread than the bias-ply aircraft tires described in equation (20). The radial tires appear to behave slightly more like the tank tread analogy in that they seek to have a larger percentage of the tread elements pass through the footprint every revolution regardless of vertical load. Although there is some scatter in a general rule to describe the behavior accurately for all three tires, an empirical relationship similar to the one presented from reference 1 appears to do a satisfactory job of approximating the effective rolling radius of the radial aircraft tire. The rolling radius for a radial aircraft tire can be approximated using the following relationship:

$$re = D/2 - 1/5 * \delta \qquad \text{(eq. 21)}$$

Figure 37 presents a plot of the rolling radius portions of figures 34-36 and shows a curve calculated for each tire using equation (21) to predict the behavior of the rolling radius.

***Rolling Resistance***

Consider the top view sketch in figure 10 in which the unbraked, yawed tire is rolling toward the top of the page. Regardless of the yaw angle, the center of pressure (that is, the centroid of the vertical ground reaction force) is seen to shift forward in the footprint. The couple produced by the vertical ground reaction force acting through this forward center of pressure tends to decelerate the tire angularly and to achieve a moment balance, there is a drag force produced at the ground plane which acts through the axle height to counteract the center of pressure moment. This drag force is typically referred to as the rolling resistance and is a function of the tire properties far more so than the nature of the frictional properties of the surface. The drag force associated with rolling in an unyawed, unbraked mode for each of the three test tires was recorded during each test run and divided by the vertical force for each test to yield the drag force coefficient according to equation (5). Figures 38, 39, and 40 present plots of rolling resistance versus multiple of rated load for the 737 nose tire, the 777 nose tire, and the 777 main tire respectively for the entire speed range tested and without regard to inflation pressure. A separate look at the data broken up with regard to speed shows no discernible trend and is thus ignored. Figure 41 presents all of the data from all three tires and it can be seen that though there is clearly scatter, the rolling resistance for a radial aircraft tire can conservatively be assumed to be approximately 0.015.

***Conicity***

A bias-ply constructed tire is, by definition and its very nature, an asymmetric composite structure. When it is deflected, because the plies are on biases at differing levels above the tread elements, a twisting motion is imposed upon the carcass structure. This twisting motion manifests itself as a slight yaw in the footprint of the otherwise unyawed tire. The uncommanded yaw in the footprint causes the tire to produce uncommanded side force as it rolls straight ahead and this is referred to as ply-

steer. A radial aircraft tire often is designed with textile materials in its carcass structure oriented in a bias fashion and thus can also exhibit elements of ply-steer, though typically it is of a less pronounced magnitude. It should also be noted that the nature of ply-steer is such that the force will always be produced towards a given side of the tire as the tire is rolled forward. In other words, if the force is produced to the left as the tire is rolled away from you, then it will be produced towards your right as the tire is rolled towards you (but still towards the tire's left as viewed from behind). Ply-steer cannot be affected by mounting the tire "backwards" on the wheel. The forces and their respective directions will be unaffected. Radial tires more typically produce uncommanded side forces during unyawed rolling due to a phenomenon referred to as conicity. In this phenomenon, one may think of the circumferential belt as being mis-aligned during construction such that one edge of the belt has a smaller radius than the other side thus taking the shape of a shallow, truncated cone. As this "cone" is rolled, it wants to trace a curved path and the tendency is to produce uncommanded side force. Hence the name "conicity". This type of uncommanded side force always produces force to the same physical side of the tire and is unaffected by rolling direction. In this case, the force can be directed towards the "other side" by reversing the way the tire is mounted on the wheel. Conicity is also much more of an unpredictable and random parameter than is ply-steer (see reference 5).

The side force associated with rolling in an unyawed, unbraked mode for each of the three test tires was recorded during each test run and divided by the vertical force for each test to yield the side force coefficient according to equation (7). To document the conicity of the radial aircraft tires, figures 42, 43, and 44 present plots of side force coefficient (denoted in the plots as conicity) versus multiple of rated load for the 737 nose tire, the 777 nose tire, and the 777 main tire respectively for the entire speed range tested and without regard to inflation pressure. Since this phenomenon is somewhat random both in magnitude and direction, no attempt at producing a generalized empirical model for predicting conicity is attempted. The data shown for the 737 nose tire exhibits more scatter than the other two larger tires, and is attributed to the smaller loads in general for this tire which decreases the signal to noise ratio of the measurements. However, it appears that a general observation regarding the magnitude of conicity for radial aircraft tires is that the value is not likely to exceed about 0.02 throughout a 15% inflation pressure range and for virtually all loads on the tire.

### Yawed-Rolling Characteristics

During this investigation the test tires were subjected to testing under yawed-rolling conditions to determine their response in side force, side force coefficient, drag force, drag force coefficient, aligning torque, overturning torque, lateral center of pressure shift, and friction force moment arm. Test parameters varied during this phase of testing included speed, inflation pressure, vertical force, yaw angle, and to some extent, surface wetness condition. Again, very limited yawed-rolling data were obtained for the 777 main tire since the test wheel bearings and test wheel itself were damaged beyond immediate repair after a single run conducted at a multiple of rated load of about 1.25.

#### *Side Force*

**Effect of Vertical Force**. Several tests were conducted to examine the effect of vertical force on the behavior of the side force with respect to yaw angle. A representative set of tests using the 777 nose tire at rated inflation pressure and a nominal speed of 100 kts is shown in figure 45 with the side force plotted as a function of yaw angle. The figure shows data for vertical forces ranging from values of 0.5 to 2.0 in multiple of rated load. The figure suggests that nearly the same side force is generated for a given yaw angle regardless of vertical force. The extremely large variation in vertical force but lack of

substantial increase in the resultant side force generated tends to mask the real effect of vertical force except when observed in a more non-dimensional fashion in the following section.

***Side Force Coefficient***

**Effect of Vertical Force**. The data from the representative set of tests from the previous section were plotted in figure 46 with side force coefficient plotted as a function of yaw angle for vertical forces ranging from values of 0.5 to 2.0 in multiple of rated load. These data were obtained using the 777 nose tire at rated inflation pressure and a nominal speed of 100 kts. The side force coefficient is literally an efficiency term that denotes how efficient the tire is at producing side force under a given vertical force. The figure shows a trend routinely seen for most tires, especially aircraft tires, in which the tire becomes less efficient at producing side force as the vertical load is increased. This effect is shown for tires of bias-ply construction as well in references 6 and 7. One possible explanation is that as the vertical force on the tire is increased, an increasing amount of 3-dimensional tire circumference and surface area must "fit" into a 2-dimensional contact patch and thus the contact patch homogeneity becomes increasingly non-linear. The tread elements near the relative center of the contact patch can actually be lifted out of contact with the surface in extreme cases. This tendency appears to be responsible, at least in part, for the degradation of cornering efficiency as vertical force is increased.

**Effect of Speed**. Several tests were conducted to examine the effect of forward speed on the behavior of the side force coefficient as a function of yaw angle. A representative set of tests using the 777 nose tire at rated inflation pressure and at rated load is shown in figure 47 with the side force coefficient plotted as a function of yaw angle for speeds ranging from a nominal 100 - 200 kts. The figure shows the expected trend of increasing side force coefficient as the yaw angle is increased up to a point where further increases in yaw angle usually result in a decrease of the side force coefficient similar to the behavior of a lift coefficient curve for a wing. Just as was reported for tires of bias-ply construction in references 6 and 7, there is no effect of speed on the cornering behavior of the radial aircraft tire worth noting on dry surfaces.

**Effect of Inflation Pressure**. Several tests were conducted to examine the effect of inflation pressure on the behavior of the side force coefficient as a function of yaw angle. A representative set of tests using the 777 nose tire at rated load and 100 kts is shown in figure 48 with the side force coefficient plotted as a function of yaw angle for rated pressure and the pressure associated with a 40 Fahrenheit degree temperature change. The figure shows that within the range of inflation pressures tested, no discernible effect on side force coefficient is present. Since other parameters associated with the footprint also appear to be unaffected by inflation pressure, such as footprint width, aspect ratio, rolling radius, etc, this result is not surprising. Based on this finding and the finding of insensitivity to speed, the remainder of the examination of the yawed-rolling generalized behavior between radial aircraft tire sizes will be without regard to speed and inflation pressure and results will be presented for rated conditions and nominal speeds unless otherwise specified.

**Effect of Tire Size**. A number of tests were conducted to examine the cornering behavior of the three tire sizes. Data for the 777 nose tire were previously presented in figure 46. Figures 49 and 50 present the same type of data with side force coefficient plotted as a function of yaw angle for various multiples of rated load for the 737 nose tire and the 777 main tire respectively. One should note that for the 737 tire, limitations of the test hardware, notably how much deflection could be imposed on the tire prior to encountering interference problems with the dynamometer on the test runway itself, caused a

functional limitation of multiple of rated load to essentially a value of 1 for this tire. For the 777 main tire, as was previously mentioned, hardware failures prevented the acquisition of data beyond the first test which was conducted at a multiple of rated load of approximately 1.25 and at a speed of approximately 200 kts. The data from the runs presented in figures 46, 49, and 50 were input into a commercially available curve-fitting program and an empirical relationship between the side force coefficient and the input parameters of yaw angle and multiple of rated load was defined. The form of the relationship was previously defined in references 6 and 7 and is a truncated bicubic equation where two variables at up to the third power are used to describe the behavior of the independent variable. Not all of the possible terms are included, but this form has previously proven to be quite adequate in modeling tire behavior. The following is the form of the bicubic representation of side force coefficient as a function of multiple of rated load and yaw angle, and since the date are non-dimensionalized, without regard to tire size:

$$\mu s = \beta 0 + \beta 1*R + \beta 2*R\text{^}2 + \beta 3*R\text{^}3 + \beta 4*\Psi + \beta 5*\Psi\text{^}2 + \beta 6*\Psi\text{^}3 + \beta 7*R*\Psi + \beta 8*R*\Psi\text{^}2 + \beta 9*R\text{^}2*\Psi \quad \text{(eq. 22)}$$

The coefficients of curve-fitting are as follows:

$\beta 0 = 0.1952$
$\beta 1 = -0.5224$
$\beta 2 = 0.4329$
$\beta 3 = -0.1140$
$\beta 4 = 0.1273$
$\beta 5 = -0.0027$
$\beta 6 = -0.0002$
$\beta 7 = -0.058$
$\beta 8 = 0.0023$
$\beta 9 = 0.0051$

Figures 49, 46, and 50 are presented again as figures 51, 52, and 53 for the 737 nose tire, 777 nose tire, and 777 main tire respectively and each load case has a line denoting the prediction of side force coefficient using equation (22) to illustrate the nature of the curve fit. Note that in figures 51 and 52, even though the positive and negative side force coefficient behavior is not completely symmetric, when the tire is at relatively light load ( R=0.5 for example ) the side force coefficient appears to begin to peak around a coefficient of approximately 0.7. The following empirical relationship was presented in reference 1 to indicate an estimate of the maximum coefficient of friction on a dry concrete surface which decreases with increasing inflation pressure:

$$\mu = 0.93 - 0.0011*P \quad \text{(eq. 23)}$$

Since the maximum friction obtainable on a dry concrete surface is likely to be mostly a function of the interaction of the tread with the surface on a very small scale, no dramatic behavior difference would be expected with a tire of different structural design so long as the footprint were a reasonable analog to the bias-ply tire the data were generated with. It appears, with limited data, that this empirical relationship is still valid for radial aircraft tires.

**Effect of Surface Wetness**. A number of yawed-rolling tests were conducted under wet conditions attempting to simulate conditions found after a typical rain shower on an ungrooved concrete runway. Figures 54 and 55 present plots of the side force coefficient versus yaw angle for the 737 nose tire and 777 nose tire respectively under wet conditions at increasing speeds. These data show the expected result of surface wetness having the effect of decreasing friction (in this case side force coefficient) and whereas speed does not have an effect under dry conditions, causing increasing speed to have an increasing negative effect on the side force coefficient obtained. The data suggests that operating at low speed ( taxi speeds, for example) under wet conditions may reduce the side force coefficient by only about 25% or less. As speed is increased to about 100 kts, the data suggest that one might expect the side force coefficient to drop by about 40% as compared to the dry value especially when the yaw angle rises past about 2 ½ degrees of yaw where the data becomes noticeably more noisy. As speed is increased to approximately 200 kts, the reduction of side force coefficient can be as high as 50-75% as compared to the dry values and again this tends to occur at higher yaw angles rather than lower ones.

***Drag Force Coefficient***

The drag force coefficient due to rolling resistance was discussed earlier. Under yawed-rolling conditions, there is additional drag force created by virtue of generating work in the tire footprint. The drag force coefficient versus yaw angle is plotted in figure 56 for all three tires at rated load except for the 777 main tire which was plotted at 1.25 rated load since those were the only test data available. The plot shows a fair amount of scatter, but the basic result of rolling resistance at zero yaw angle being approximated by the value 0.015 still appears valid. Additionally, there is a slight increase in the drag force coefficient as yaw angle is increased in either direction. A simple model for this behavior is:

$$\mu d = 0.015 + 0.001*ABS(\Psi) \qquad \text{(eq. 24)}$$

***Aligning Torque***

As previously mentioned, the aligning torque is developed as a result of the centroid of the side forces in the yawed, rolling tire footprint moving aft of the steering axis and is a moment that generally resists the further increase of yaw angle as long as the yaw angle is within certain limits about zero yaw angle. Figure 57 shows a plot of the typical behavior of the aligning torque for the 777 nose tire at rated load. The plot shows that as the yaw angle is increased up to about 6 degrees, that the moment continues to rise in response to the increased yaw angle. This moment is representative of the moment required to steer the tire at these conditions and would, for example, provide a target value for the minimum moment required of a steering actuator. After reaching a maximum value, it can be seen that further increases in yaw angle result in a decrease in the restorative yaw moment the tire produces. Since this phenomenon relies, in part, on how far aft of the steering axis the centroid of side force moves, one approach to modeling the aligning torque is to use a term associated with the tire size in addition to a term associated with multiple of the rated load and yaw angle. The most useful place to examine the aligning torque is at rated conditions, and between the yaw values that the torque continues to rise. Figure 58 presents a plot of aligning torque for the 737 nose tire, the 777 nose tire, and the 777 main tire respectively as a function of yaw angle at rated load conditions. The plot shows essentially linear behavior in the positive to negative 5 degrees range shown for each tire. For each tire shown, a

model to predict the aligning torque is also plotted and appears to do a satisfactory job of approximating the aligning torque of the radial aircraft tire. The aligning torque for a radial aircraft tire up to approximately 5 degrees yaw angle can be approximated using the following relationship:

$$Mz = 0.85*R*D^{2.5}*\Psi \qquad \text{(eq. 25)}$$

***Overturning Torque***

As previously mentioned, the overturning torque is developed as a result of the side force acting laterally with a moment arm of the axle height in addition to the vertical force acting through a laterally-shifted center of pressure. The moment contribution of the side force is typically the larger of the two moments that add together to form the overturning torque. The axle height and the lateral stiffness of the tire footprint contribute to the moment arms used in the calculations, so it is natural to attempt modeling again with at least a term descriptive of the tire geometry, and so again the tire diameter is used. Figure 59 presents a plot of overturning torque for the 737 nose tire, the 777 nose tire, and the 777 main tire respectively as a function of yaw angle at rated load conditions. The plot shows that the overturning torque is reasonably linear over the range tested and particularly within about positive and negative 5 degrees. Note that the overturning torque for the 777 main tire is reasonably well-behaved in the positive yaw direction but begins to become unpredictable in the negative yaw direction. This is due to the fact that the bearing failures discussed earlier appear to have begun about 2/3 through the test, which coincides with the time that the yaw angle was passing through about –2 to –3 degrees. An empirical relationship was developed to predict the overturning torque for the radial aircraft tire and is shown in the following formula:

$$Mx = 0.11*D^{3.5}*\Psi \qquad \text{(eq. 26)}$$

**Effect of Surface Wetness**. A number of yawed-rolling tests were conducted under wet conditions attempting to simulate conditions found after a typical rain shower on an ungrooved concrete runway. Figure 60 present plots of the overturning torque as a function of yaw angle for dry and wet surfaces with the 777 nose tire under rated conditions. The figure shows essentially the same behavior as that shown for the side force coefficient in figures 54 and 55, with a reduction in the overturning torque of about 40% at 100 kts on the wet surface. This is not surprising since the overturning torque is, of course, dominated by the side force acting through the axle height.

***Lateral Center of Pressure Shift***

As shown in figure 10, the lateral center of pressure shift is the arm through which the centroid of the vertical force creates a component of the overturning torque. One can visualize the tire under yawed-rolling conditions and the fact that the footprint is displaced toward the direction of yaw angle since it can be thought of as a lateral spring. The lateral center of pressure shift is determined through test data by the method described in equation (10). Though the initial appearance of the parameter looks to be a measure of the tire lateral stiffness, it really should not be substituted for a true lateral load-deflection test if those are the data being sought since the lateral center of pressure shift is in a sense the distance to an imaginary point in the footprint and one that can only be “calculated” as opposed to

measured directly. Figure 61 presents a plot of lateral center of pressure shift as a function of yaw angle for the three tire sizes and differing conditions; the 737 nose tire at rated load and pressure but slow speed, the 777 nose tire at rated pressure and 100 kts but at multiples of rated load of 1 and 2, and the 777 main tire at rated pressure but at 200 kts and a multiple of rated load of 1.25. All of these data are plotted as a single data set after noticing that there did not seem to be a trend based on tire size. Thus there did not appear to be a need to non-dimensionalize the data. A linear curve was fit to the data and forced to intercept the origin and is also shown on the figure. The following empirical relationship may be used to predict the lateral center of pressure shift for a radial aircraft tire:

$$Cp = 0.2*\Psi \qquad \text{(eq. 27)}$$

***Friction Force Moment Arm***

As shown in figure 10, the friction force moment arm is the arm through which the centroid of the side force of the yawed, rolling tire creates a component that tends to align the tire with the direction of motion. Just as for the lateral center of pressure shift, this moment arm is the distance from the steering axis to an imaginary, calculated point aft of the steering axis. It is useful only in the sense that it relates the side force to aligning torque and in a sense, provides a measure of how efficiently the side force manifests itself as aligning torque by observing the yaw angle where the moment arm reaches a peak. Figure 62 presents a plot of the friction force moment arm as a function of positive yaw angle for the same tires and conditions as described for figure 61 above. The figure shows that, in general, the friction force moment arm reaches a peak around 2 degrees of yaw angle. The curve for the 737 nose tire and the 777 nose tire at rated load are seen to reach a value of approximately zero at about 8 degrees of yaw angle. This suggests that the aligning torque has reached a value of zero as well, indicating that the yaw behavior of the tire has become neutrally stable and that further increases in yaw angle are either neutrally stable or unstable if the tire were in a free-castor mode and able to reach that angle. The figure shows a fairly significant effect of vertical force by observing the 777 nose tire data at rated load and twice rated load, where the friction force moment arm almost triples for the load factor of two. The effect of tire size appears to be related in a basic sense, with the trend of friction force moment arm rising with tire size. Rather than defining a new empirical relationship to describe the friction force moment arm, combining three relationships that are already developed is the suggested method to predict the friction force moment arm. Equation (11), which described the friction force moment arm, can be rewritten and combined with equation (7) and equation (24) to yield the following relationship:

$$FFma = (0.85*R*D^{2.5}*\Psi) / (\mu s*Fz) \qquad \text{(eq. 28)}$$

where $\mu s$ must be evaluated with the formula in equation (22).

## Concluding Remarks

In an effort to update the 1960 document entitled “Mechanical Properties of Pneumatic Tires With Special Reference to Modern Aircraft Tires”, the NASA Langley Research Center Aircraft Landing Dynamics Facility was used to conduct an experimental study. The goal was to acquire mechanical properties behavior of modern aircraft tires of radial construction as opposed to those of

bias-ply construction from the 1960 report. A further goal was to determine if any parameters that can be measured statically vary with high forward speed or not as was suggested in the original R-64 report. Additionally, where possible, empirical relationships were developed to predict certain elements of radial aircraft tire behavior.

An experimental investigation was conducted to determine the effects of various parameters on the mechanical properties of three modern radial aircraft tires representing the range of sizes likely to be encountered on typical modern commercial jet transport aircraft. The mechanical properties investigated included static load-deflection behavior, footprint area, footprint aspect ratio, contact pressure ratio, footprint half-width, rolling radius and axle height, rolling drag coefficient, conicity, side force response, drag force response, aligning torque, overturning torque, lateral center of pressure shift, and friction force moment arm. The parameters that were varied to evaluate these mechanical properties included vertical load, tire inflation pressure, forward speed, yaw angle, and surface wetness condition. The ranges of load, speed, pressure, yaw angle, and surface wetness were designed to represent the likely variations encountered in actual aircraft operations.

The results of the investigation indicate that the modern radial aircraft tire is very stable dimensionally regarding footprint area, contact pressure ratio, and footprint aspect ratio. The response of these parameters to variations in inflation pressure equal to a 40-Fahrenheit degree temperature change, as might be seen in actual flight operations, was small. The footprint area of the radial tire was found to be smaller than the contact area that would be associated with the inflation pressure at a given load. This difference was far larger than the slight variations in footprint area due to the range of inflation pressures tested. Thus the contact pressure ratio was found to be greater than 1 for all conditions tested and also that it could be represented by a linear function based on a multiple of rated load. Further study and comparison of this contact pressure ratio with bias-ply tire behavior with regard to its influence on hydroplaning behavior is recommended.

The static load-deflection behavior of the radial tires was found to follow the same behavior trends as for bias-ply aircraft tires. Though percent deflection is less-often used in describing radial tire rated conditions, it was observed that each tire deflected similarly as a function of multiple of rated load. A relationship to describe this behavior with a slight modifier for tire size was presented.

The response of certain radial tire parameters to at-speed but zero-yaw conditions also appeared stable in terms of inflation pressure and forward speed. The footprint half-width was found to be unaffected by either speed or inflation pressure for the ranges tested. A relationship to predict the footprint half-width based on tire size and multiple of rated load was presented. Due to the stability of this parameter, it is clear that laboratory measurement of the radial aircraft tire footprint half-width is adequate for dynamics analyses. The rolling radius of the radial aircraft tire was found to be independent of inflation pressure or forward speed. The variation in axle height was found to be small for the range of speeds tested. The maximum change in axle height based on variations in pressures still caused the at-speed behavior to be less deflected than the static deflection which again suggests that this pressure range has little effect on the overall deflection or behavior of the tire. This slight variation decreased when calculating the effective axle height, or the rolling radius. The rolling radius was found, as it was for bias-ply aircraft tires, to be universally more than the value of axle height at any time. No single empirical model appeared to fit the test data as well as the curve fits reported in R-64 for bias-ply aircraft tires due to directional scatter in the test data, i.e. no coherent trend due to tire size was observed. However, a general empirical model was developed that simply makes use of a different coefficient than the existing model and permits gross estimates of the rolling radius for a radial aircraft tire. Rolling resistance was found to be generally unaffected by speed or inflation pressure and that the drag force coefficient associated with rolling the radial aircraft tire straight ahead can be conservatively

estimated at 0.015. Conicity was found to be present in these radial aircraft tires and it appeared to be random, given the small number of tires tested, as described in other references. The value of conicity appears to be bounded by a side force coefficient of approximately 0.02.

A number of parameters describing the radial aircraft tire's response to yawed rolling were investigated. For the individual tire, there appeared to be little effect on the side force as a function of yaw angle when varying vertical force. However, a more proper understanding of the true behavior is to observe the effect of vertical force on the side force coefficient, and when this is done one can see that as the vertical force is increased, the radial aircraft tire becomes less efficient at producing side force as is classically seen. No effect of speed on the side force coefficient was observed so long as the tire was operated on a dry concrete surface, repeating the results of many previous studies at the facility. Likewise, no effect of inflation pressure within the range tested on the side force coefficient was observed. Again, it appears that within the range of pressures tested (which amounts to approximately +/- 15 psi for most of these tires) that no observable change in performance is present, perhaps making it possible to consider relaxing the required tolerance in radial aircraft tire pressures during routine flight operations and checks. Using the nondimensionalized side force coefficient, comparisons of the three radial tire sizes could be made directly. It was found that a single empirical relationship, though complicated, could describe the side force coefficient for any of the radial aircraft tires. The effect of wetness on the radial aircraft tire side force coefficient was as expected and confirmed that under wet conditions, increasing speed causes an increase in the amount of friction loss as compared to a dry surface. Though not tested in the present study, the amount of friction loss is also highly affected by water depth on the runway. In general, with moderate wetness present, one can expect an approximate 40% decrease as compared to dry friction levels as the speed is increased to about 100 kts, and an approximate 50-75% decrease as compared to dry friction levels as the speed is increased to about 200 kts. The drag force coefficient was seen to exhibit scatter during yawed testing which is possibly due to the noisy nature of dynamic rotation of an unbalanced tire coupled with tire cornering. Regardless, a trend was observed wherein as yaw angle was increased, the drag force coefficient increased slightly as well. A simple model to describe this linear behavior was presented.

Aligning torque, since it relies heavily on side force and tire geometry, was found to be predictable using functions of multiple of rated load, yaw angle, and tire size. It was found to vary approximately linearly within about +/-5 degrees of yaw angle. The response of overturning torque to yaw angle was found to be approximately the same shape as the side force response, except slightly more linear since it has added to it a moment based on lateral center of pressure shift times the vertical force. An empirical relationship based on tire diameter and yaw angle for rated load conditions was developed based on the observations that the footprint configuration is stable with regard to inflation pressure and that the side force is insensitive with regard to variations in speed and inflation pressure. The prediction of overturning torque could be modified to be more general to include the effect of side forces and axle heights developed at other than the rated load but was not attempted in this report. While the effect of wetness was discussed earlier for side force coefficient, for completeness the overturning torque was examined for the effect of wetness and should have responded similarly. It was found to respond to the effect of wetness and speed in the same manner, though no empirical relationship was offered. The lateral center of pressure shift was found to be remarkably similar in magnitude between the three tire sizes tested and an empirical relationship was presented. The lateral center of pressure shift was modeled as linear with yaw angle alone. Finally, the friction force moment arm was examined and found to increase with increasing tire size, just as the side forces generated also increase with tire size. This parameter was also found to reach a peak value at low yaw angles of about

2 degrees. The friction force moment arm was also seen to vary substantially with multiple of rated load, with a doubling in vertical force resulting in a tripling of the friction force moment arm.

## Appendix A

Footprint Images of Radial Aircraft Tires

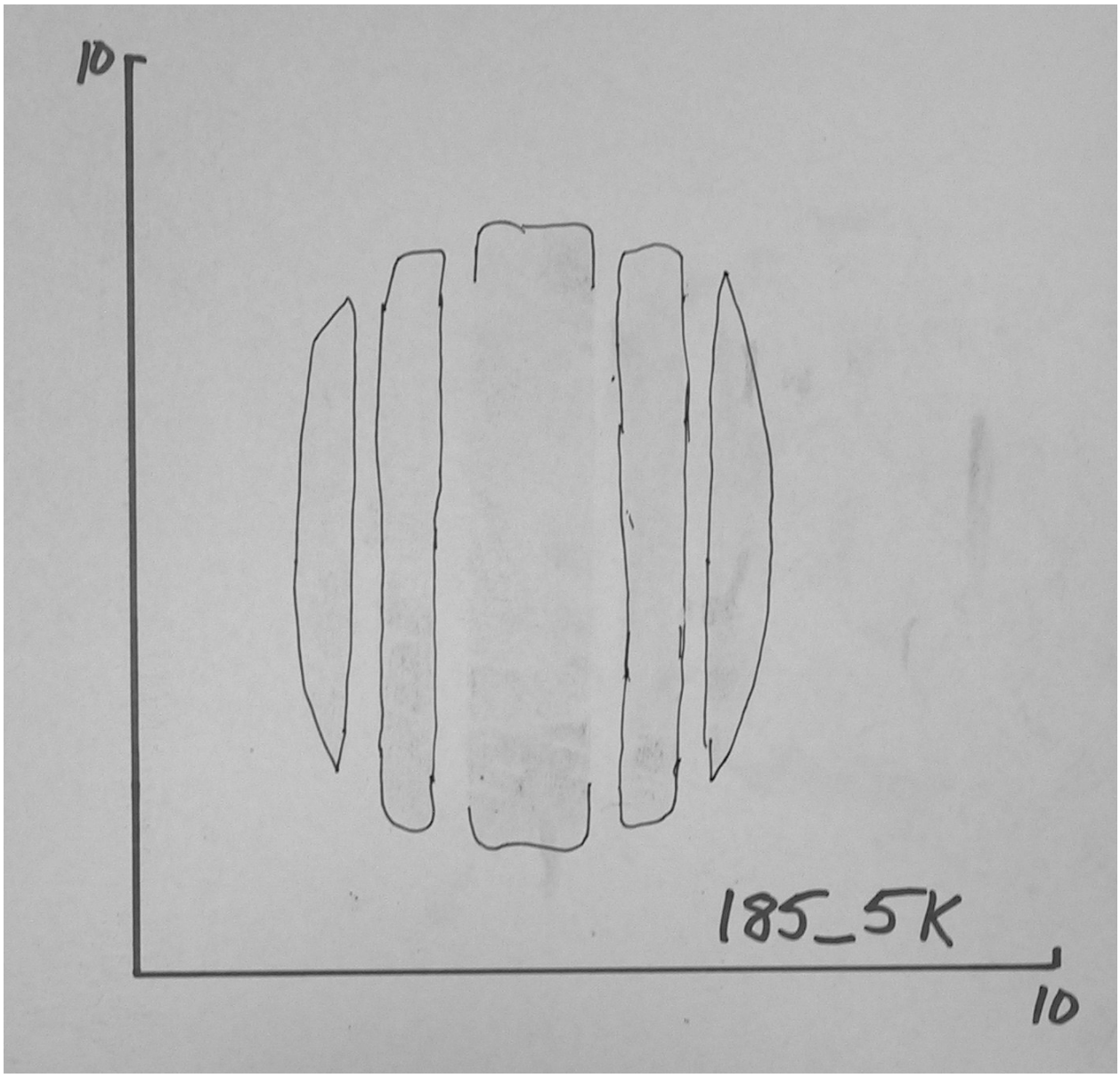


Figure A1. 737 nose tire; 185 psi; 5000 lb.

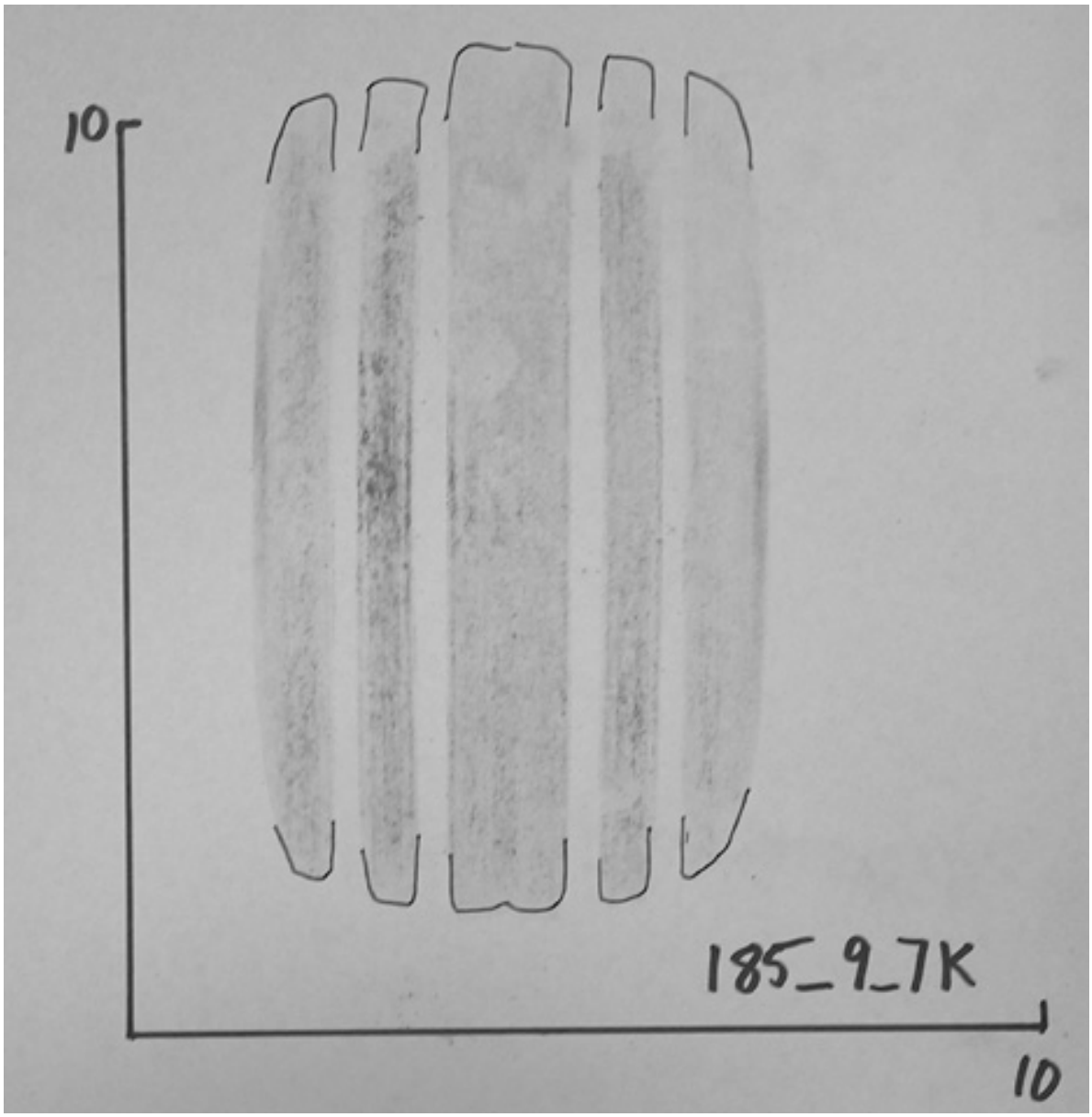


Figure A2. 737 nose tire; 185 psi; 9700 lb.

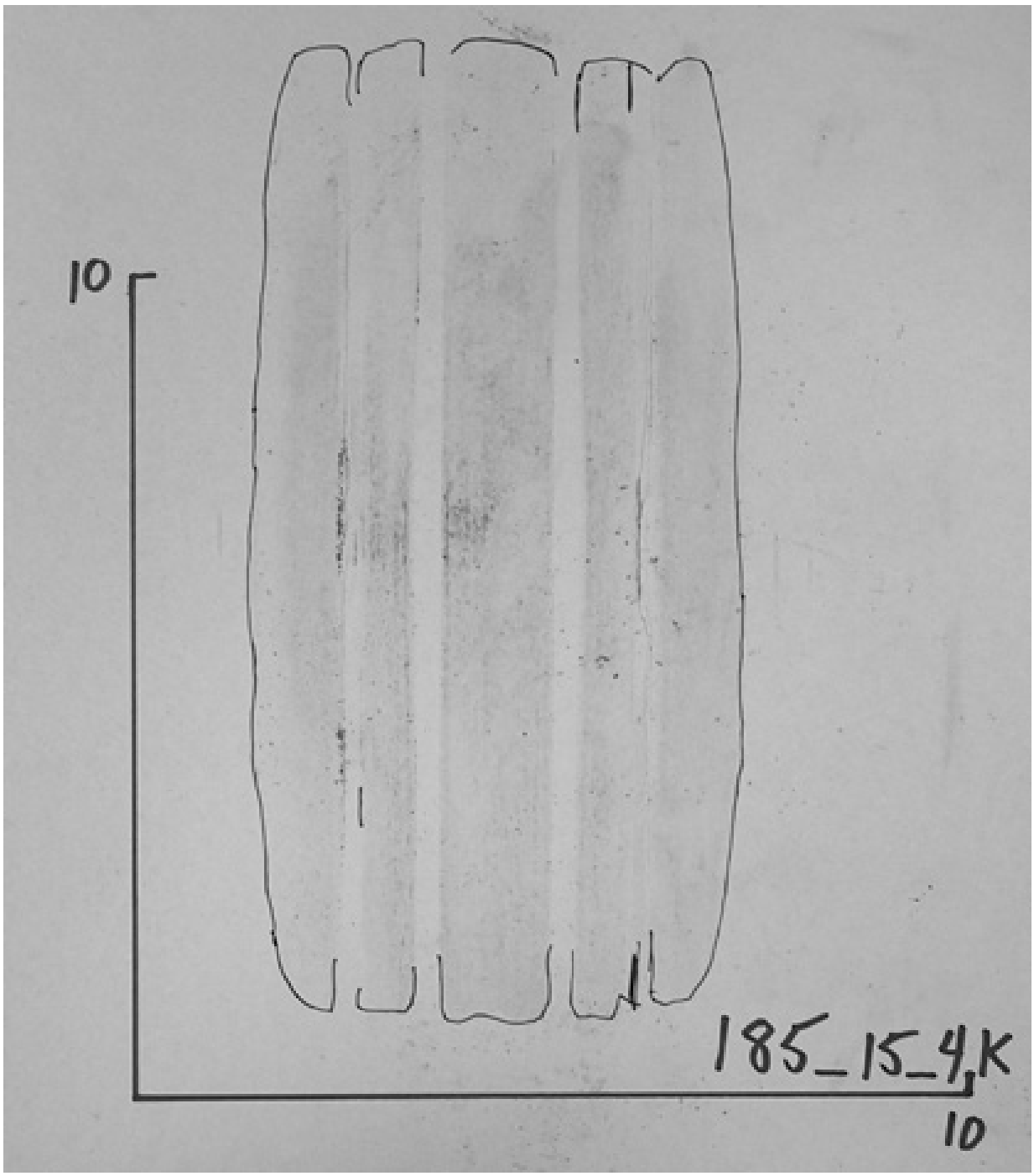


Figure A3. 737 nose tire; 185 psi; 15400 lb.

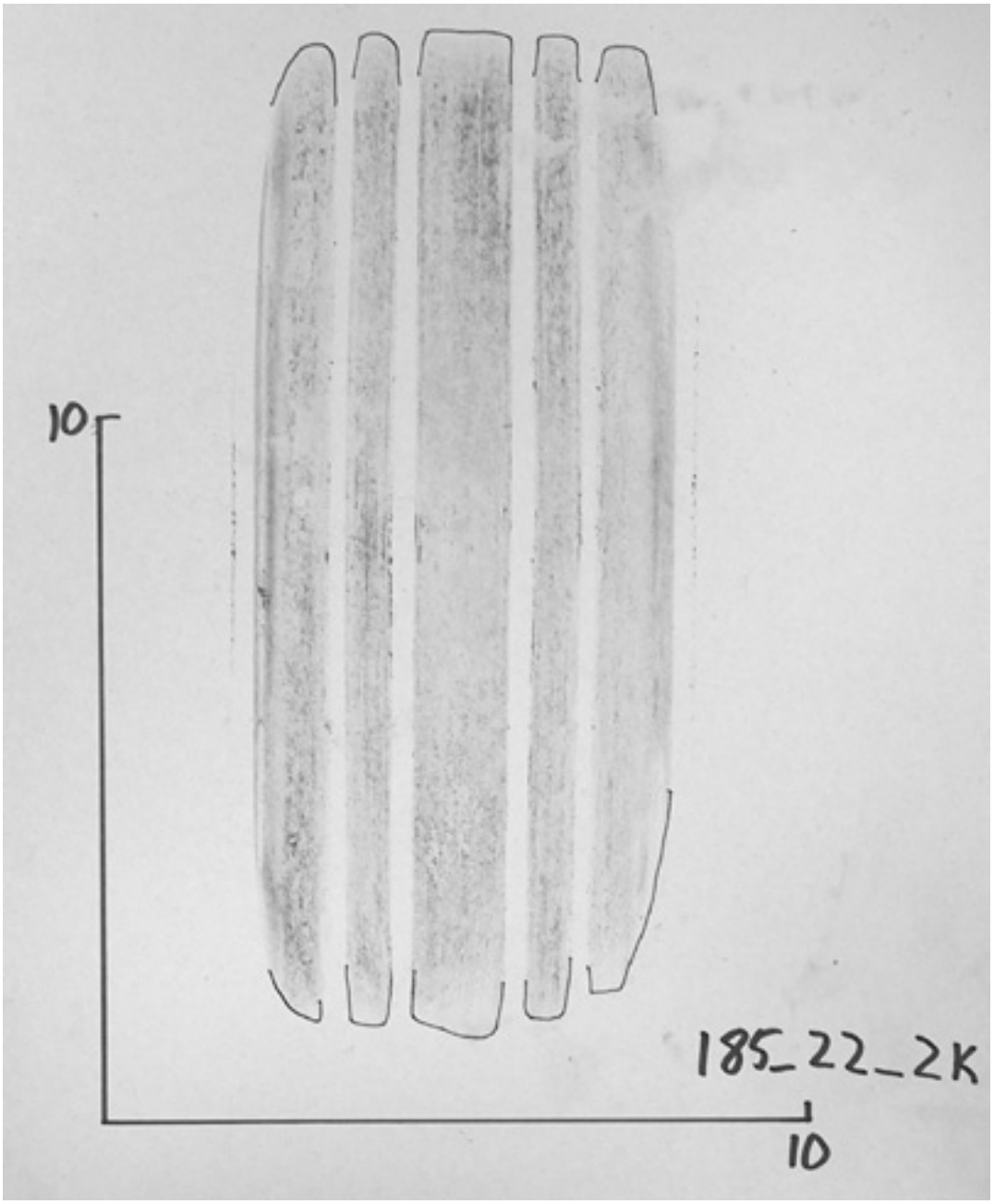


Figure A4. 737 nose tire; 185 psi; 22200 lb.

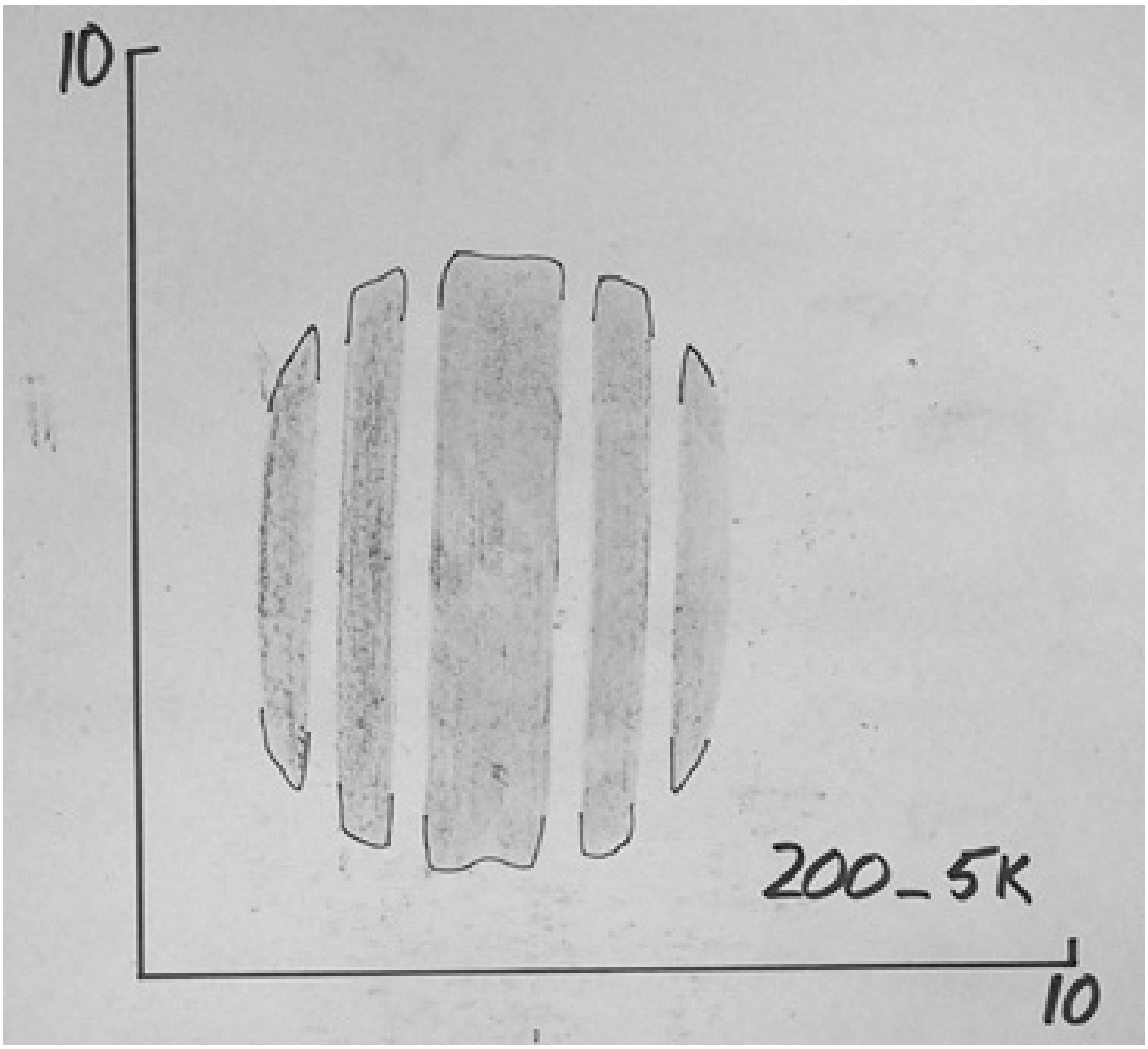


Figure A5. 737 nose tire; 200psi; 5000 lb.

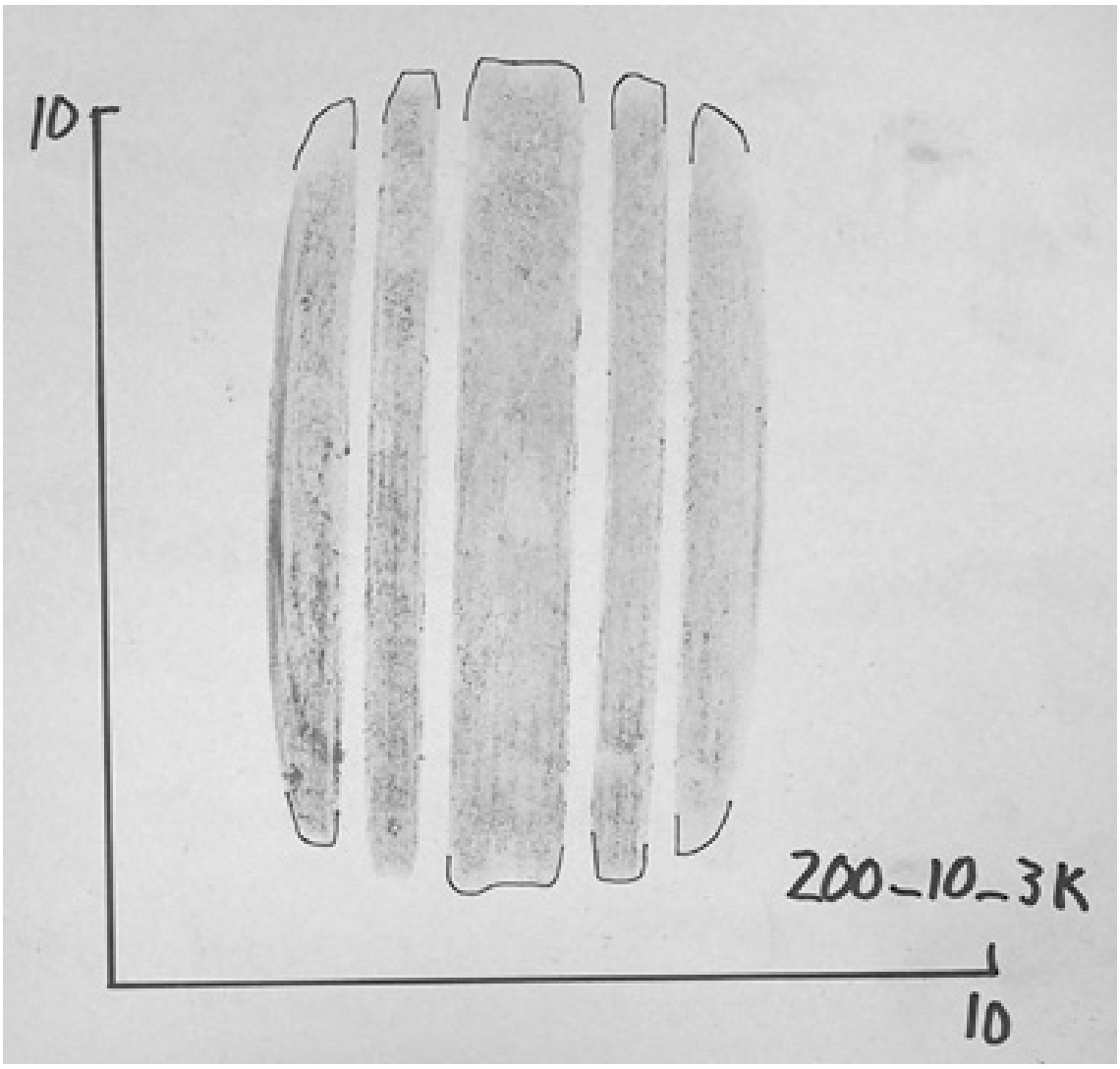


Figure A6. 737 nose tire; 200 psi; 10300 lb.

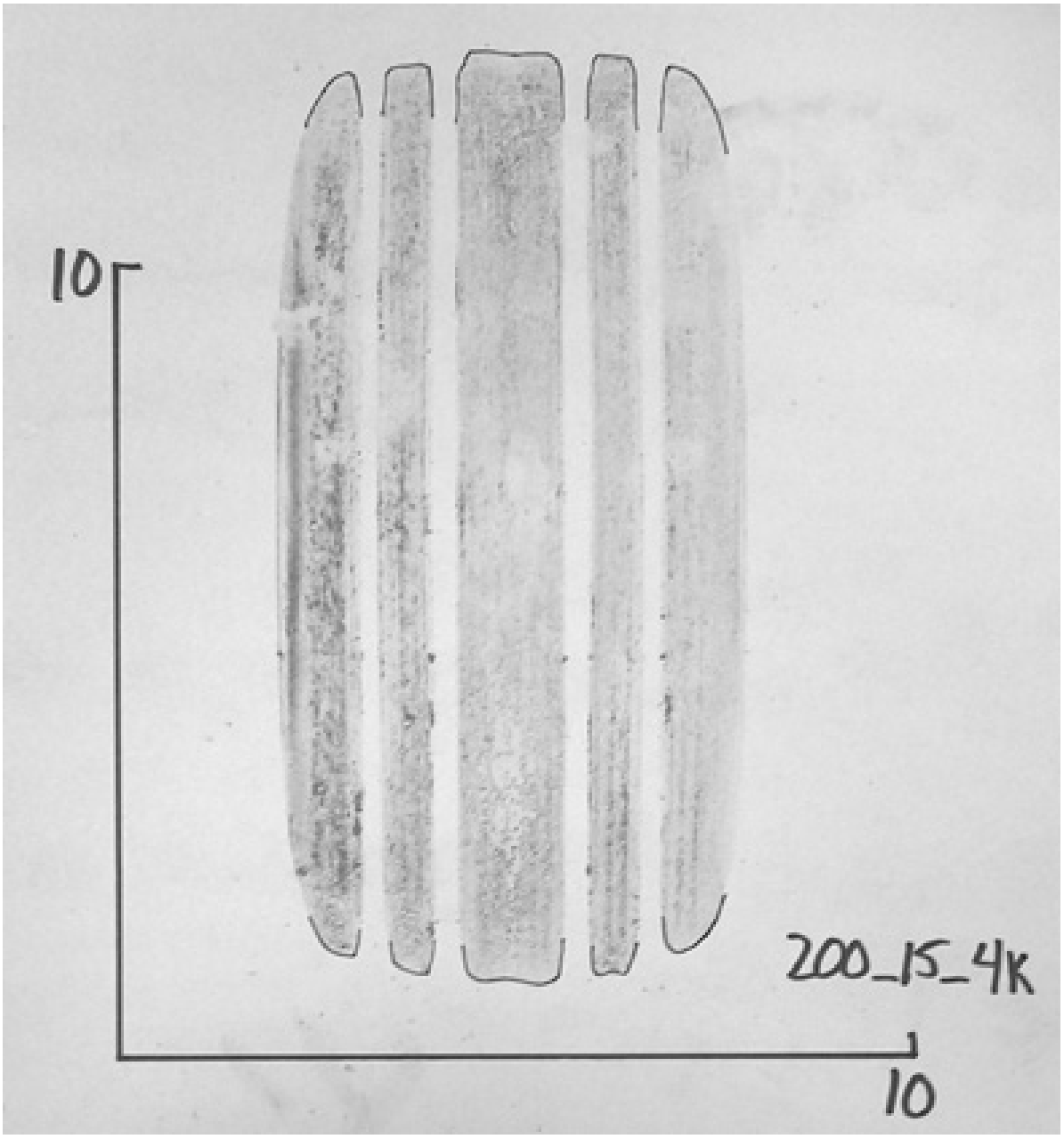


Figure A7. 737 nose tire; 200 psi; 15400 lb.

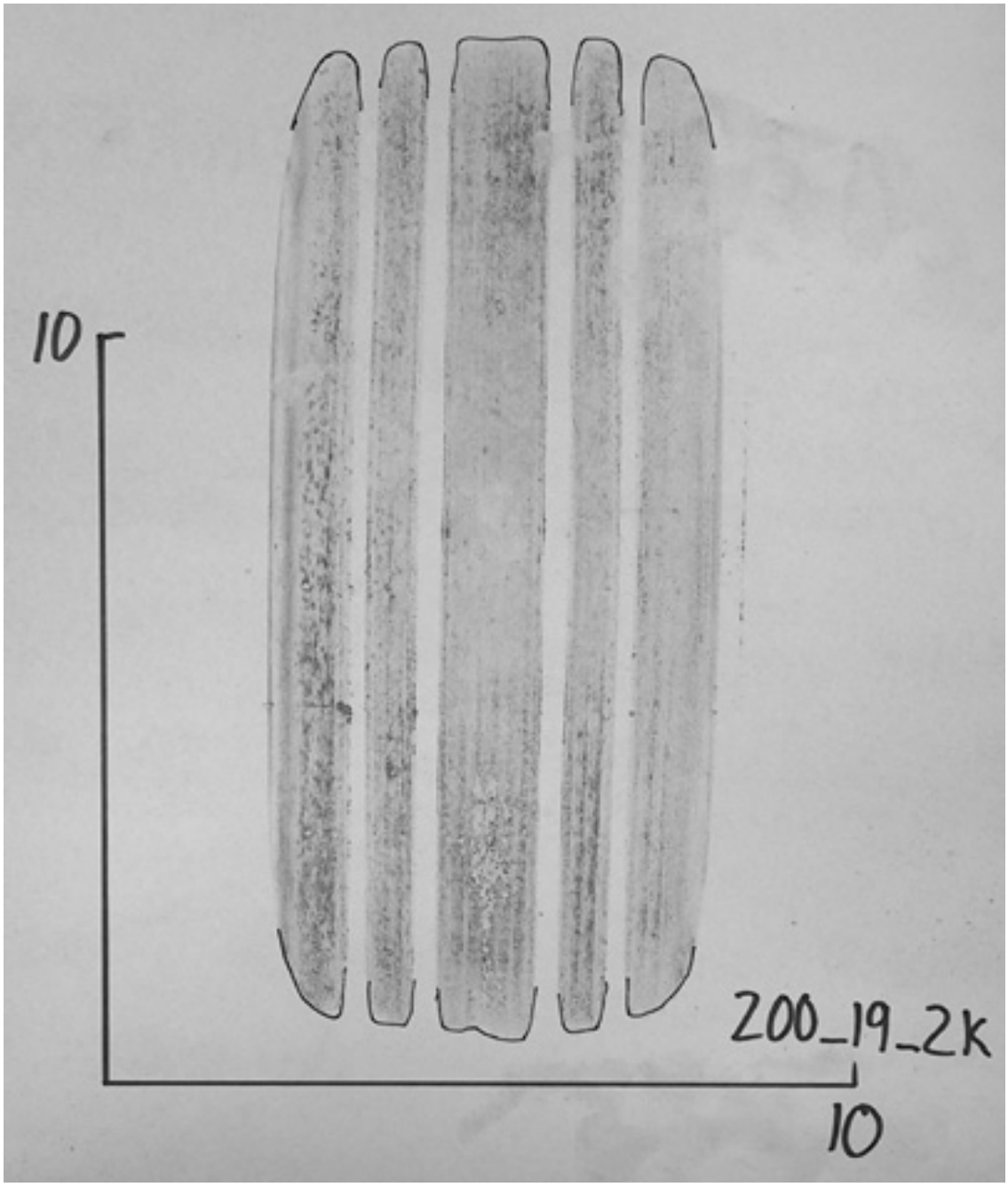


Figure A8. 737 nose tire; 200 psi; 19200 lb.

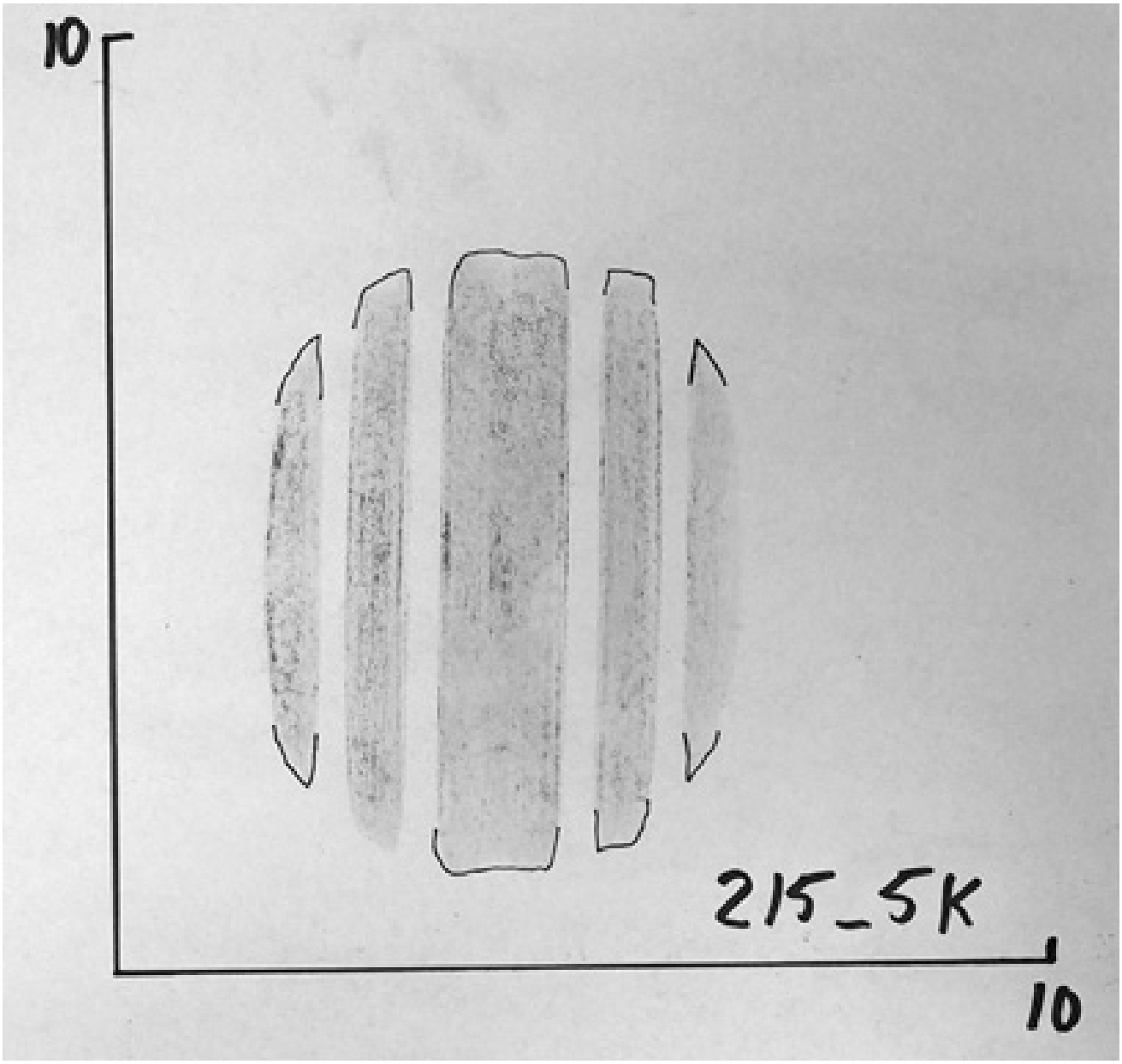


Figure A9. 737 nose tire; 215 psi; 5000 lb.

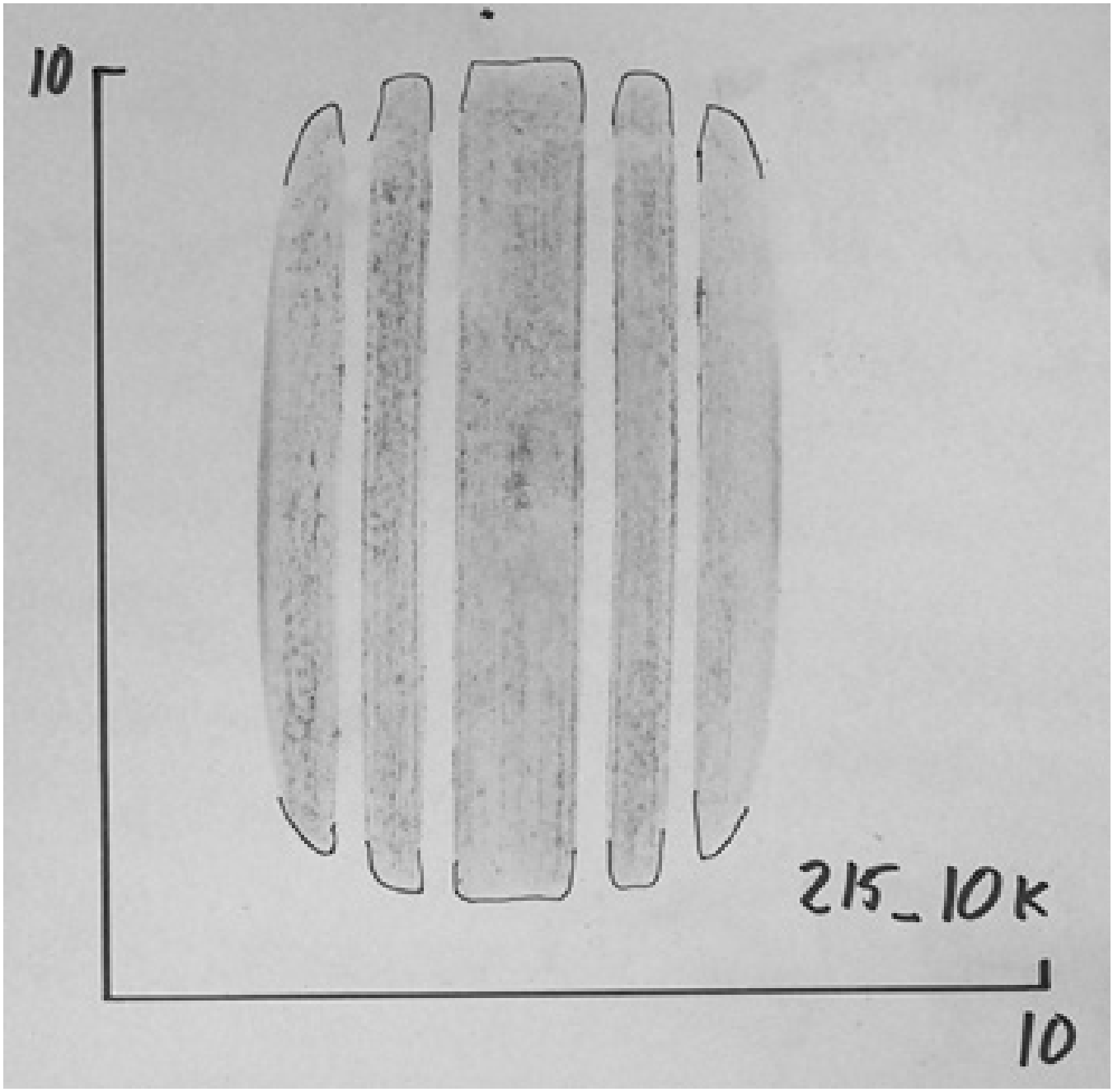


Figure A10. 737 nose tire; 215 psi; 10000 lb.

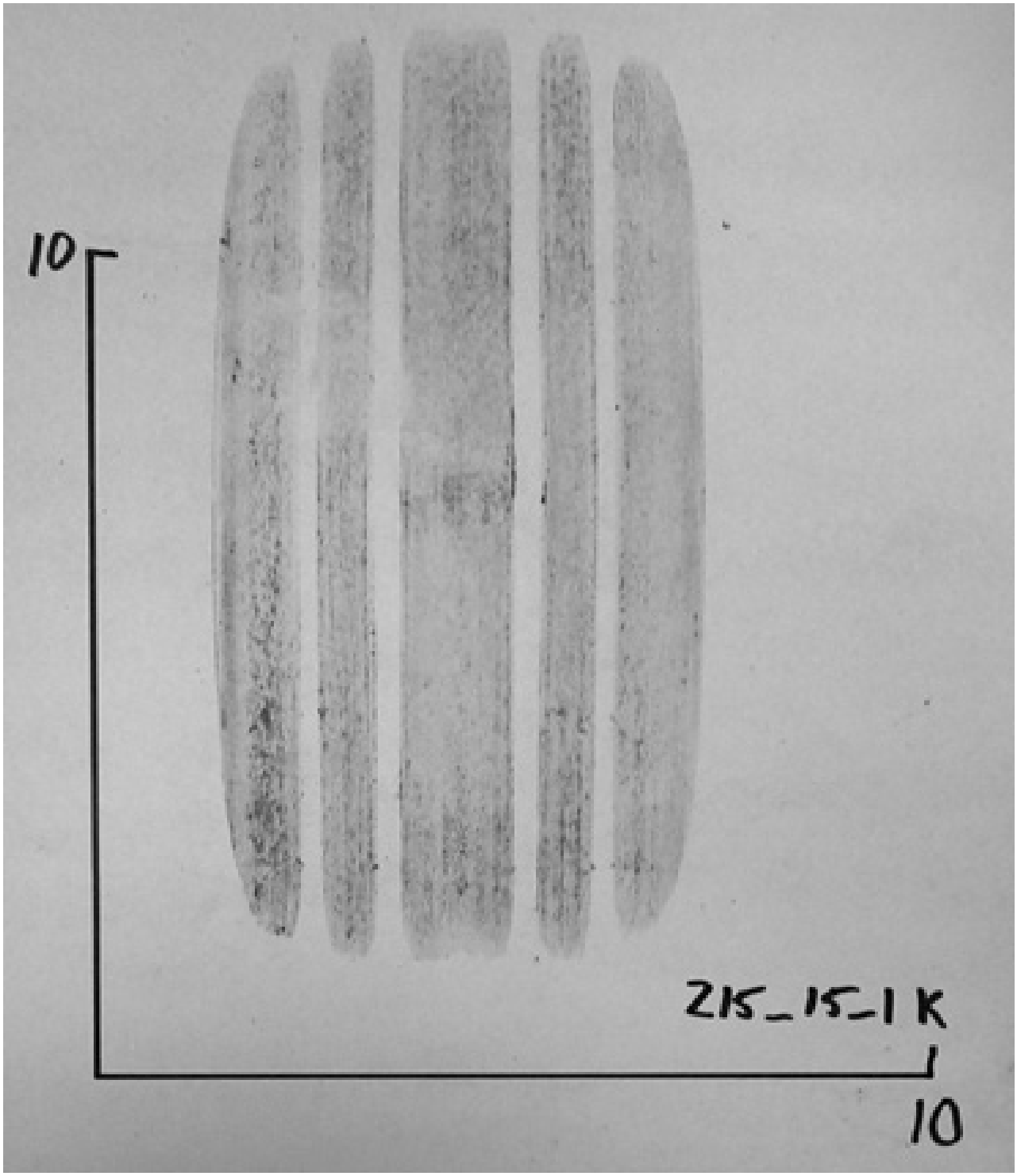


Figure A11. 737 nose tire; 215 psi; 15100 lb.

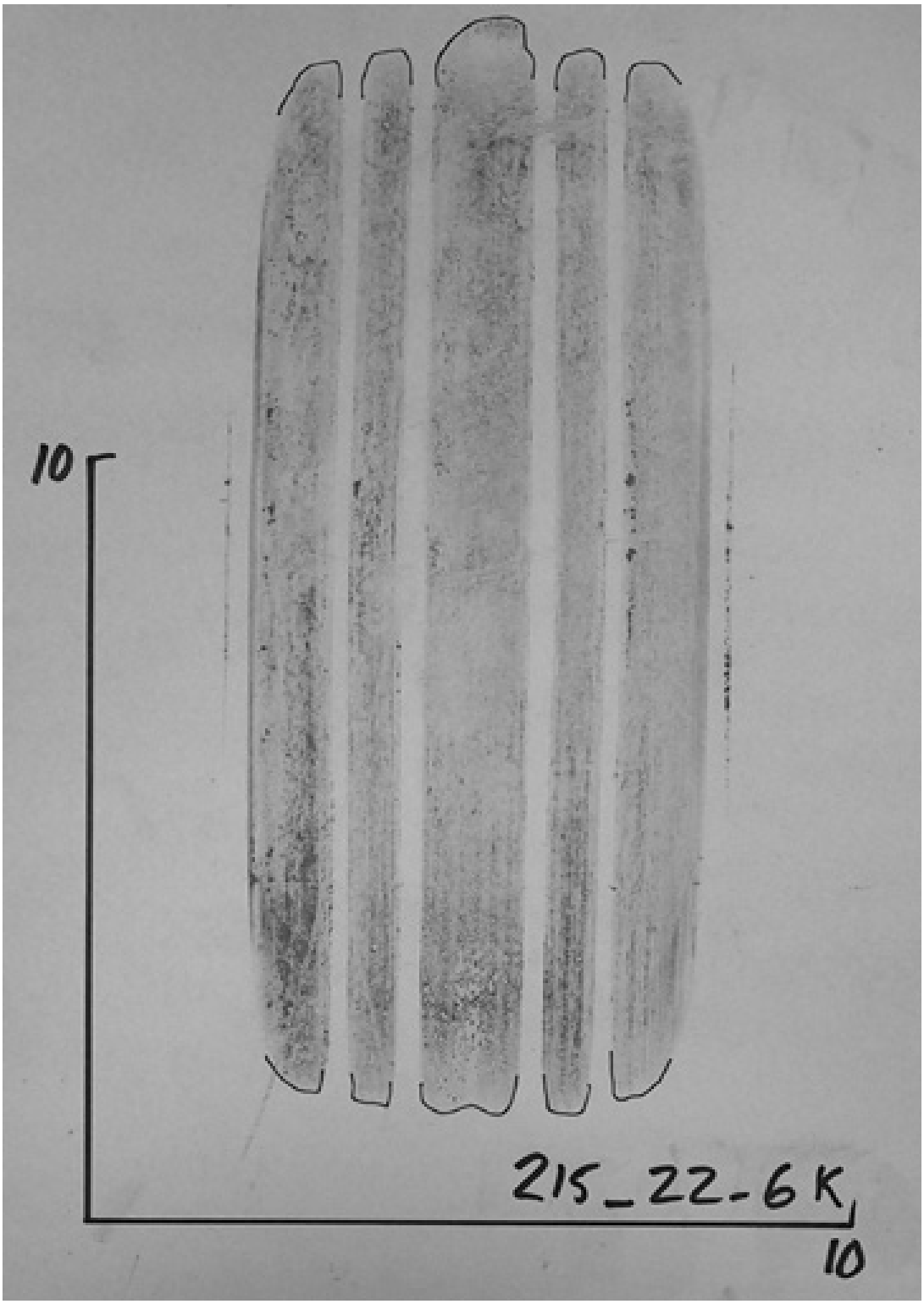


Figure A12. 737 nose tire; 215 psi; 22600 lb.

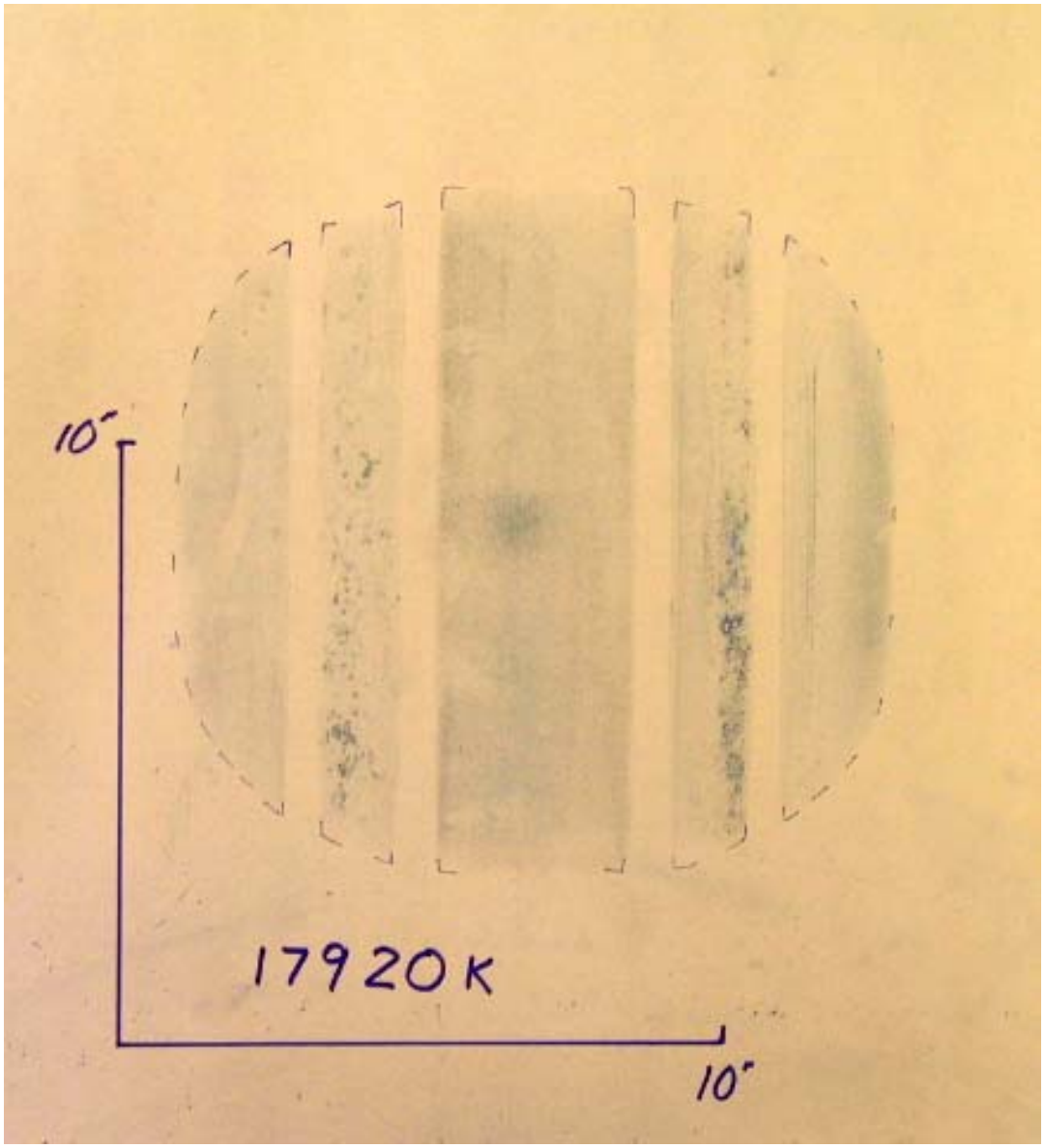


Figure A13. 777 nose tire; 179 psi; 20000 lb.

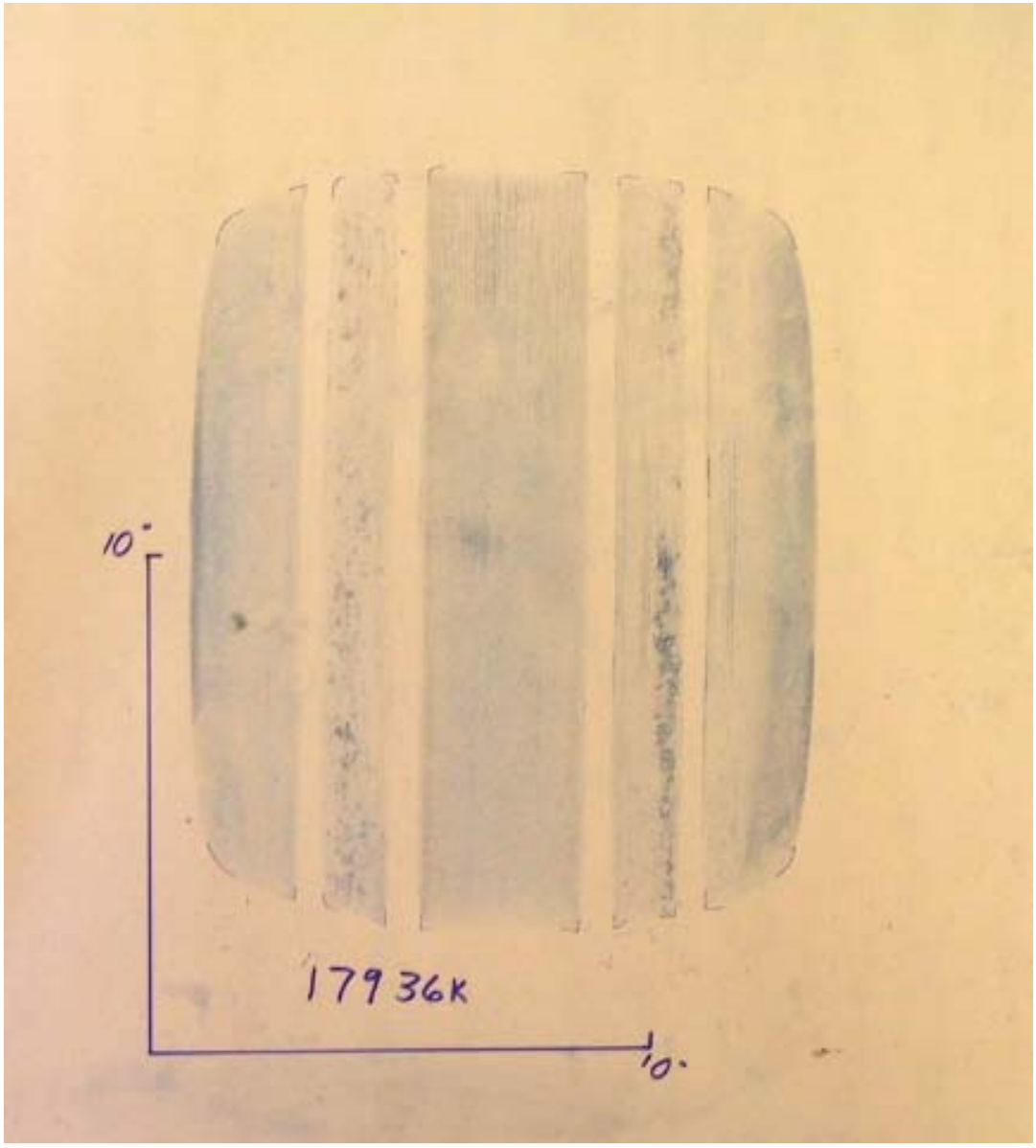


Figure A14. 777 nose tire; 179 psi; 36000 lb.

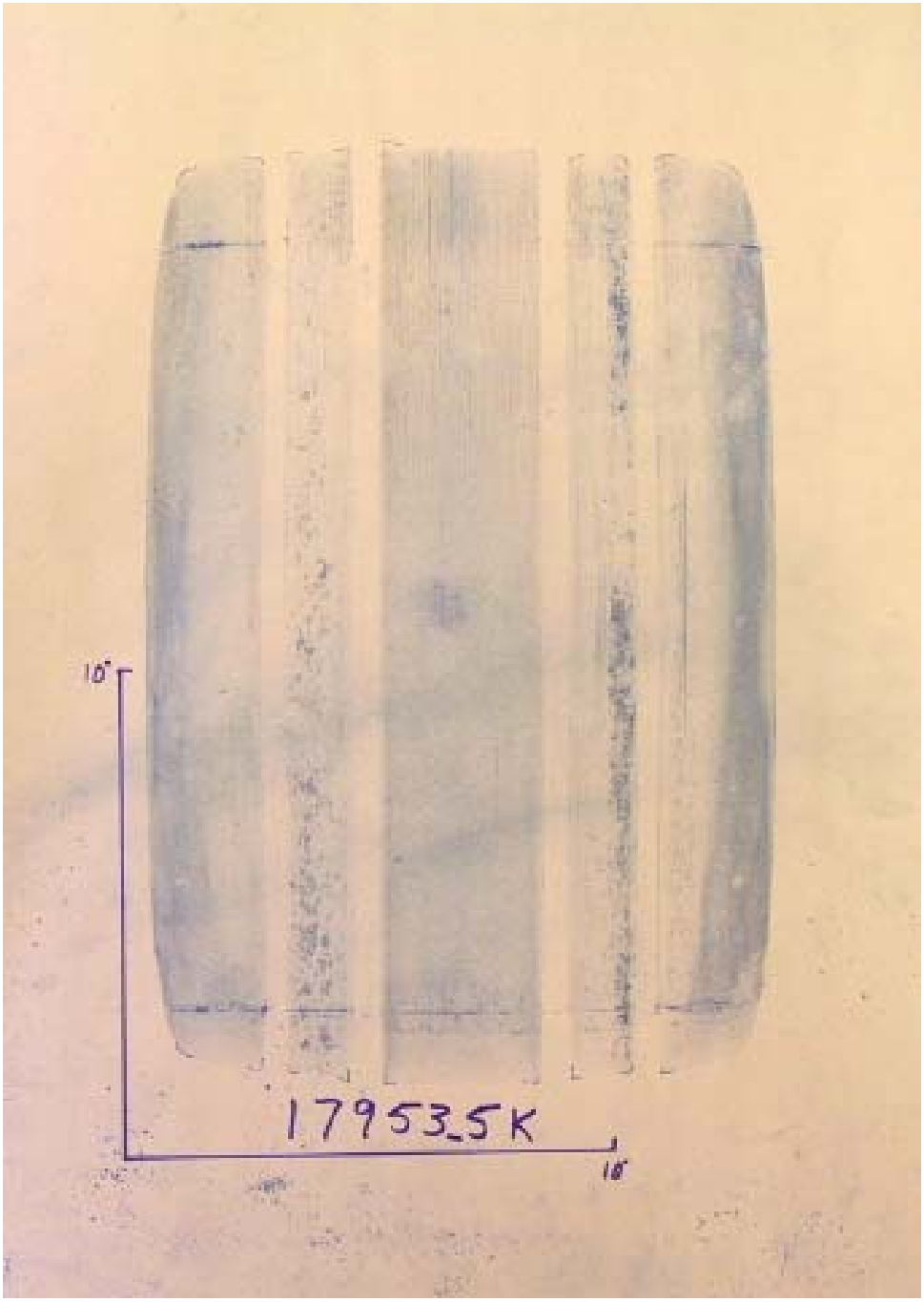


Figure A15. 777 nose tire; 179 psi; 535000 lb.

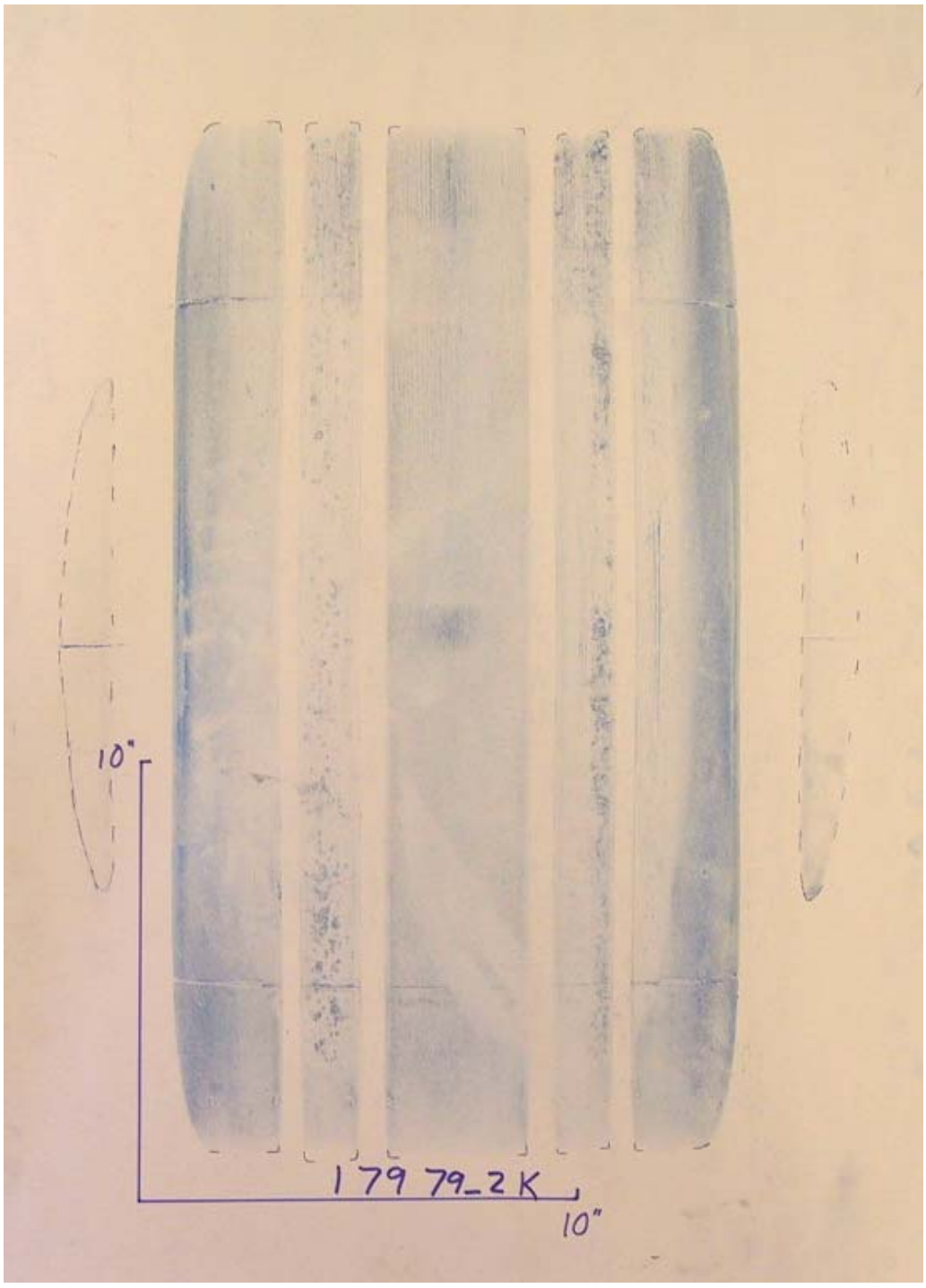


Figure A16. 777 nose tire; 179 psi; 79200 lb.

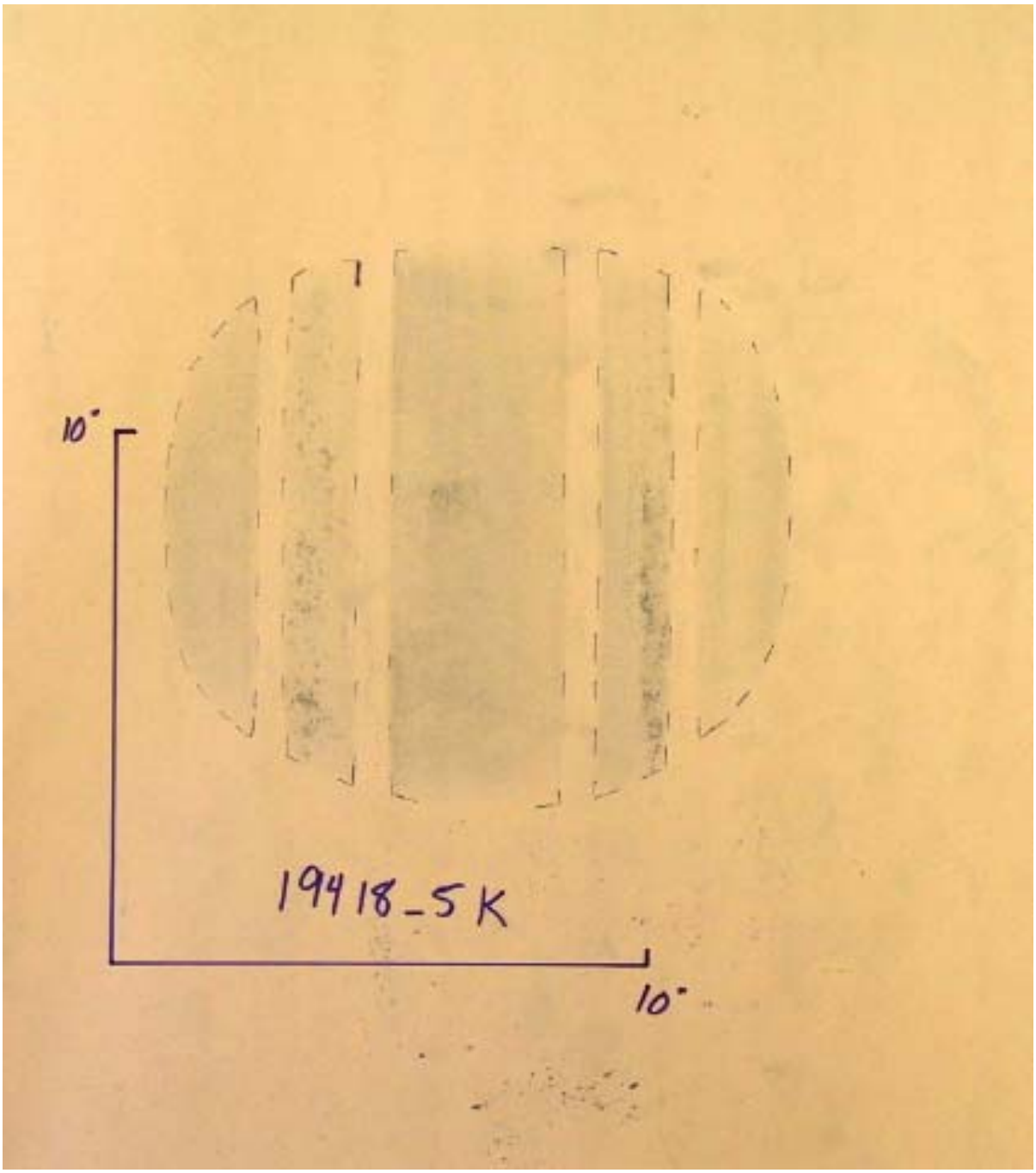


Figure A17. 777 nose tire; 194 psi; 18500 lb.

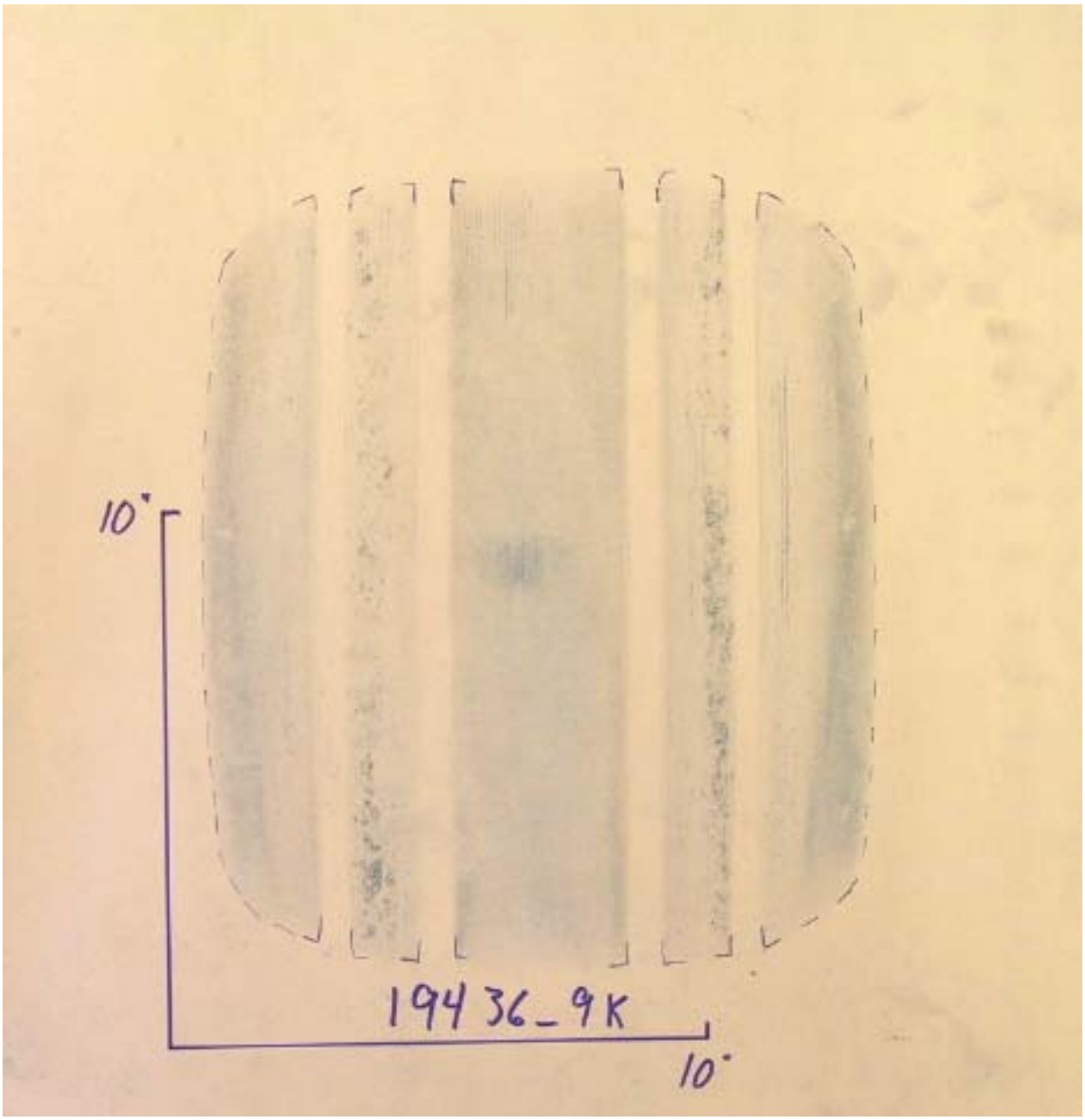


Figure A18. 777 nose tire; 194 psi; 36900 lb.

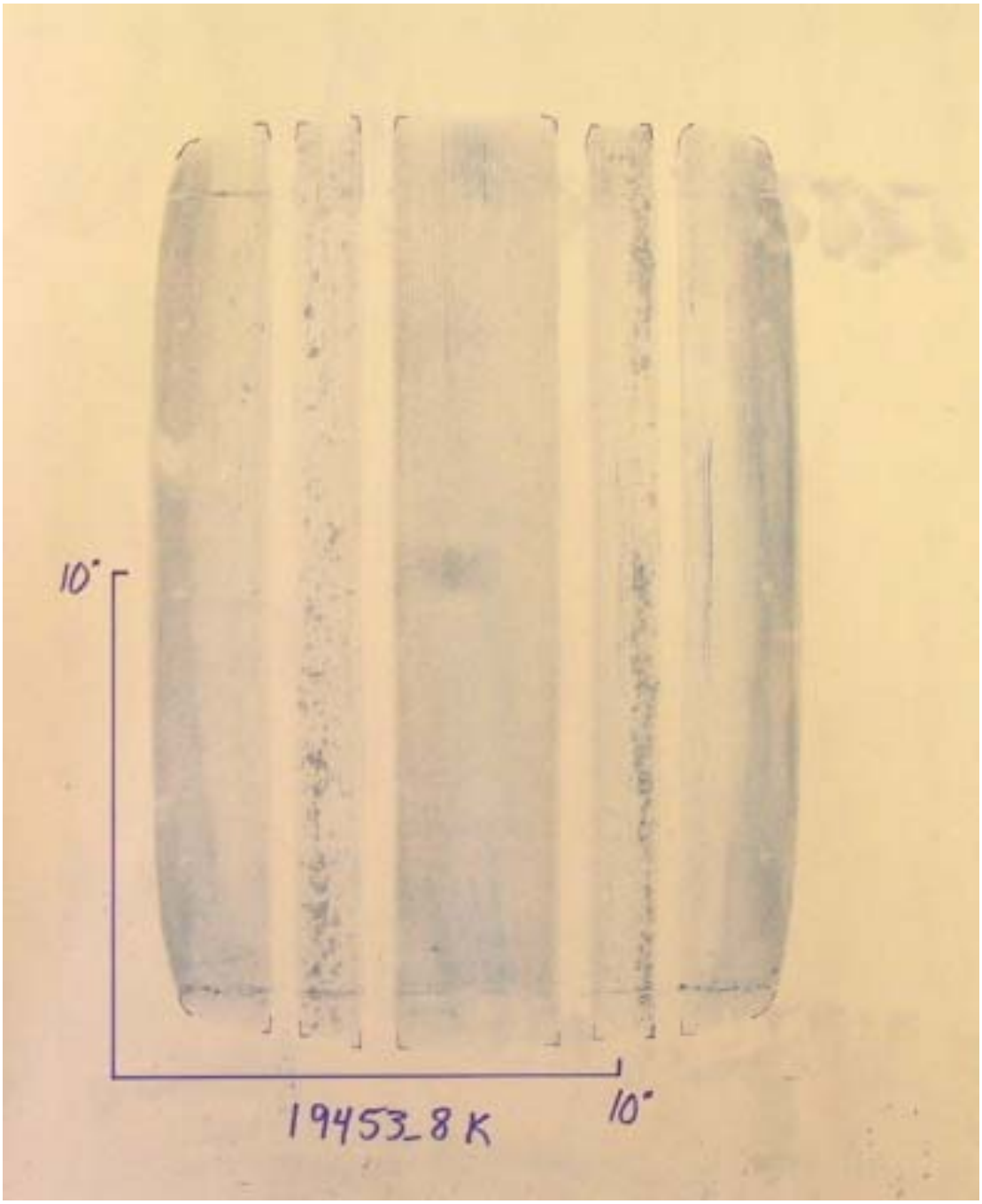


Figure A19. 777 nose tire; 194 psi; 53800 lb.

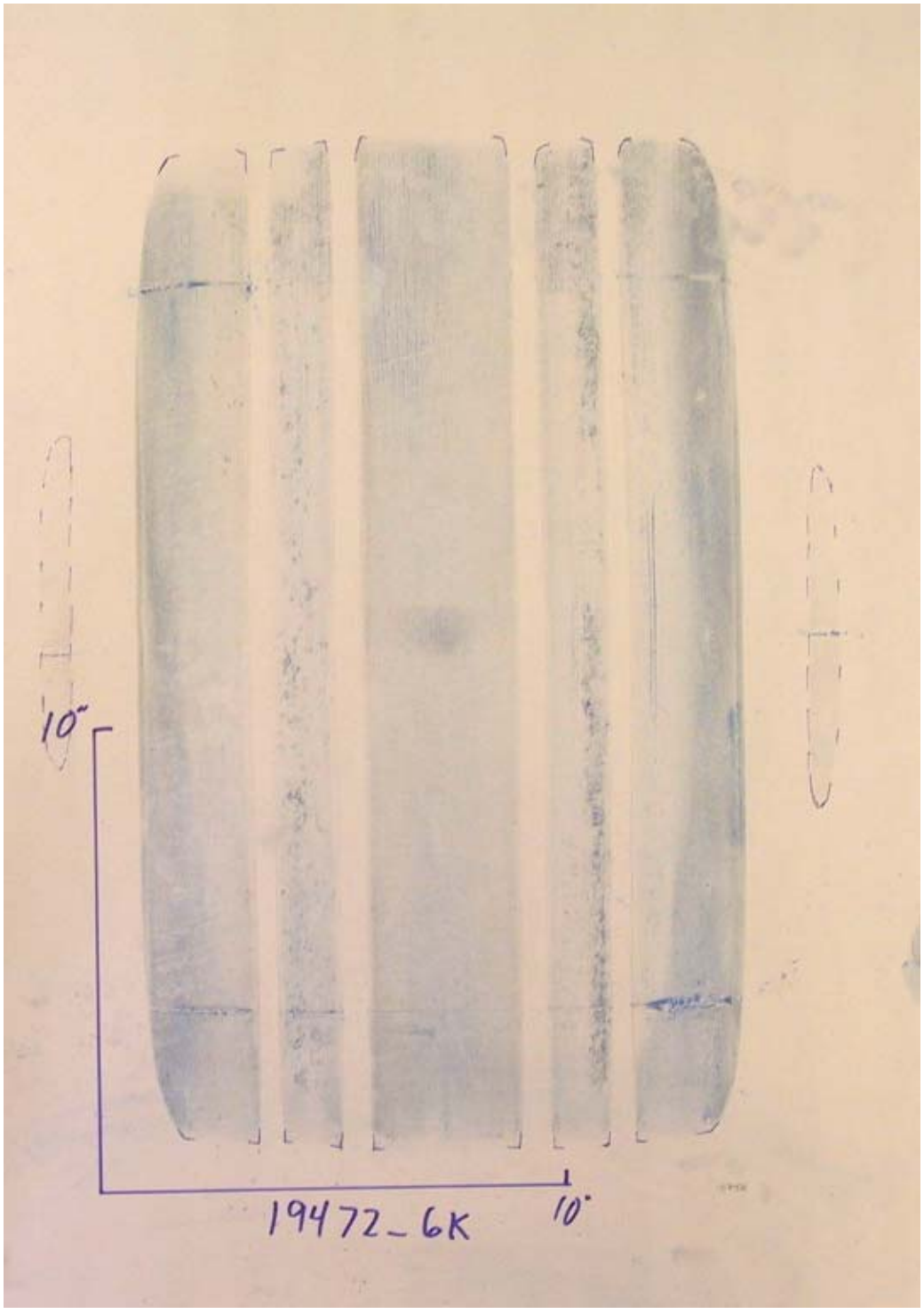


Figure A20. 777 nose tire; 194 psi; 72600 lb.

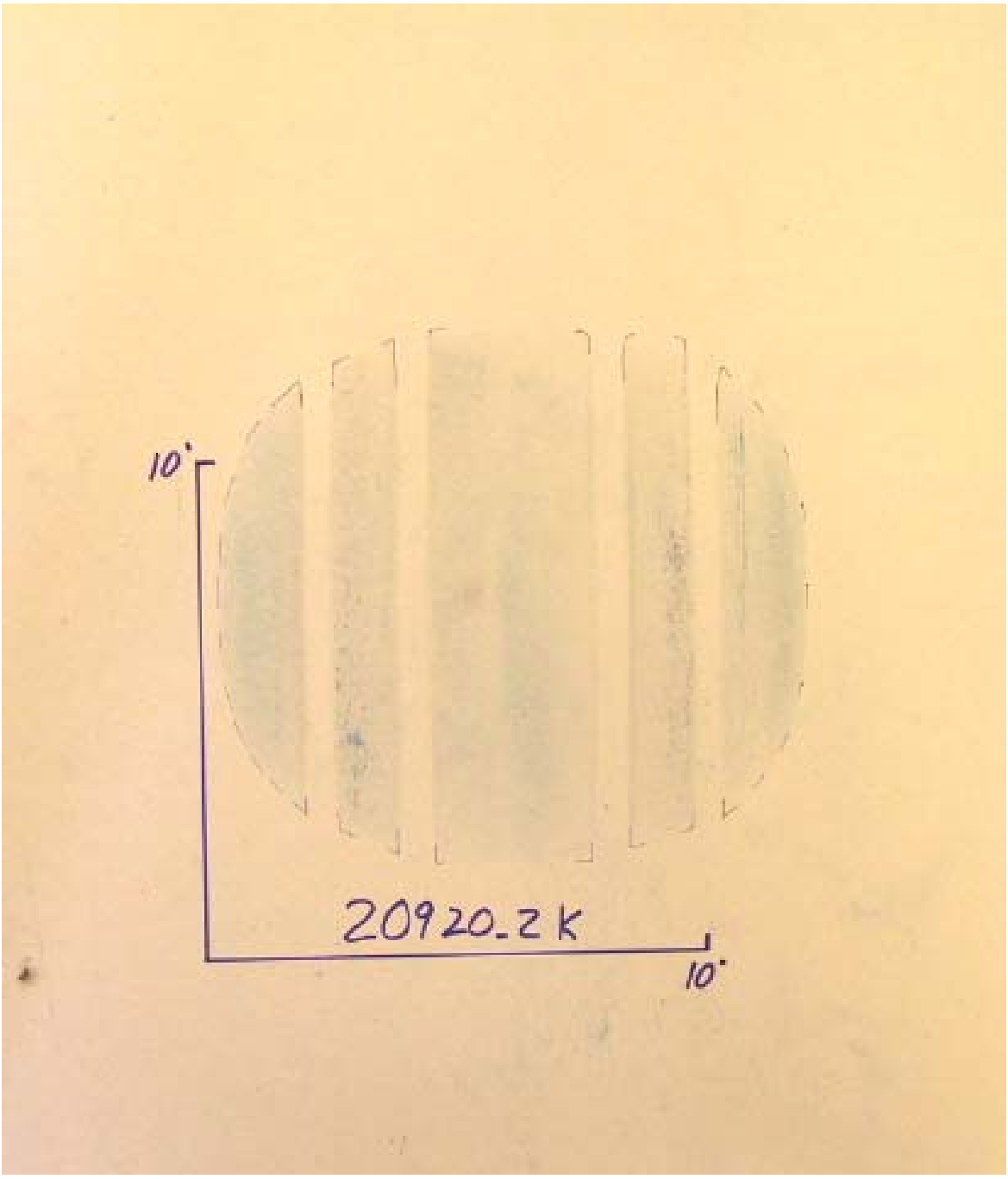


Figure A21. 777 nose tire; 209 psi; 20200 lb.

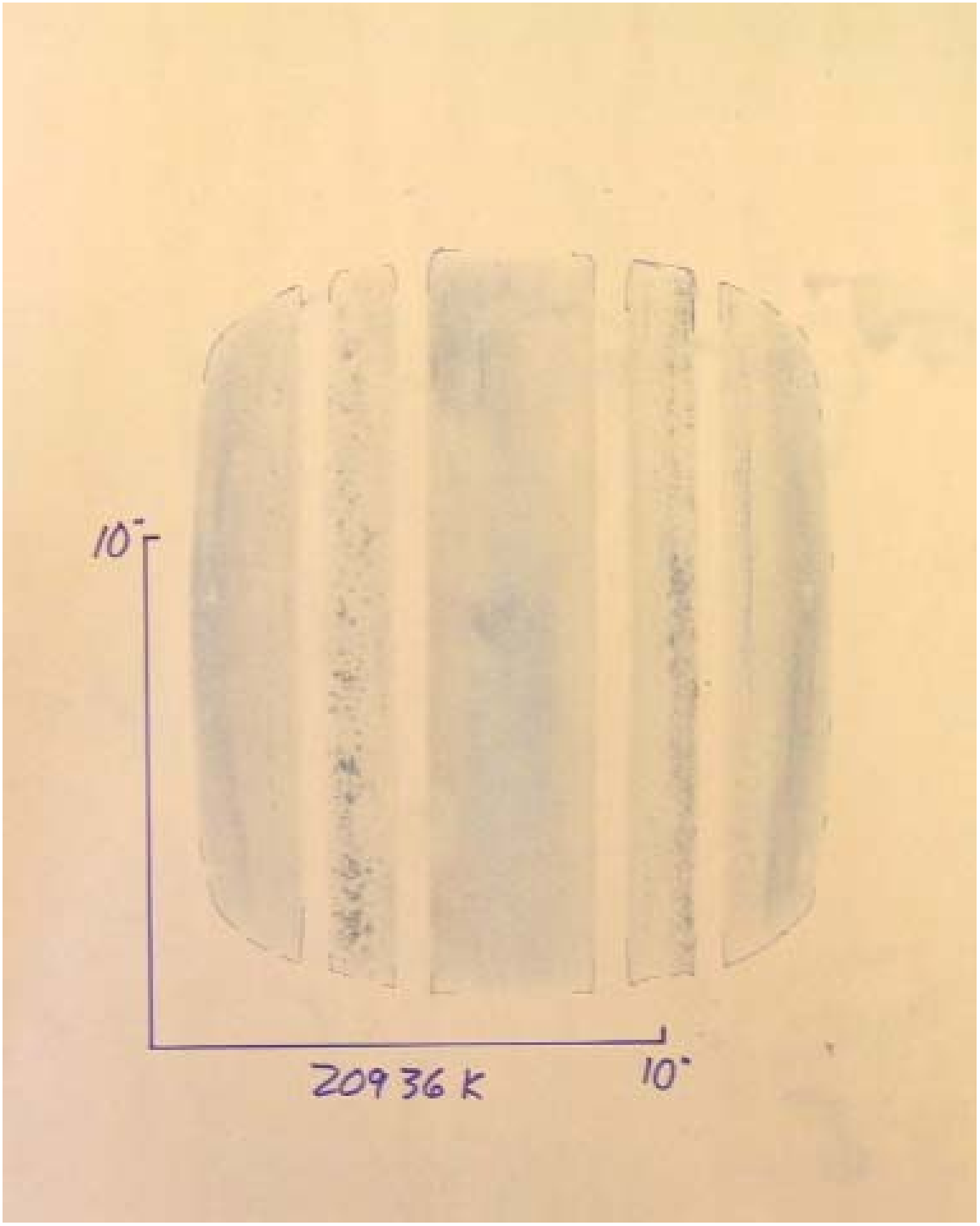


Figure A22. 777 nose tire; 209 psi; 36000 lb.

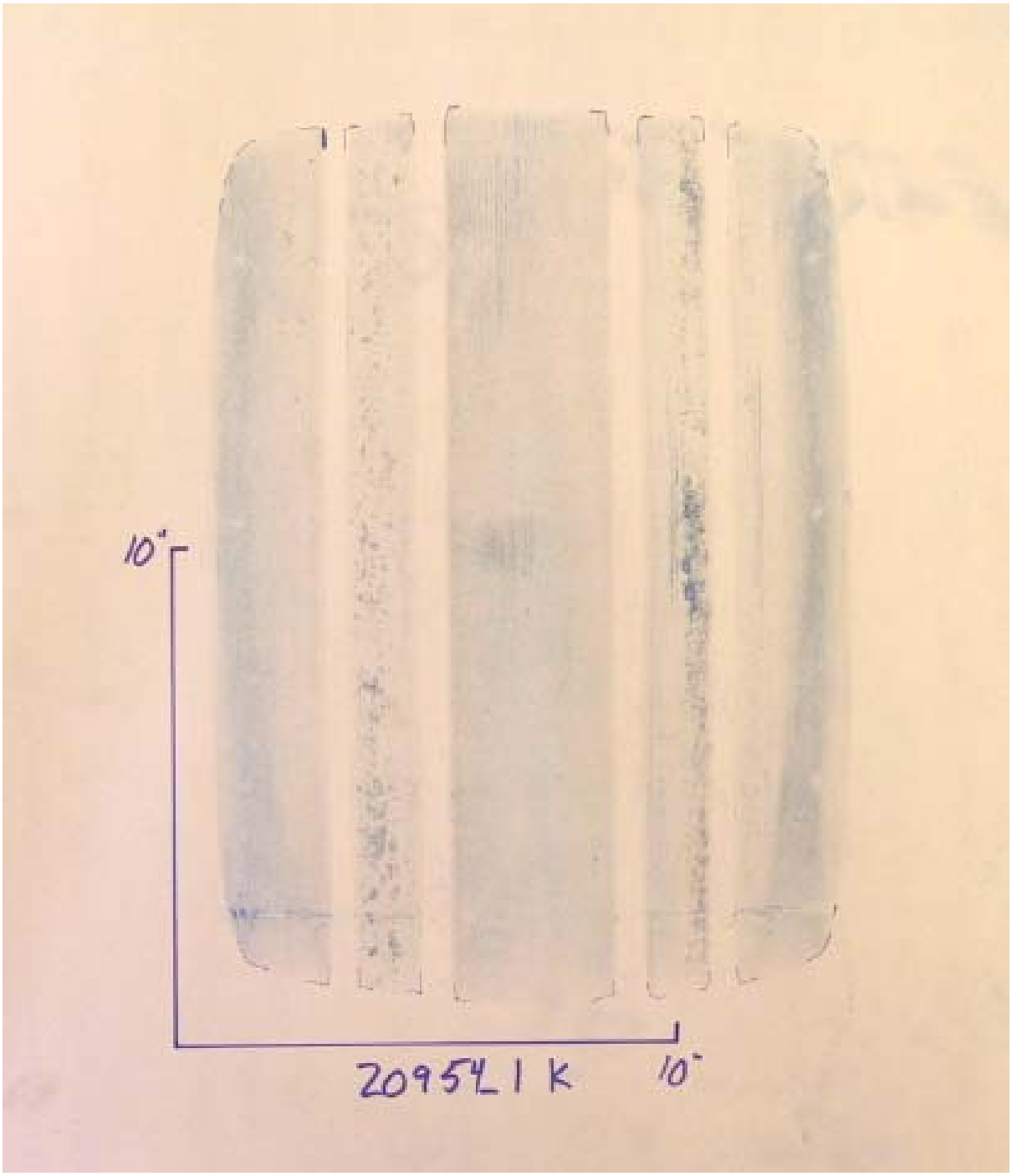


Figure A23. 777 nose tire; 209 psi; 54100 lb.

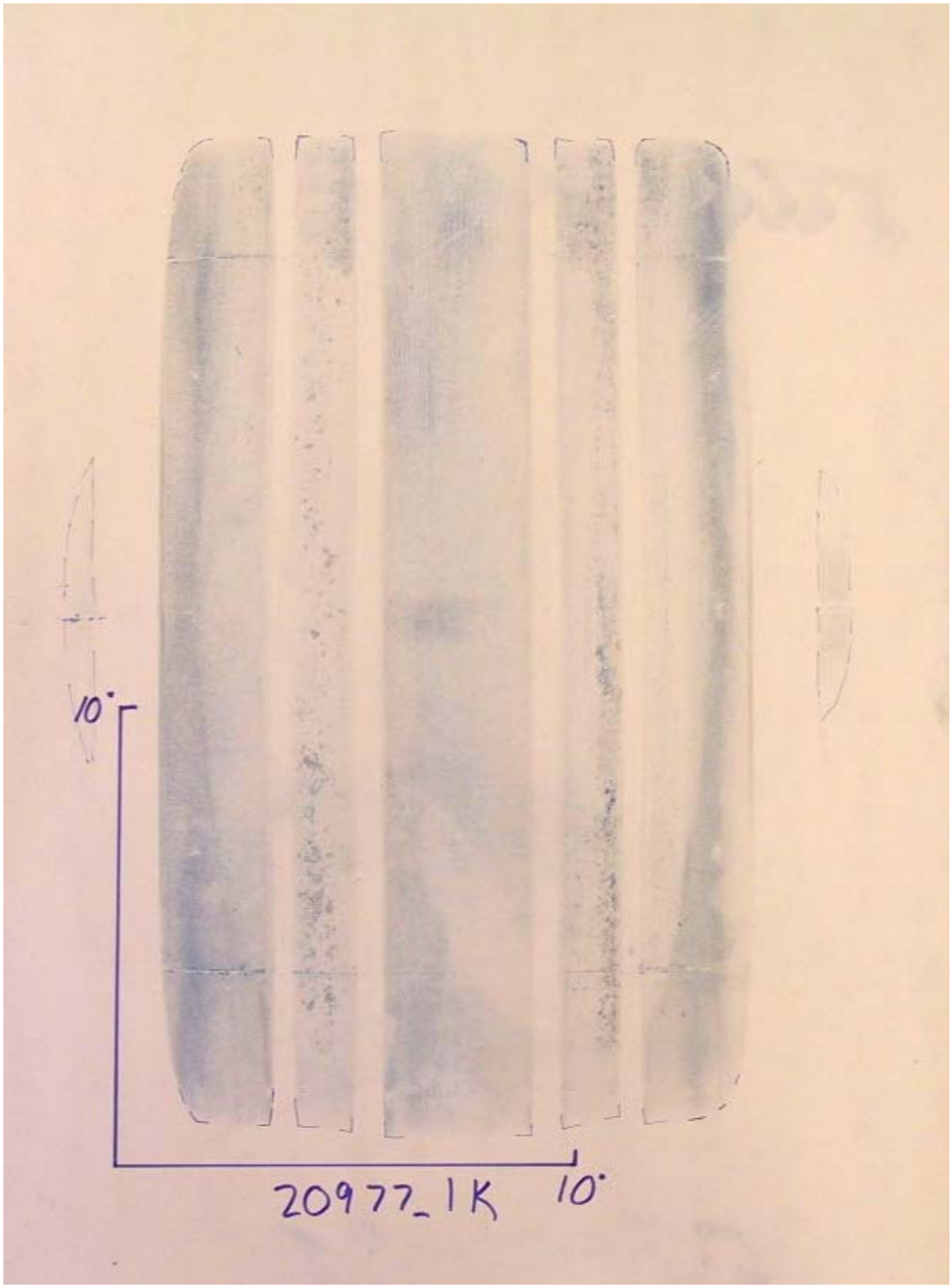


Figure A24. 777 nose tire; 209 psi; 77100 lb.

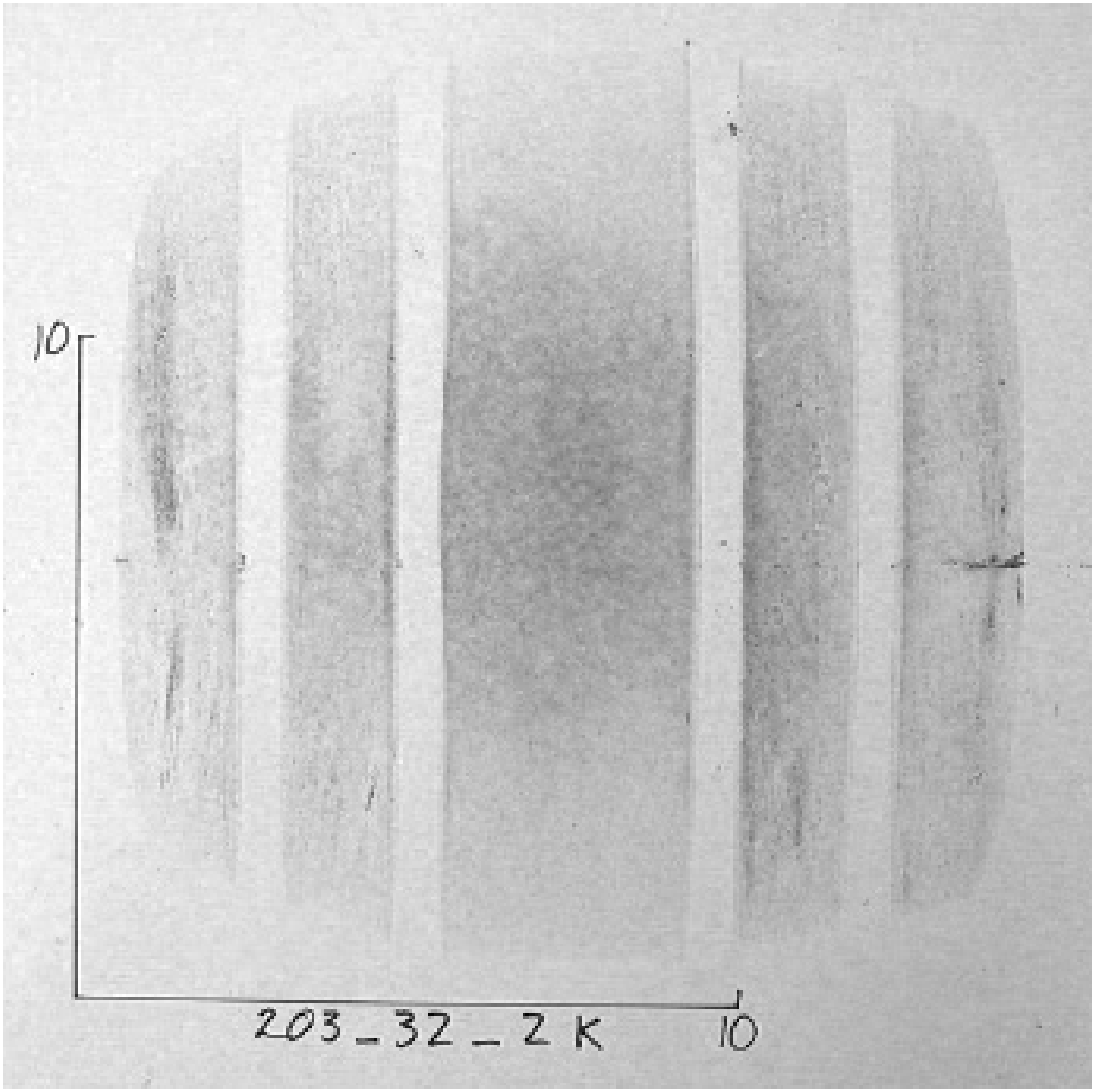


Figure A25. 777 main tire; 203 psi; 32200 lb.

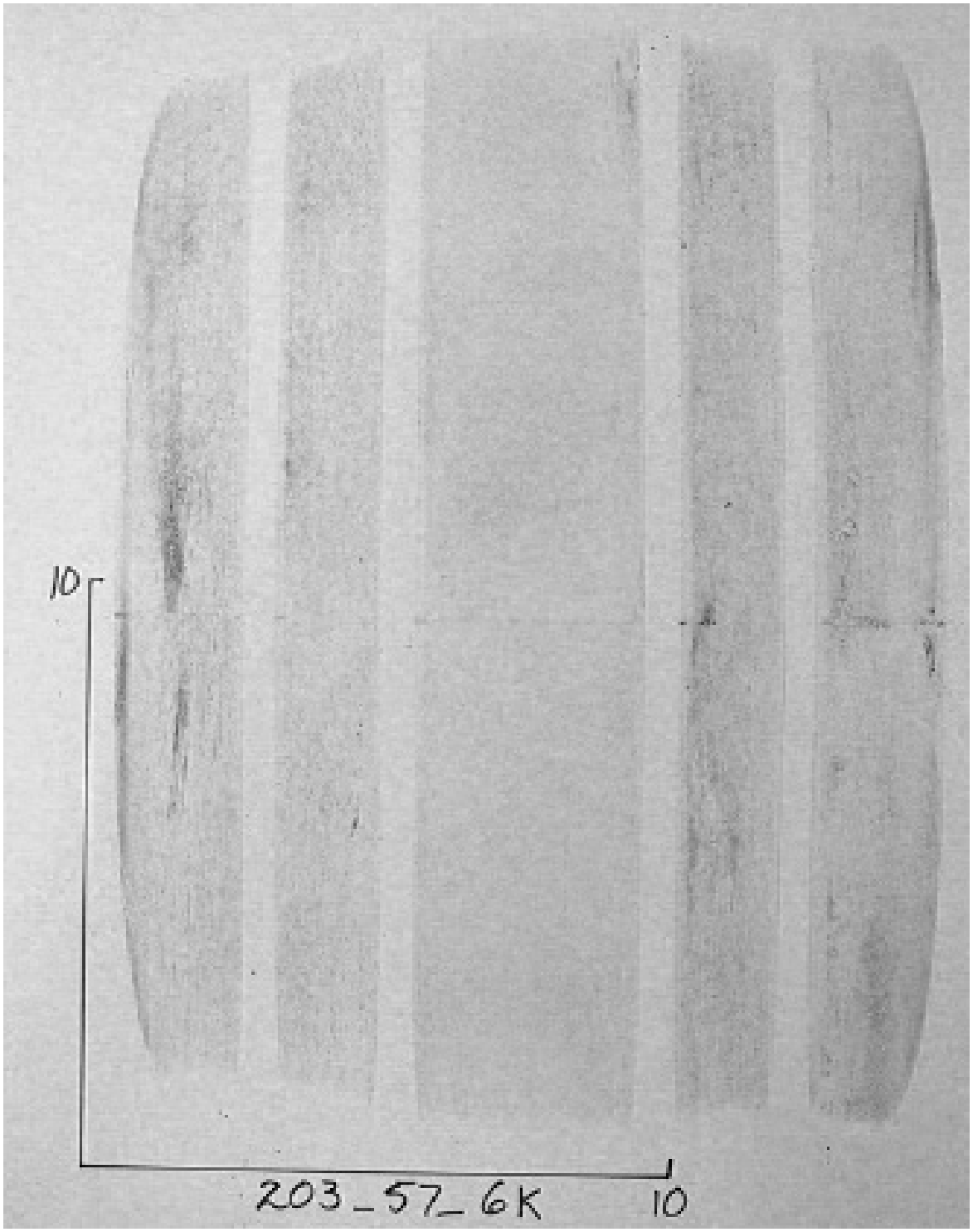


Figure A26. 777 main tire; 203 psi; 57600 lb.

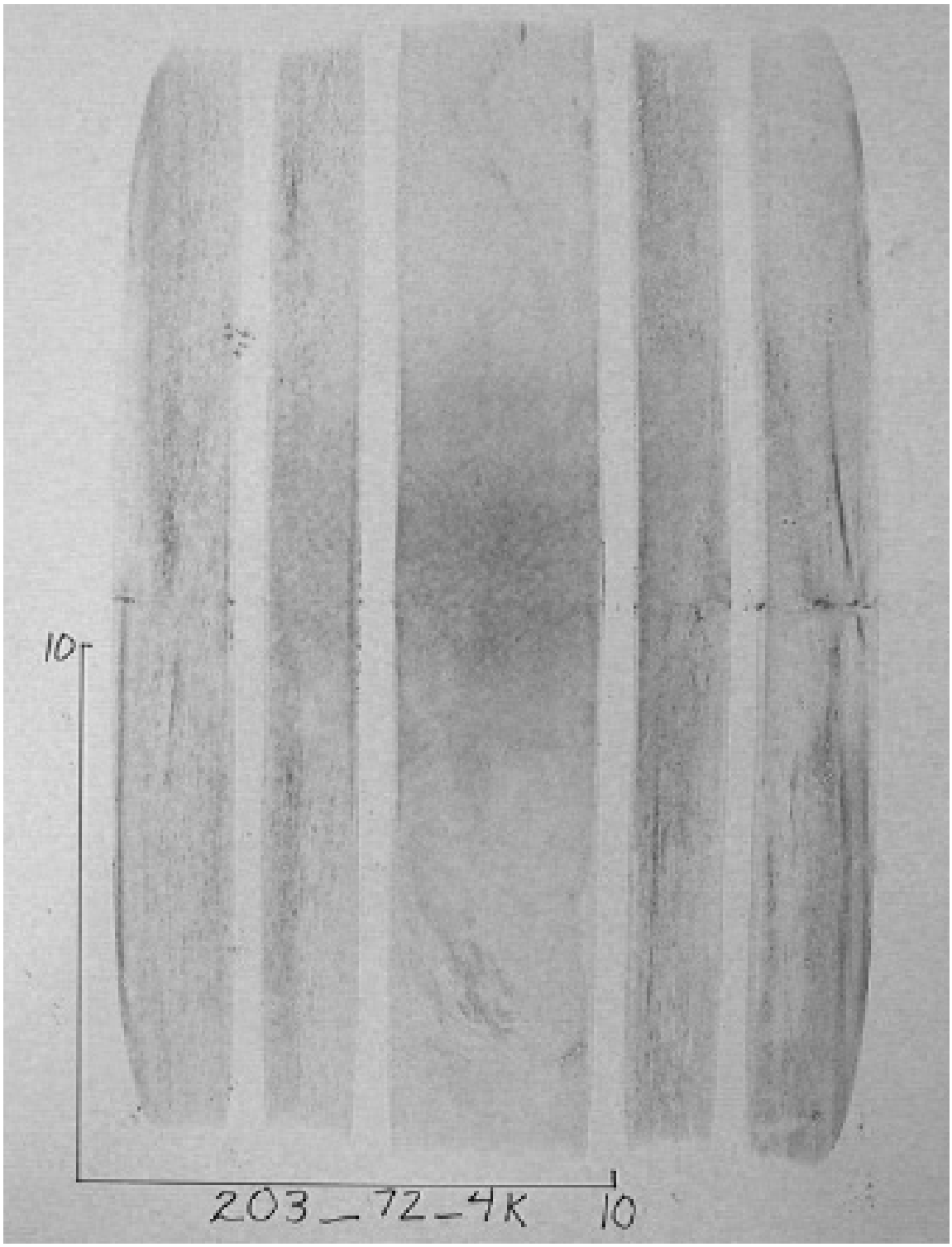


Figure A27. 777 main tire; 203 psi; 72400 lb.

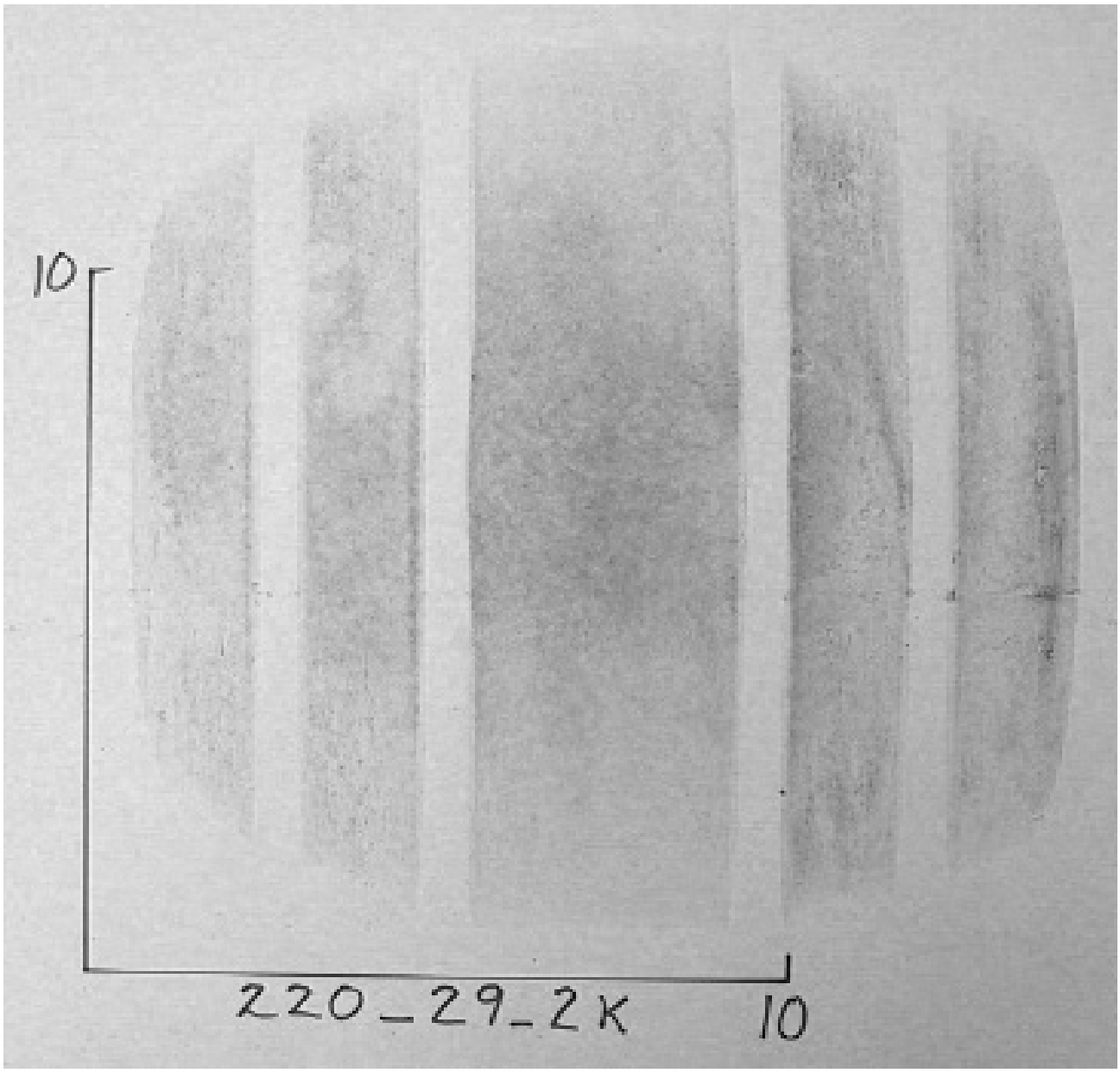


Figure A28. 777 main tire; 220 psi; 29200 lb.

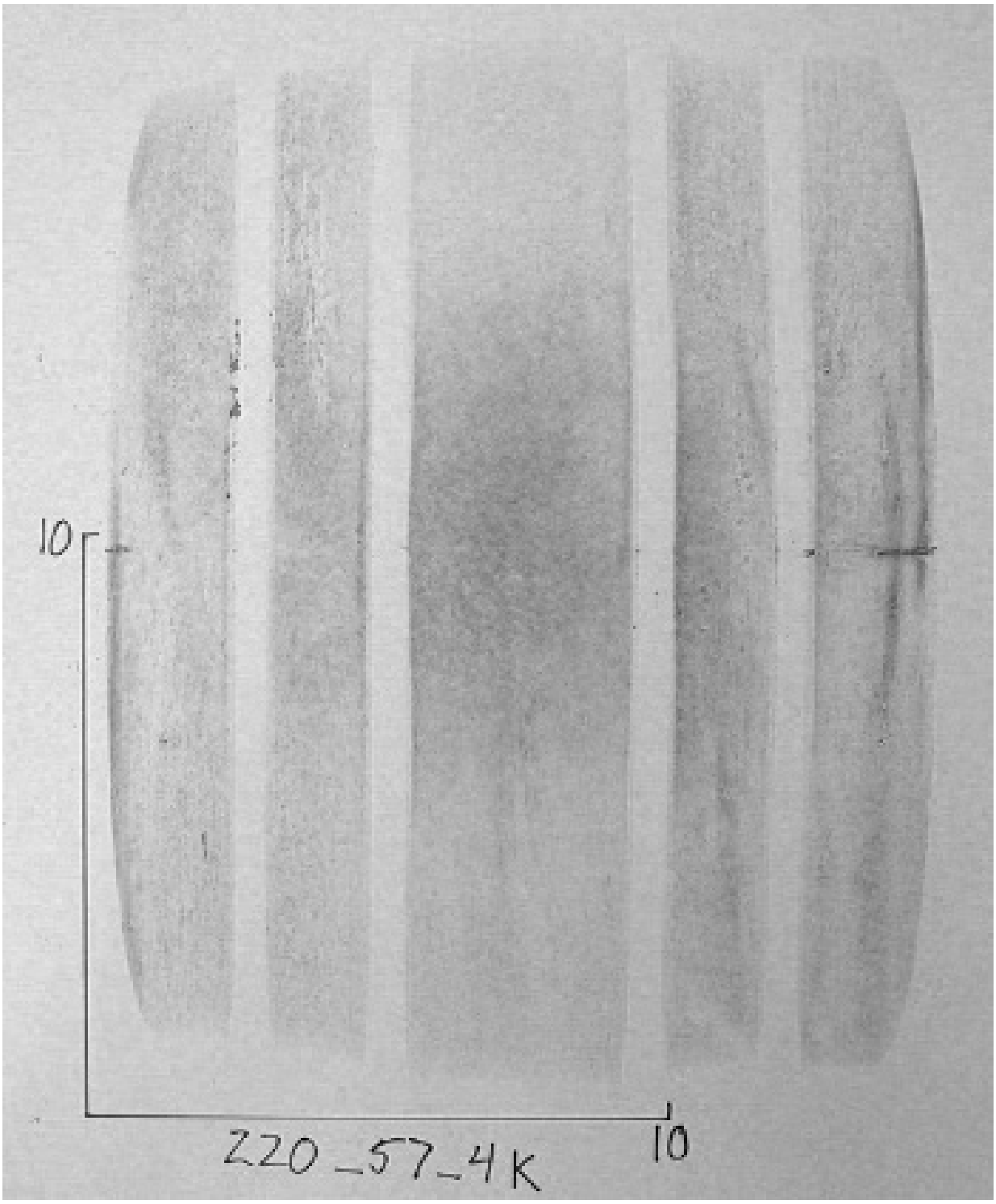


Figure A29. 777 main tire; 220 psi; 57400 lb.

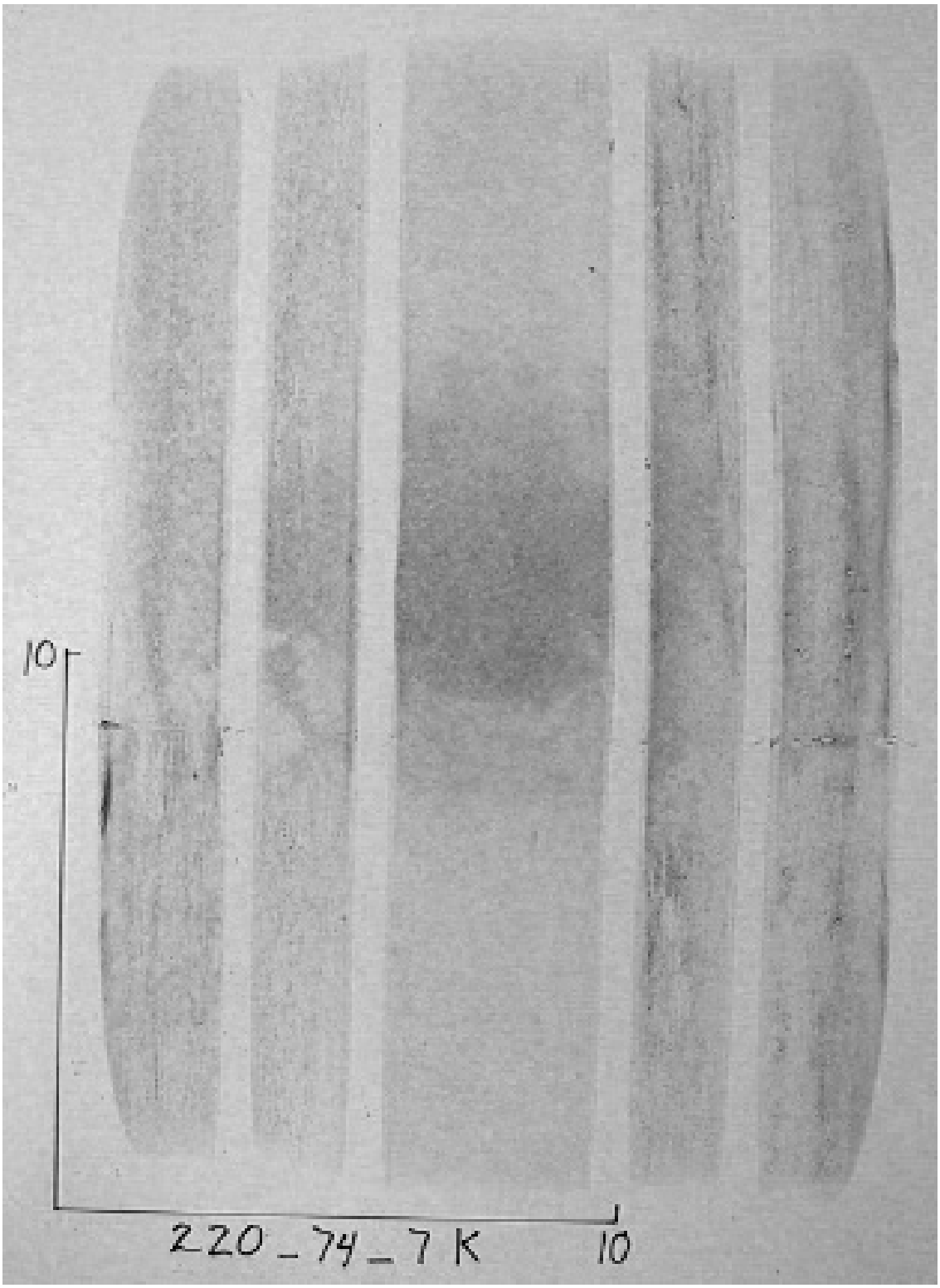


Figure A30. 777 main tire; 220 psi; 74700 lb.

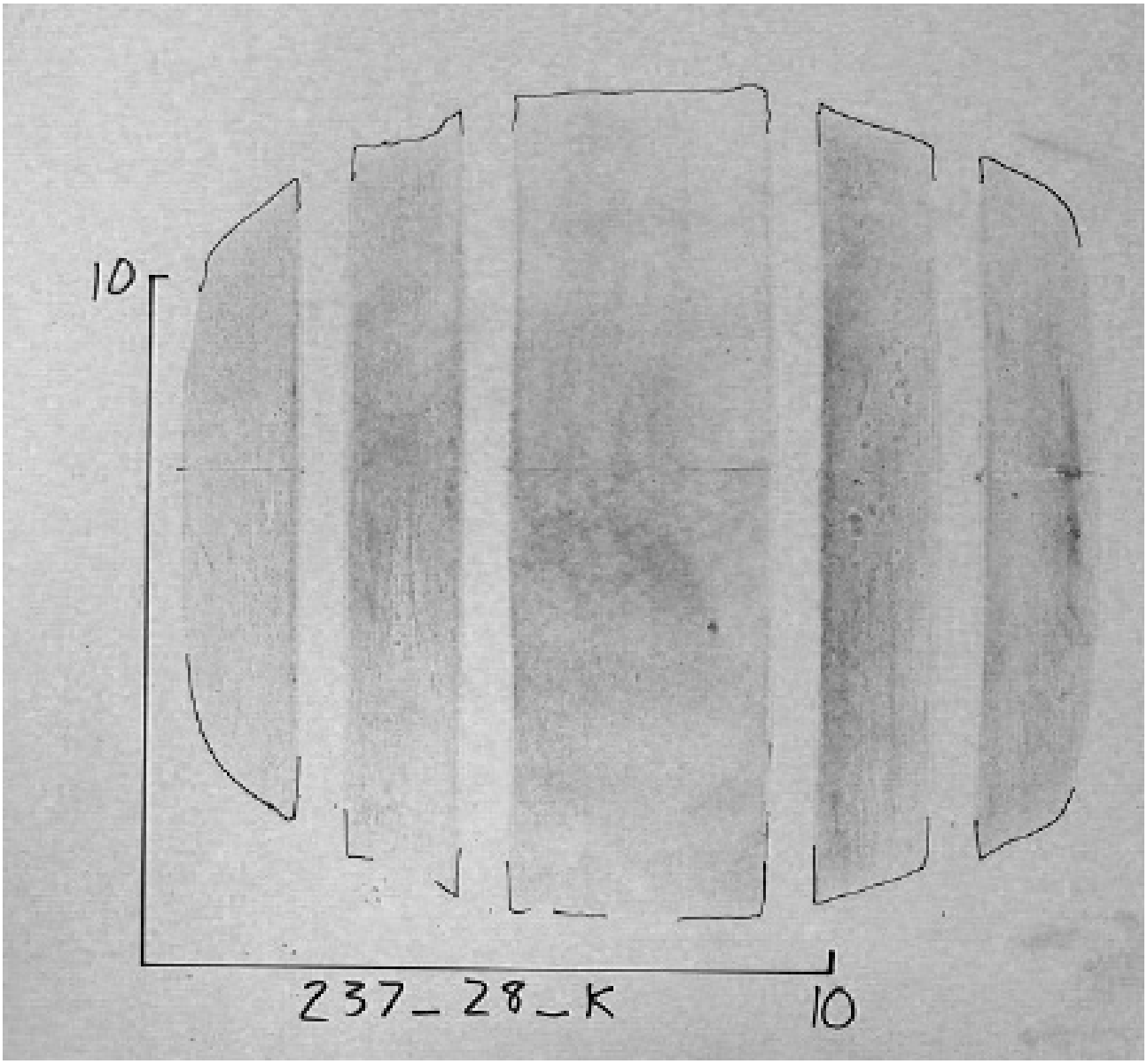


Figure A31. 777 main tire; 237 psi; 28000 lb.

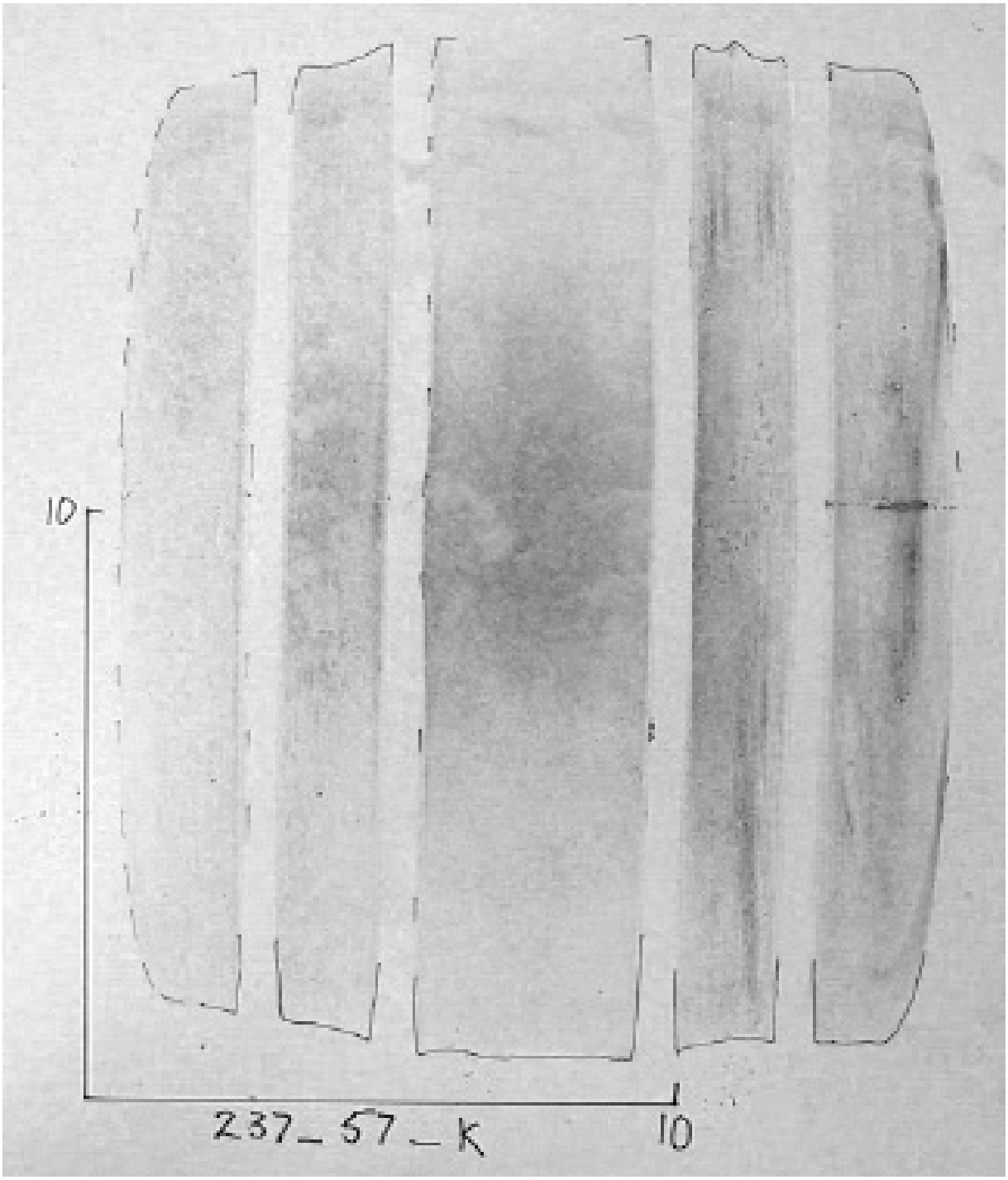


Figure A32. 777 main tire; 237 psi; 57000 lb.

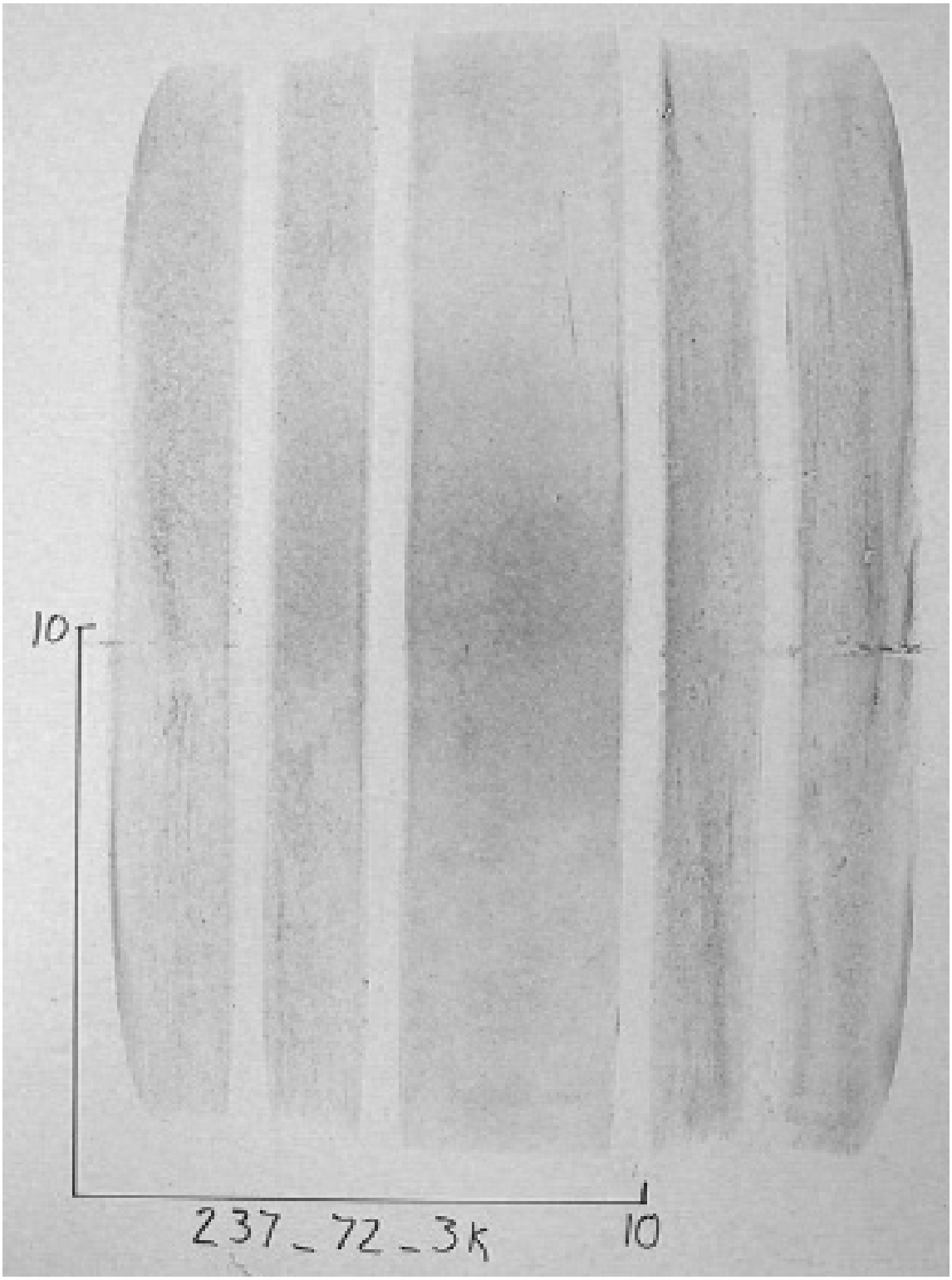


Figure A33. 777 main tire; 237 psi; 72300 lb.

## References


1. Smiley, Robert F.; and Horne, Walter B.: *Mechanical Properties of Pneumatic Tires With Special Reference to Modern Aircraft Tires*. NASA TR R-64, 1960
2. Davis, Pamela A.; Stubbs, Sandy M.; and Tanner, John A.*: Langley Aircraft Landing Dynamics Facility*. NASA RP 1189, October 1987
3. Leland, Trafford J. W.; Yager, Thomas J.; and Joyner, Upshur T.*: Effects of Pavement Texture on Wet-Runway Braking Performance*. NASA TN D-4323, 1968
4. Horne, Walter B.; Yager, Thomas J.; and Ivey, Don L.*: Recent Studies to Investigate Effects of Tire Footprint Aspect Ratio on Dynamic Hydroplaning Speed*. Presented at the Joint ASTM E-17/F-9 Symposium on Tire/Pavement Interface, Columbus, OH, June 5-6, 1985
5. Clark, Samuel K., ed.: *Mechanics of Pneumatic Tires*. 2nd ed. U.S. Department of Transportation, National Highway Safety Administration
6. Daugherty, Robert H.; Stubbs, Sandy, M.; and Robinson, Martha P.*: Cornering Characteristics of the Main-Gear Tire of the Space Shuttle Orbiter*. NASA TP 2790, March 1988
7. Vogler, William A.; and Tanner, John A.: *Cornering Characteristics of the Nose-Gear Tire of the Space Shuttle Orbiter*. NASA TP 1917, October 1981

Table 1. 737 Nose Tire Test Matrix and Results

**737 Nose Tire Testing**

**R-64 Update**

***ALDF Test Matrix***

| Run # | Date | Track Run # | Nominal Speed, kts | Nominal Load, lb | Tire Press | Yaw Angle | Surface Cond | Footprint Width | Axle Height inches | Carriage Dist, feet | Carriage Time,sec | Carriage Speed,fps | Tire Revs | Time for Tire Revs | Dist trav during tire revs | Rolling Radius, in | Vert Load, lbs | Drag Load, lbs | Side Load, lbs | Multiple of Rated Load |
|---|---|---|---|---|---|---|---|---|---|---|---|---|---|---|---|---|---|---|---|---|
| 1 | 22-Jul | 494 | 100 | 5000 | 215 | 0 | Dry | 5.35 | 12.76 | 100 | 0.686 | 145.77 | 10 | 0.469 | 68.37 | 13.0572 | 7350 | -200 | -310 | 0.761658 |
| 2 | 22-Jul | 495 | 100 | 10000 | 215 | 0 | Dry | 5.56 | 12.28 | 100 | 0.678 | 147.49 | 10 | 0.463 | 68.29 | 13.04225 | 10510 | -270 | -470 | 1.0891192 |
| 3 | 22-Jul | 496 | 100 | 16000 | 215 | 0 | Dry | 5.72 | 11.91 | 100 | 0.675 | 148.15 | 10 | 0.46 | 68.15 | 13.01534 | 12490 | -240 | -730 | 1.2943005 |
| 4 | 23-Jul | 497 | 100 | 5000 | 200 | 0 | Dry | 5.27 | 12.91 | 100 | 0.666 | 150.15 | 10 | 0.457 | 68.62 | 13.10519 | 6000 | 70 | -90 | 0.6217617 |
| 5 | 23-Jul | 498 | 100 | 10000 | 200 | 0 | Dry | 5.49 | 12.52 | 100 | 0.662 | 151.06 | 10 | 0.455 | 68.73 | 13.12668 | 8730 | -30 | -180 | 0.9046632 |
| 6 | 23-Jul | 499 | 100 | 16000 | 200 | 0 | Dry | 5.67 | 12.54 | 100 | 0.675 | 148.15 | 10 | 0.457 | 67.70 | 12.93045 | 11550 | 0 | -470 | 1.1968912 |
| 7 | 23-Jul | 501 | 100 | 5000 | 185 | 0 | Dry | 5.22 | 12.91 | 100 | 0.656 | 152.44 | 10 | 0.45 | 68.60 | 13.10117 | 4590 | -60 | -70 | 0.4756477 |
| 8 | 23-Jul | 500 | 100 | 10000 | 185 | 0 | Dry | 5.54 | 12.4 | 100 | 0.669 | 149.48 | 10 | 0.455 | 68.01 | 12.98933 | 8660 | 0 | -170 | 0.8974093 |
| 9 | 26-Jul | 503 | 100 | 16000 | 185 | 0 | Dry | 5.63 | 11.54 | 100 | 0.675 | 148.15 | 10 | 0.457 | 67.70 | 12.93045 | 11110 | 50 | -460 | 1.1512953 |
| 10 | 29-Jul | 504 | 150 | 5000 | 215 | 0 | Dry | 4.83 | 13.42 | 100 | 0.46 | 217.39 | 10 | 0.318 | 69.13 | 13.20294 | 3670 | 70 | -140 | 0.3803109 |
| 11 | 29-Jul | 505 | 150 | 10000 | 215 | 0 | Dry | 5.43 | | 100 | 0.458 | 218.34 | 10 | 0.315 | 68.78 | 13.1355 | 8770 | 0 | -180 | 0.9088083 |
| 12 | 29-Jul | 506 | 150 | 16000 | 215 | 0 | Dry | 5.65 | | 100 | 0.452 | 221.24 | 10 | 0.31 | 68.58 | 13.09859 | 12810 | 0 | -430 | 1.3274611 |
| 13 | 29-Jul | 507 | 150 | 5000 | 200 | 0 | Dry | 5.02 | 12.76 | 100 | 0.452 | 221.24 | 10 | 0.314 | 69.47 | 13.26761 | 4300 | 40 | 0 | 0.4455959 |
| 14 | 29-Jul | 508 | 150 | 10000 | 200 | 0 | Dry | 5.46 | 12.46 | 100 | 0.445 | 224.72 | 10 | 0.305 | 68.54 | 13.09005 | 8790 | 0 | -200 | 0.9108808 |
| 15 | 30-Jul | 509 | 150 | 16000 | 200 | 0 | Dry | 5.63 | 12.09 | 100 | 0.465 | 215.05 | 10 | 0.317 | 68.17 | 13.0199 | 12290 | 160 | -320 | 1.2735751 |
| 16 | 30-Jul | 510 | 150 | 5000 | 185 | 0 | Dry | 5.03 | | 100 | 0.46 | 217.39 | 10 | 0.318 | 69.13 | 13.20294 | 3930 | 90 | -50 | 0.4072539 |
| 17 | 30-Jul | 512 | 150 | 10000 | 185 | 0 | Dry | 5.48 | | 100 | 0.458 | 218.34 | 10 | 0.315 | 68.78 | 13.1355 | 9040 | 20 | -140 | 0.9367876 |
| 18 | 30-Jul | 513 | 150 | 16000 | 185 | 0 | Dry | 5.62 | 12.28 | 100 | 0.458 | 218.34 | 10 | 0.312 | 68.12 | 13.0104 | 11330 | 0 | -280 | 1.1740933 |
| 19 | 31-Jul | 514 | 200 | 5000 | 215 | 0 | Dry | 4.89 | 13.49 | 100 | 0.346 | 289.02 | 10 | 0.241 | 69.65 | 13.30278 | 3800 | | | 0.3937824 |
| 20 | 31-Jul | 515 | 200 | 10000 | 215 | 0 | Dry | 5.49 | 12.76 | 100 | 0.347 | 288.18 | 10 | 0.24 | 69.16 | 13.2094 | 9350 | 80 | -200 | 0.9689119 |
| 21 | 31-Jul | 516 | 200 | 16000 | 215 | 0 | Dry | 5.65 | 12.28 | 100 | 0.346 | 289.02 | 10 | 0.238 | 68.79 | 13.13718 | 13720 | 180 | -500 | 1.4217617 |
| 22 | 1-Aug | 517 | 200 | 5000 | 200 | 0 | Dry | 4.38 | 13.45 | 100 | 0.346 | 289.02 | 10 | 0.24 | 69.36 | 13.24758 | 4790 | 210 | 70 | 0.4963731 |
| 23 | 1-Aug | 518 | 200 | 10000 | 200 | 0 | Dry | 5.49 | 12.65 | 100 | 0.347 | 288.18 | 10 | 0.239 | 68.88 | 13.15436 | 9100 | 130 | | 0.9430052 |
| 24 | 2-Aug | 521 | 200 | 16000 | 200 | 0 | Dry | 6.70 | 12.24 | 100 | 0.348 | 287.36 | 10 | 0.24 | 68.97 | 13.17144 | 12300 | 130 | | 1.2746114 |
| 25 | 2-Aug | 522 | 200 | 5000 | 185 | 0 | Dry | 5.09 | 13.28 | 100 | 0.347 | 288.18 | 10 | 0.24 | 69.16 | 13.2094 | 5000 | 100 | | 0.5181347 |
| 26 | 2-Aug | 523 | 200 | 10000 | 185 | 0 | Dry | 5.49 | 12.77 | 100 | 0.354 | 282.49 | 10 | 0.242 | 68.36 | 13.0561 | 8730 | 170 | | 0.9046632 |
| 27 | 6-Aug | 524 | 200 | 16000 | 185 | 0 | Dry | 5.62 | 12.16 | 100 | 0.35 | 285.71 | 10 | 0.24 | 68.57 | 13.09618 | 11560 | 310 | | 1.1979275 |
| 28 | 1-Aug | 718 | Tow | 5000 | 215 | 0 | Dry | 5.32 | 12.93 | 40 | 3.537 | 11.31 | 5 | 3.023 | 34.19 | 13.05853 | 5340 | 30 | -100 | 0.5533679 |
| 29 | 1-Aug | 719 | Tow | 10000 | 215 | 0 | Dry | 5.50 | 12.58 | 40 | 3.103 | 12.89 | 5 | 2.749 | 35.44 | 13.53581 | 7870 | 60 | 0 | 0.815544 |
| 30 | 1-Aug | 720 | Tow | 16000 | 215 | 0 | Dry | 5.65 | 12.04 | 40 | 3.215 | 12.44 | 5 | 2.781 | 34.60 | 13.21635 | 12060 | 50 | -160 | 1.2497409 |
| 31 | 1-Aug | 721 | Tow | 5000 | 200 | 0 | Dry | 5.15 | 13.15 | 40 | 3.215 | 12.44 | 5 | 2.765 | 34.40 | 13.14031 | 4540 | 100 | -80 | 0.4704663 |
| 32 | 1-Aug | 722 | Tow | 10000 | 200 | 0 | Dry | 5.59 | 12.14 | 40 | 3.312 | 12.08 | 5 | 2.845 | 34.36 | 13.12452 | 9720 | 70 | -40 | 1.0072539 |
| 33 | 1-Aug | 723 | Tow | 16000 | 200 | 0 | Dry | 5.72 | 11.92 | 40 | 3.328 | 12.02 | 5 | 2.83 | 34.01 | 12.99255 | 11200 | 0 | 0 | 1.1606218 |
| 34 | 1-Aug | 724 | Tow | 5000 | 185 | 0 | Dry | 5.05 | 12.96 | 40 | 3.103 | 12.89 | 5 | 2.733 | 35.23 | 13.45703 | 3190 | 40 | -120 | 0.3305699 |
| 35 | 1-Aug | 725 | Tow | 10000 | 185 | 0 | Dry | 5.58 | 12.06 | 40 | 3.505 | 11.41 | 5 | 2.99 | 34.12 | 13.0339 | 8670 | 50 | -160 | 0.8984456 |
| 36 | 1-Aug | 726 | Tow | 16000 | 185 | 0 | Dry | 5.73 | 11.97 | 40 | 3.376 | 11.85 | 5 | 2.894 | 34.29 | 13.09747 | 9470 | 50 | -100 | 0.9813472 |
| 37 | 8-Aug | 534 | 100 | 5000 | 200 | variable | Dry | | | | | | | | | | | | | |
| 38 | 8-Aug | 535 | 100 | 10000 | 200 | variable | Dry | | | | | | | | | | | | | |
| 39 | 8-Aug | 536 | 100 | 16000 | 200 | variable | Dry | | | | | | | | | | | | | |
| 40 | 8-Aug | 537 | 100 | 5000 | 200 | variable | Wet | | | | | | | | | | | | | |
| 41 | 8-Aug | 538 | 100 | 10000 | 200 | variable | Wet | | | | | | | | | | | | | |
| 42 | | | 100 | 16000 | 200 | variable | Wet | Did not run...tire wear prevents max load | | | | | | | | | | | | |
| 43 | 7-Aug | 531 | 150 | 5000 | 200 | variable | Dry | | | | | | | | | | | | | |
| 44 | 7-Aug | 532 | 150 | 10000 | 200 | variable | Wet | | | | | | | | | | | | | |
| 45 | 7-Aug | 533 | 150 | 16000 | 200 | variable | Wet | | | | | | | | | | | | | |
| 46 | 6-Aug | 525 | 200 | 5000 | 200 | variable | Wet | | | | | | | | | | | | | |
| 47 | 6-Aug | 526 | 200 | 10000 | 200 | variable | Wet | | | | | | | | | | | | | |
| 48 | 7-Aug | 530 | 200 | 16000 | 200 | variable | Wet | | | | | | | | | | | | | |
| 49 | 6-Aug | 527 | 200 | 5000 | 200 | variable | Dry | | | | | | | | | | | | | |
| 50 | 6-Aug | 528 | 200 | 10000 | 200 | variable | Dry | | | | | | | | | | | | | |
| 51 | 7-Aug | 529 | 200 | 16000 | 200 | variable | Dry | | | | | | | | | | | | | |
| 52 | 12-Aug | 731 | Tow | 5000 | 200 | variable | Wet | | | | | | | | | | | | | |
| 53 | 12-Aug | 732 | Tow | 10000 | 200 | variable | Wet | | | | | | | | | | | | | |
| 54 | | | Tow | 16000 | 200 | variable | Wet | Did not run...tire wear prevents max load | | | | | | | | | | | | |
| 55 | 12-Aug | 729 | Tow | 5000 | 200 | variable | Dry | | | | | | | | | | | | | |
| 56 | 12-Aug | 730 | Tow | 10000 | 200 | variable | Dry | | | | | | | | | | | | | |
| 57 | | | Tow | 16000 | 200 | variable | Dry | Did not run...tire wear prevents max load | | | | | | | | | | | | |

| Footprint Area Testing | | | | Footprint length | | |
|---|---|---|---|---|---|---|
| STATIC | 5000 | 185 | 5.15 | 6.68 | 5000 | 0.5181347 |
| STATIC | 10000 | 185 | 5.64 | 9.5 | 9700 | 1.0051813 |
| STATIC | 16000 | 185 | 5.93 | 11.96 | 15400 | 1.5958549 |
| STATIC | 22000 | 185 | 6.58 | 14.26 | 22200 | 2.3005181 |
| STATIC | 5000 | 200 | 5.10 | 6.5 | 5000 | 0.5181347 |
| STATIC | 10000 | 200 | 5.70 | 9.36 | 10300 | 1.0673575 |
| STATIC | 16000 | 200 | 5.92 | 11.7 | 15400 | 1.5958549 |
| STATIC | 22000 | 200 | 6.30 | 13.3 | 19200 | 1.9896373 |
| STATIC | 5000 | 215 | 5.15 | 6.58 | 5000 | 0.5181347 |
| STATIC | 10000 | 215 | 5.62 | 9.04 | 10000 | 1.0362694 |
| STATIC | 16000 | 215 | 5.93 | 11.18 | 15100 | 1.5647668 |
| STATIC | 22000 | 215 | 6.63 | 14.2 | 22600 | 2.3419689 |

Table 2. 777 Nose Tire Test Matrix and Results

**777 Nose Tire Testing**
**R-64 Update**
***ALDF Test Matrix***

| Run # | Date | Track Run # | Nominal Speed, kts | Nominal Load, lb | Tire Press | Yaw Angle | Surface Condition | Footprint Width | Axle Height inches | Carriage Dist, feet | Carriage Time,sec | Carriage Speed,ft/sec | Tire Revs | Time for Tire Revs | Dist trav during tire revs | Rolling Radius, in | Vert Load, lbs | Drag Load, lbs | Side Load, lbs | Multiple of Rated Load |
|---|---|---|---|---|---|---|---|---|---|---|---|---|---|---|---|---|---|---|---|---|
| 1 | 23-May | 431 | 100 | N/A pins | N/A | neg 8 to 8 | Dry | | | | | | | | | | | | | |
| 2 | 23-May | 432 | 100 | Dead | 209 | 0 | Dry | | 19.70 | 100 | 0.737 | 135.69 | 10 | 0.783 | 106.24 | 20.29064 | 20000 | 60 | 110 | 0.5540166 |
| 3 | 24-May | 433 | 100 | Dead | 194 | 0 | Dry | 11.80 | 19.21 | 100 | 0.699 | 143.06 | 10 | 0.743 | 106.29 | 20.30079 | 19100 | 120 | 380 | 0.5290859 |
| 4 | 4-Jun | 435 | 100 | Dead | 179 | 0 | Dry | 11.94 | 19.26 | 100 | 0.733 | 136.43 | 10 | 0.778 | 106.14 | 20.27109 | 19300 | -100 | 100 | 0.534626 |
| 5 | 6-Jun | 437 | 100 | 36000 | 209 | 0 | Dry | 12.48 | 18.55 | 100 | 0.685 | 145.99 | 10 | 0.727 | 106.13 | 20.2696 | 34300 | 300 | 250 | 0.9501385 |
| 6 | 6-Jun | 438 | 100 | 36000 | 194 | 0 | Dry | 12.48 | 18.43 | 100 | 0.669 | 149.48 | 10 | 0.706 | 105.53 | 20.15487 | 33500 | 250 | 320 | 0.9279778 |
| 7 | 4-Jun | 436 | 100 | 36000 | 179 | 0 | Dry | 12.50 | 17.92 | 100 | 0.725 | 137.93 | 10 | 0.764 | 105.38 | 20.12597 | 32900 | 190 | 270 | 0.9113573 |
| 8 | 6-Jun | 439 | 100 | 54000 | 209 | 0 | Dry | 12.70 | 17.10 | 100 | 0.675 | 148.15 | 10 | 0.715 | 105.93 | 20.23036 | 48100 | 470 | 410 | 1.33241 |
| 9 | 11-Jun | 440 | 100 | 54000 | 194 | 0 | Dry | 12.09 | 16.88 | 100 | 0.707 | 141.44 | 10 | 0.748 | 105.80 | 20.20615 | 50900 | 570 | 460 | 1.4099723 |
| 10 | 11-Jun | 441 | 100 | 54000 | 179 | 0 | Dry | 12.95 | 16.26 | 100 | 0.701 | 142.65 | 10 | 0.738 | 105.28 | 20.10865 | 52900 | 530 | 70 | 1.465374 |
| 11 | 12-Jun | 443 | 100 | 72000 | 209 | 0 | Dry | 16.65 | 17.01 | 100 | 0.695 | 143.88 | 10 | 0.730 | 105.04 | 20.06039 | 66600 | 650 | 440 | 1.8448753 |
| 12 | 12-Jun | 444 | 100 | 72000 | 194 | 0 | Dry | 17.38 | 16.52 | 100 | 0.686 | 145.77 | 10 | 0.721 | 105.10 | 20.07301 | 68600 | 870 | 100 | 1.900277 |
| 13 | 11-Jun | 442 | 100 | 72000 | 179 | 0 | Dry | 17.69 | 15.13 | 100 | 0.711 | 140.65 | 10 | 0.744 | 104.64 | 19.98503 | 66800 | 950 | -100 | 1.8504155 |
| 14 | 12-Jun | 445 | 150 | Dead | 209 | 0 | Dry | 12.00 | 19.48 | 100 | 0.505 | 198.02 | 10 | 0.540 | 106.93 | 20.42226 | 20000 | 140 | 150 | 0.5540166 |
| 15 | 12-Jun | 446 | 150 | Dead | 194 | 0 | Dry | 12.08 | 19.40 | 100 | 0.471 | 212.31 | 10 | 0.505 | 107.22 | 20.47726 | 19200 | 170 | 140 | 0.531856 |
| 16 | 12-Jun | 447 | 150 | Dead | 179 | 0 | Dry | 12.01 | 19.24 | 100 | 0.473 | 211.42 | 10 | 0.505 | 106.77 | 20.39068 | 19300 | 130 | 20 | 0.534626 |
| 17 | 13-Jun | 448 | 150 | 36000 | 209 | 0 | Dry | 12.50 | 18.54 | 100 | 0.479 | 208.77 | 10 | 0.505 | 105.43 | 20.13526 | 35300 | 340 | 370 | 0.9776393 |
| 18 | 13-Jun | 449 | 150 | 36000 | 194 | 0 | Dry | 12.52 | 18.23 | 100 | 0.479 | 208.77 | 10 | 0.508 | 106.05 | 20.25488 | 35000 | | 250 | 0.9695291 |
| 19 | 13-Jun | 450 | 150 | 36000 | 179 | 0 | Dry | 12.56 | 18.04 | 100 | 0.476 | 210.08 | 10 | 0.503 | 105.67 | 20.18192 | 34300 | 440 | 250 | 0.9501385 |
| 20 | 13-Jun | 451 | 150 | 54000 | 209 | 0 | Dry | 12.92 | 16.67 | 100 | 0.482 | 207.47 | 10 | 0.510 | 105.81 | 20.20806 | 51400 | 810 | 250 | 1.4238227 |
| 21 | 14-Jun | 452 | 150 | 54000 | 194 | 0 | Dry | 12.96 | 16.70 | 100 | 0.486 | 205.76 | 10 | 0.511 | 105.14 | 20.08103 | 52900 | 710 | 440 | 1.465374 |
| 22 | 14-Jun | 453 | 150 | 54000 | 179 | 0 | Dry | 12.99 | 16.55 | 100 | 0.474 | 210.97 | 10 | 0.498 | 105.06 | 20.06561 | 53600 | | 340 | 1.4847645 |
| 23 | 14-Jun | 454 | 150 | 72000 | 209 | 0 | Dry | 16.98 | 16.59 | 100 | 0.475 | 210.53 | 10 | 0.502 | 105.68 | 20.1842 | 69400 | 950 | 270 | 1.9224377 |
| 24 | 18-Jun | 455 | 150 | 72000 | 194 | 0 | Dry | 17.16 | 16.00 | 100 | 0.490 | 204.08 | 10 | 0.518 | 105.71 | 20.18994 | 69100 | 960 | 230 | 1.9141274 |
| 25 | 18-Jun | 456 | 150 | 72000 | 179 | 0 | Dry | 17.82 | 15.51 | 100 | 0.495 | 202.02 | 10 | 0.518 | 104.65 | 19.986 | 69700 | 1000 | 220 | 1.9307479 |
| 26 | 18-Jun | 458 | 200 | Dead | 209 | 0 | Dry | 11.94 | 19.18 | 100 | 0.361 | 277.01 | 10 | 0.387 | 107.20 | 20.47412 | 21000 | | 200 | 0.5817175 |
| 27 | 19-Jun | 459 | 200 | Dead | 194 | 0 | Dry | 11.90 | 19.00 | 100 | 0.362 | 276.24 | 10 | 0.387 | 106.91 | 20.41756 | 20000 | | 360 | 0.5540166 |
| 28 | 19-Jun | 460 | 200 | Dead | 179 | 0 | Dry | 11.98 | 19.00 | 100 | 0.366 | 273.22 | 10 | 0.391 | 106.83 | 20.40314 | 19800 | 300 | 200 | 0.5484765 |
| 29 | 24-Jun | 461 | 200 | 36000 | 209 | 0 | Dry | 12.45 | 18.50 | 100 | 0.350 | 285.71 | 10 | 0.373 | 106.57 | 20.35364 | 35000 | 540 | 470 | 0.9695291 |
| 30 | 24-Jun | 462 | 200 | 36000 | 194 | 0 | Dry | 12.46 | 18.44 | 100 | 0.355 | 281.69 | 10 | 0.377 | 106.20 | 20.28217 | 35000 | 500 | 300 | 0.9695291 |
| 31 | 24-Jun | 463 | 200 | 36000 | 179 | 0 | Dry | 12.47 | 18.02 | 100 | 0.352 | 284.09 | 10 | 0.375 | 106.53 | 20.34651 | 35000 | 500 | 190 | 0.9695291 |
| 32 | 25-Jun | 464 | 200 | 54000 | 209 | 0 | Dry | 12.90 | 17.01 | 100 | 0.350 | 285.71 | 10 | 0.373 | 106.57 | 20.35364 | 50200 | 840 | 480 | 1.3905817 |
| 33 | 25-Jun | 466 | 200 | 54000 | 194 | 0 | Dry | 13.04 | 16.52 | 100 | 0.350 | 285.71 | 10 | 0.373 | 106.57 | 20.35364 | 54500 | 780 | 300 | 1.5096953 |
| 34 | 25-Jun | 467 | 200 | 54000 | 179 | 0 | Dry | 13.06 | 16.45 | 100 | 0.350 | 285.71 | 10 | 0.371 | 106.00 | 20.24451 | 56000 | 860 | 100 | 1.5512465 |
| 35 | 26-Jun | 469 | 200 | 72000 | 209 | 0 | Dry | 16.13 | 16.71 | 100 | 0.355 | 281.69 | 10 | 0.376 | 105.92 | 20.22837 | 64900 | 1100 | 370 | 1.7977839 |
| 36 | 26-Jun | 471 | 200 | 72000 | 194 | 0 | Dry | 17.22 | 16.00 | 100 | 0.346 | 289.02 | 10 | 0.366 | 105.78 | 20.20256 | 67600 | 1000 | 250 | 1.8725762 |
| 37 | 25-Jun | 468 | 200 | 72000 | 179 | 0 | Dry | 17.70 | 15.60 | 100 | 0.354 | 282.49 | 10 | 0.373 | 105.37 | 20.12366 | 67300 | 1100 | 200 | 1.8642659 |
| 38 | 5-Jun | 700 | Tow | Dead | 209 | 0 | Dry | 11.95 | 19.00 | 40 | 6.660 | 6.01 | 4 | 7.060 | 42.40 | 20.24566 | 20600 | 80 | 310 | 0.5706371 |
| 39 | 5-Jun | 704 | Tow | Dead | 194 | 0 | Dry | 11.95 | 18.90 | 40 | 8.100 | 4.94 | 4 | 8.680 | 42.86 | 20.46615 | 20400 | 70 | 240 | 0.565097 |
| 40 | 5-Jun | 708 | Tow | Dead | 179 | 0 | Dry | 11.95 | 18.83 | 40 | 6.660 | 6.01 | 4 | 6.940 | 41.68 | 19.90154 | 19200 | 60 | 300 | 0.531856 |
| 41 | 5-Jun | 701 | Tow | 36000 | 209 | 0 | Dry | 12.50 | 17.84 | 40 | 7.010 | 5.71 | 4 | 8.077 | 46.09 | 22.00581 | 37100 | 300 | 480 | 1.0277008 |
| 42 | 5-Jun | 705 | Tow | 36000 | 194 | 0 | Dry | 12.50 | 17.72 | 40 | 7.203 | 5.55 | 4 | 7.691 | 42.71 | 20.39251 | 35400 | 270 | 420 | 0.9806094 |
| 43 | 5-Jun | 709 | Tow | 36000 | 179 | 0 | Dry | 12.67 | 17.47 | 40 | 7.379 | 5.42 | 4 | 7.871 | 42.67 | 20.37201 | 35000 | 290 | 320 | 0.9695291 |
| 44 | 5-Jun | 702 | Tow | 54000 | 209 | 0 | Dry | 12.80 | 16.53 | 30 | 5.990 | 5.01 | 3 | 6.280 | 31.45 | 20.02323 | 54800 | 600 | 400 | 1.5180055 |
| 45 | 5-Jun | 706 | Tow | 54000 | 194 | 0 | Dry | 12.94 | 16.31 | 40 | 7.580 | 5.28 | 4 | 8.020 | 42.32 | 20.20722 | 53300 | 560 | 460 | 1.4764543 |
| 46 | 5-Jun | 710 | Tow | 54000 | 179 | 0 | Dry | 12.93 | 16.04 | 40 | 8.100 | 4.94 | 4 | 8.460 | 41.73 | 19.92384 | 52400 | 570 | 290 | 1.4515235 |
| 47 | 5-Jun | 703 | Tow | 72000 | 209 | 0 | Dry | 16.81 | 15.42 | 40 | 8.970 | 4.46 | 4 | 9.200 | 41.03 | 19.5883 | 71100 | 890 | 420 | 1.9695291 |
| 48 | 5-Jun | 707 | Tow | 72000 | 194 | 0 | Dry | 17.42 | 15.13 | 40 | 8.330 | 4.80 | 4 | 8.650 | 41.54 | 19.83227 | 70400 | 1040 | 340 | 1.9501385 |
| 49 | 5-Jun | 711 | Tow | 72000 | 179 | 0 | Dry | 18.17 | 14.60 | 40 | 7.200 | 5.56 | 4 | 7.640 | 42.44 | 20.26573 | 72400 | 1200 | 400 | 2.0055402 |
| 50 | 28-Jun | 472 | 100 | 18000 | 194 | variable | Dry | | | | | | | | | | | | | |
| 51 | 8-Jul | 474 | 100 | 36000 | 209 | variable | Dry | | | | | | | | | | | | | |
| 52 | 8-Jul | 475 | 100 | 36000 | 194 | variable | Dry | | | | | | | | | | | | | |
| 53 | 8-Jul | 476 | 100 | 36000 | 194 | variable | **Wet** | | | | | | | | | | | | | |
| 54 | 9-Jul | 477 | 100 | 36000 | 179 | variable | Dry | | | | | | | | | | | | | |
| 55 | 9-Jul | 478 | 100 | 54000 | 194 | variable | Dry | | | | | | | | | | | | | |
| 56 | 9-Jul | 479 | 100 | 72000 | 194 | variable | Dry | | | | | | | | | | | | | |
| 57 | 9-Jul | 480 | 150 | 18000 | 194 | variable | Dry | | | | | | | | | | | | | |
| 58 | 9-Jul | 481 | 150 | 36000 | 209 | variable | Dry | | | | | | | | | | | | | |
| 59 | 10-Jul | 482 | 150 | 36000 | 194 | variable | Dry | | | | | | | | | | | | | |
| 60 | 10-Jul | 483 | 150 | 36000 | 194 | variable | **Wet** | | | | | | | | | | | | | |
| 61 | 10-Jul | 484 | 150 | 36000 | 179 | variable | Dry | | | | | | | | | | | | | |
| 62 | 10-Jul | 485 | 150 | 54000 | 194 | variable | Dry | | | | | | | | | | | | | |
| 63 | 11-Jul | 486 | 150 | 72000 | 194 | variable | Dry | | | | | | | | | | | | | |
| 64 | 11-Jul | 487 | 200 | 18000 | 194 | variable | Dry | | | | | | | | | | | | | |
| 65 | 11-Jul | 488 | 200 | 36000 | 209 | variable | Dry | | | | | | | | | | | | | |
| 66 | 11-Jul | 489 | 200 | 36000 | 194 | variable | Dry | | | | | | | | | | | | | |
| 67 | 11-Jul | 490 | 200 | 36000 | 194 | variable | **Wet** | | | | | | | | | | | | | |
| 68 | 12-Jul | 491 | 200 | 36000 | 179 | variable | Dry | | | | | | | | | | | | | |
| 69 | 12-Jul | 492 | 200 | 54000 | 194 | variable | Dry | | | | | | | | | | | | | |
| 70 | 12-Jul | 493 | 200 | 72000 | 194 | variable | Dry | | | | | | | | | | | | | |

| Footprint Area Testing | | | | | Footprint Length, in | | | | | |
|---|---|---|---|---|---|---|---|---|---|---|
| Static | Dead | 179 | | 12.00 | 18.57 | 11.5 | | | 20000 | | | 0.5540166 |
| Static | 36000 | 179 | | 12.66 | 17.15 | 15.35 | | | 36000 | | | 0.9972299 |
| Static | 54000 | 179 | | 13.00 | 15.68 | 19.3 | | | 53500 | | | 1.4819945 |
| Static | 72000 | 179 | | 18.32 | 13.90 | 23.72 | | | 79200 | | | 2.1939058 |
| Static | Dead | 194 | | 11.72 | 18.87 | 10.56 | | | 18900 | | | 0.5124654 |
| Static | 36000 | 194 | | 12.56 | 17.34 | 14.9 | | | 36800 | | | 1.0221607 |
| Static | 54000 | 194 | | 13.00 | 16.05 | 18.52 | | | 53800 | | | 1.4903047 |
| Static | 72000 | 194 | | 17.25 | 14.75 | 22.02 | | | 72600 | | | 2.0110803 |
| Static | Dead | 209 | | 11.80 | 18.90 | 10.72 | | | 20200 | | | 0.5595668 |
| Static | 36000 | 209 | | 12.56 | 17.70 | 14.48 | | | 36000 | | | 0.9972299 |
| Static | 54000 | 209 | | 13.00 | 16.30 | 18.02 | | | 54100 | | | 1.498615 |
| Static | 72000 | 209 | | 17.32 | 14.80 | 22.2 | | | 77100 | | | 2.1357341 |

Table 3. 777 Main Tire Test Matrix and Results

**777 Main Tire Testing**

**R-64 Update**

***ALDF Test Matrix***

| Run # | Date | Track Run # | Nominal Speed, kts | Nominal Load, lb | Tire Press | Yaw Angle | Surface Cond | Footprint Width | Axle Height inches | Carriage Dist, feet | Carriage Time,sec | Carriage Speed,fps | Tire Revs | Time for Tire Revs | Dist trav during tire revs | Rolling Radius, in | Vert Load, lbs | Drag Load, lbs | Side Load, lbs | Multiple of Rated Load |
|---|---|---|---|---|---|---|---|---|---|---|---|---|---|---|---|---|---|---|---|---|
| 1 | 27-Aug | 541 | 100 | 29000 | 237 | 0 | Dry | 13.33 | 22.66 | 100 | 0.645 | 155.04 | 10 | 0.823 | 127.60 | 24.36921 | 29660 | 160 | -450 | 0.5194396 |
| 2 | 27-Aug | 540 | 100 | 57000 | 237 | 0 | Dry | 14.00 | 21.21 | 100 | 0.653 | 153.14 | 10 | 0.825 | 126.34 | 24.12916 | 57590 | 670 | -750 | 1.0085814 |
| 3 | 27-Aug | 539 | 100 | 72000 | 237 | 0 | Dry | 14.00 | 20.52 | 100 | 0.654 | 152.91 | 10 | 0.823 | 125.84 | 24.03386 | 70000 | 840 | -730 | 1.2259194 |
| 4 | 29-Aug | 544 | 100 | 29000 | 220 | 0 | Dry | 13.40 | 22.59 | 100 | 0.641 | 156.01 | 10 | 0.814 | 126.99 | 24.25313 | 30000 | 360 | -1300 | 0.525394 |
| 5 | 27-Aug | 543 | 100 | 57000 | 220 | 0 | Dry | 13.95 | 20.93 | 100 | 0.646 | 154.80 | 10 | 0.817 | 126.47 | 24.1541 | 56700 | 640 | -1170 | 0.9929947 |
| 6 | 27-Aug | 542 | 100 | 72000 | 220 | 0 | Dry | 14.02 | 20.52 | 100 | 0.648 | 154.32 | 10 | 0.818 | 126.23 | 24.10903 | 69160 | 740 | -950 | 1.2112084 |
| 7 | 29-Aug | 547 | 100 | 29000 | 203 | 0 | Dry | 13.51 | 22.66 | 100 | 0.629 | 158.98 | 10 | 0.797 | 126.71 | 24.19965 | 30360 | 190 | -630 | 0.5316988 |
| 8 | 29-Aug | 546 | 100 | 57000 | 203 | 0 | Dry | 14.03 | 20.74 | 100 | 0.643 | 155.52 | 10 | 0.81 | 125.97 | 24.05888 | 58030 | 620 | -810 | 1.0162872 |
| 9 | 29-Aug | 545 | 100 | 72000 | 203 | 0 | Dry | 14.11 | 20.07 | 100 | 0.635 | 157.48 | 10 | 0.796 | 125.35 | 23.94091 | 70000 | 1010 | -1570 | 1.2259194 |
| 10 | 3-Sep | 550 | 150 | 29000 | 237 | 0 | Dry | 13.42 | 22.36 | 100 | 0.439 | 227.79 | 10 | 0.559 | 127.33 | 24.31917 | 30000 | 370 | -420 | 0.525394 |
| 11 | 3-Sep | 548 | 150 | 72000 | 237 | 0 | Dry | 14.13 |  | 100 | 0.436 | 229.36 | 10 | 0.55 | 126.15 | 24.09226 | 71770 | 1000 | -500 | 1.2569177 |
| 12 | 3-Sep | 551 | 150 | 29000 | 220 | 0 | Dry | 13.40 | 22.39 | 100 | 0.436 | 229.36 | 10 | 0.556 | 127.52 | 24.35509 | 30390 | 440 | -340 | 0.5322242 |
| 13 | 4-Sep | 555 | 150 | 57000 | 220 | 0 | Dry | 14.10 | 21.11 | 100 | 0.439 | 227.79 | 10 | 0.556 | 126.65 | 24.18865 | 57590 | 790 | -710 | 1.0085814 |
| 14 | 4-Sep | 553 | 150 | 72000 | 220 | 0 | Dry | 14.16 | 20.33 | 100 | 0.447 | 223.71 | 10 | 0.563 | 125.95 | 24.05483 | 74290 | 1160 | -810 | 1.3010508 |
| 15 | 3-Sep | 552 | 150 | 29000 | 203 | 0 | Dry | 13.48 | 22.33 | 100 | 0.434 | 230.41 | 10 | 0.551 | 126.96 | 24.24729 | 29660 | 390 | -470 | 0.5194396 |
| 16 | 4-Sep | 556 | 150 | 72000 | 203 | 0 | Dry | 14.25 | 20.37 | 70 | 0.297 | 235.69 | 6 | 0.322 | 75.89 | 24.15726 | 70000 | 960 | -810 | 1.2259194 |
| 17 | 5-Sep | 559 | 200 | 29000 | 237 | 0 | Dry | 13.46 | 22.93 | 100 | 0.335 | 298.51 | 10 | 0.428 | 127.76 | 24.40059 | 30000 | 540 | -340 | 0.525394 |
| 18 | 4-Sep | 558 | 200 | 57000 | 237 | 0 | Dry | 14.04 | 21.44 | 100 | 0.327 | 305.81 | 10 | 0.417 | 127.52 | 24.35509 | 56700 | 1060 | -630 | 0.9929947 |
| 19 | 4-Sep | 557 | 200 | 72000 | 237 | 0 | Dry | 14.23 | 19.7 | 100 | 0.326 | 306.75 | 10 | 0.415 | 127.30 | 24.31263 | 71550 | 1130 | -680 | 1.2530648 |
| 20 | 5-Sep | 562 | 200 | 29000 | 220 | 0 | Dry | 13.55 |  | 100 | 0.33 | 303.03 | 10 | 0.42 | 127.27 | 24.3073 | 30580 | 440 | -580 | 0.5355517 |
| 21 | 5-Sep | 561 | 200 | 57000 | 220 | 0 | Dry | 14.05 | 21.7 | 100 | 0.326 | 306.75 | 10 | 0.416 | 127.61 | 24.37121 | 57590 | 860 | -670 | 1.0085814 |
| 22 | 5-Sep | 560 | 200 | 72000 | 220 | 0 | Dry | 14.32 | 19.85 | 100 | 0.329 | 303.95 | 10 | 0.418 | 127.05 | 24.26508 | 73000 | 1310 | -830 | 1.2784588 |
| 23 | 5-Sep | 565 | 200 | 29000 | 203 | 0 | Dry | 13.59 | 22.69 | 100 | 0.328 | 304.88 | 10 | 0.42 | 128.05 | 24.45552 | 30400 | 490 | -360 | 0.5323993 |
| 24 | 5-Sep | 564 | 200 | 57000 | 203 | 0 | Dry | 14.06 | 21.18 | 100 | 0.326 | 306.75 | 10 | 0.413 | 126.69 | 24.19546 | 58370 | 940 | -640 | 1.0222417 |
| 25 | 5-Sep | 563 | 200 | 72000 | 203 | 0 | Dry | 14.30 | 20.22 | 100 | 0.329 | 303.95 | 10 | 0.416 | 126.44 | 24.14898 | 71130 | 1060 | -850 | 1.2457093 |
| 26 | 6-Sep | 734 | Tow | 29000 | 237 | 0 | Dry | 13.56 | 22.49 | 50 | 4.9 | 10.20 | 5 | 6.251 | 63.79 | 24.36435 | 30300 | 200 | -360 | 0.530648 |
| 27 | 6-Sep | 735 | Tow | 57000 | 237 | 0 | Dry | 14.17 | 20.76 | 50 | 5.981 | 8.36 | 4 | 6.135 | 51.29 | 24.48793 | 60350 | 590 | -800 | 1.0569177 |
| 28 | 6-Sep | 736 | Tow | 72000 | 237 | 0 | Dry | 14.46 | 19.9 | 50 | 5.055 | 9.89 | 4 | 5.093 | 50.38 | 24.0527 | 77830 | 890 | -1250 | 1.3630473 |
| 29 | 6-Sep | 737 | Tow | 29000 | 220 | 0 | Dry | 13.54 | 22.43 | 50 | 4.823 | 10.37 | 4 | 4.842 | 50.20 | 23.96729 | 31280 | 270 | -430 | 0.5478109 |
| 30 | 6-Sep | 738 | Tow | 57000 | 220 | 0 | Dry | 14.09 | 20.83 | 50 | 5.325 | 9.39 | 4 | 5.441 | 51.09 | 24.3933 | 57730 | 620 | -720 | 1.0110333 |
| 31 | 6-Sep | 739 | Tow | 72000 | 220 | 0 | Dry | 14.45 | 19.47 | 40 | 5.035 | 7.94 | 3 | 4.707 | 37.39 | 23.80591 | 77340 | 940 | -1140 | 1.3544658 |
| 32 | 6-Sep | 740 | Tow | 29000 | 203 | 0 | Dry | 13.62 | 22.24 | 40 | 4.611 | 8.67 | 3 | 4.437 | 38.49 | 24.50386 | 30000 | 250 | -200 | 0.525394 |
| 33 | 6-Sep | 741 | Tow | 57000 | 203 | 0 | Dry | 14.22 | 20.46 | 30 | 3.916 | 7.66 | 3 | 4.92 | 37.69 | 23.99517 | 57340 | 640 | -740 | 1.0042032 |
| 34 | 6-Sep | 742 | Tow | 72000 | 203 | 0 | Dry | 14.60 | 19.35 | 40 | 5.17 | 7.74 | 3 | 4.823 | 37.32 | 23.75565 | 74630 | 890 | -1210 | 1.3070053 |
| 35 |  |  | 100 | 29000 | 220 | variable | Dry | See note run 49 |  |  |  |  |  |  |  |  |  |  |  |  |
| 36 |  |  | 100 | 57000 | 220 | variable | Dry | See note run 49 |  |  |  |  |  |  |  |  |  |  |  |  |
| 37 |  |  | 100 | 72000 | 220 | variable | Dry | See note run 49 |  |  |  |  |  |  |  |  |  |  |  |  |
| 38 |  |  | 100 | 29000 | 220 | variable | Wet | See note run 49 |  |  |  |  |  |  |  |  |  |  |  |  |
| 39 |  |  | 100 | 57000 | 220 | variable | Wet | See note run 49 |  |  |  |  |  |  |  |  |  |  |  |  |
| 40 |  |  | 100 | 72000 | 220 | variable | Wet | See note run 49 |  |  |  |  |  |  |  |  |  |  |  |  |
| 41 |  |  | 150 | 29000 | 220 | variable | Wet | See note run 49 |  |  |  |  |  |  |  |  |  |  |  |  |
| 42 |  |  | 150 | 57000 | 220 | variable | Wet | See note run 49 |  |  |  |  |  |  |  |  |  |  |  |  |
| 43 |  |  | 150 | 72000 | 220 | variable | Wet | See note run 49 |  |  |  |  |  |  |  |  |  |  |  |  |
| 44 |  |  | 200 | 29000 | 220 | variable | Wet | See note run 49 |  |  |  |  |  |  |  |  |  |  |  |  |
| 45 |  |  | 200 | 57000 | 220 | variable | Wet | See note run 49 |  |  |  |  |  |  |  |  |  |  |  |  |
| 46 |  |  | 200 | 72000 | 220 | variable | Wet | See note run 49 |  |  |  |  |  |  |  |  |  |  |  |  |
| 47 |  |  | 200 | 29000 | 220 | variable | Dry | See note run 49 |  |  |  |  |  |  |  |  |  |  |  |  |
| 48 |  |  | 200 | 57000 | 220 | variable | Dry | See note run 49 |  |  |  |  |  |  |  |  |  |  |  |  |
| 49 | 9-Sep | 566 | 200 | 72000 | 220 | variable | Dry | Catastrophic bearing failure…no other yawed runs possible |  |  |  |  |  |  |  |  |  |  |  |  |
| 50 |  |  | Tow | 29000 | 220 | variable | Dry | See note run 49 |  |  |  |  |  |  |  |  |  |  |  |  |
| 51 |  |  | Tow | 57000 | 220 | variable | Dry | See note run 49 |  |  |  |  |  |  |  |  |  |  |  |  |
| 52 |  |  | Tow | 72000 | 220 | variable | Dry | See note run 49 |  |  |  |  |  |  |  |  |  |  |  |  |
| 53 |  |  | Tow | 29000 | 220 | variable | Wet | See note run 49 |  |  |  |  |  |  |  |  |  |  |  |  |
| 54 |  |  | Tow | 57000 | 220 | variable | Wet | See note run 49 |  |  |  |  |  |  |  |  |  |  |  |  |
| 55 |  |  | Tow | 72000 | 220 | variable | Wet | See note run 49 |  |  |  |  |  |  |  |  |  |  |  |  |
|  |  |  |  |  |  |  |  |  |  |  |  |  |  |  |  |  |  |  |  |  |
|  |  |  |  |  |  |  |  |  |  |  |  |  |  |  |  |  |  |  |  |  |
|  |  |  |  |  |  |  |  |  | Footprint |  |  |  |  |  |  |  |  |  |  |  |
|  |  |  | **Footprint Area Testing** |  |  |  |  |  | Length |  |  |  |  |  |  |  |  |  |  |  |
|  |  |  | Static | 29000 | 203 |  |  | 13.62 | 13.62 |  |  |  |  |  |  |  | 32200 |  |  | 0.5639229 |
|  |  |  | Static | 57000 | 203 |  |  | 14.18 | 18.7 |  |  |  |  |  |  |  | 57600 |  |  | 1.0087566 |
|  |  |  | Static | 72000 | 203 |  |  | 14.34 | 21.27 |  |  |  |  |  |  |  | 72400 |  |  | 1.267951 |
|  |  |  | Static | 29000 | 220 |  |  | 13.50 | 12.52 |  |  |  |  |  |  |  | 29200 |  |  | 0.5113835 |
|  |  |  | Static | 57000 | 220 |  |  | 14.17 | 17.84 |  |  |  |  |  |  |  | 57400 |  |  | 1.0052539 |
|  |  |  | Static | 72000 | 220 |  |  | 14.37 | 20.76 |  |  |  |  |  |  |  | 74700 |  |  | 1.3082312 |
|  |  |  | Static | 29000 | 237 |  |  | 13.38 | 11.92 |  |  |  |  |  |  |  | 28000 |  |  | 0.4903678 |
|  |  |  | Static | 57000 | 237 |  |  | 14.12 | 17.25 |  |  |  |  |  |  |  | 57000 |  |  | 0.9982487 |
|  |  |  | Static | 72000 | 237 |  |  | 14.35 | 19.84 |  |  |  |  |  |  |  | 72300 |  |  | 1.2661996 |

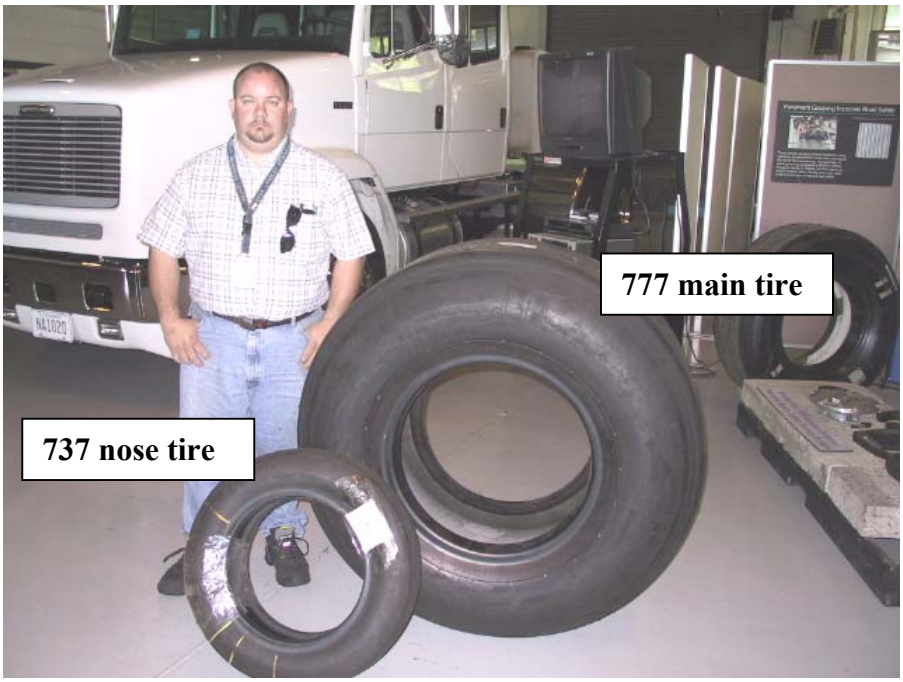


Figure 1. Photograph of the 737 nose tire and 777 main tire.

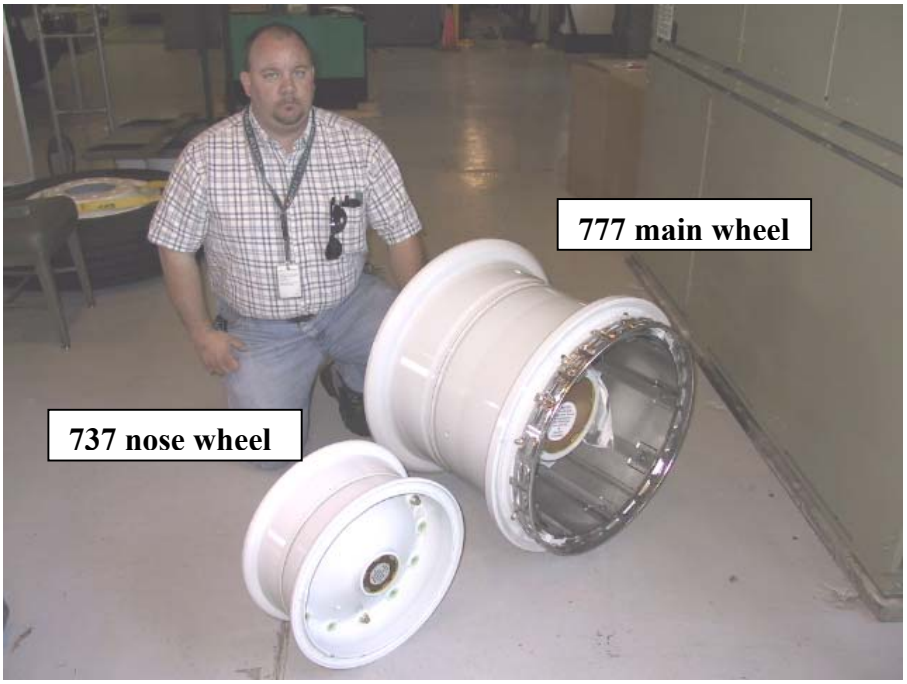


Figure 2. Photograph of the 737 nose wheel and 777 main wheel.

Figure 3. Photograph of the Aircraft Landing Dynamics Facility.

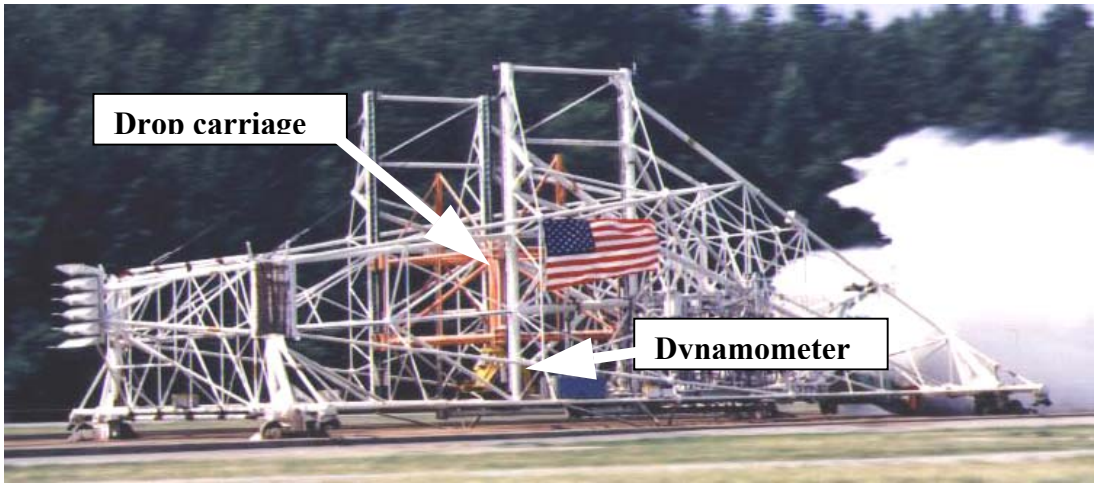


Figure 4. Photograph of the ALDF test carriage.

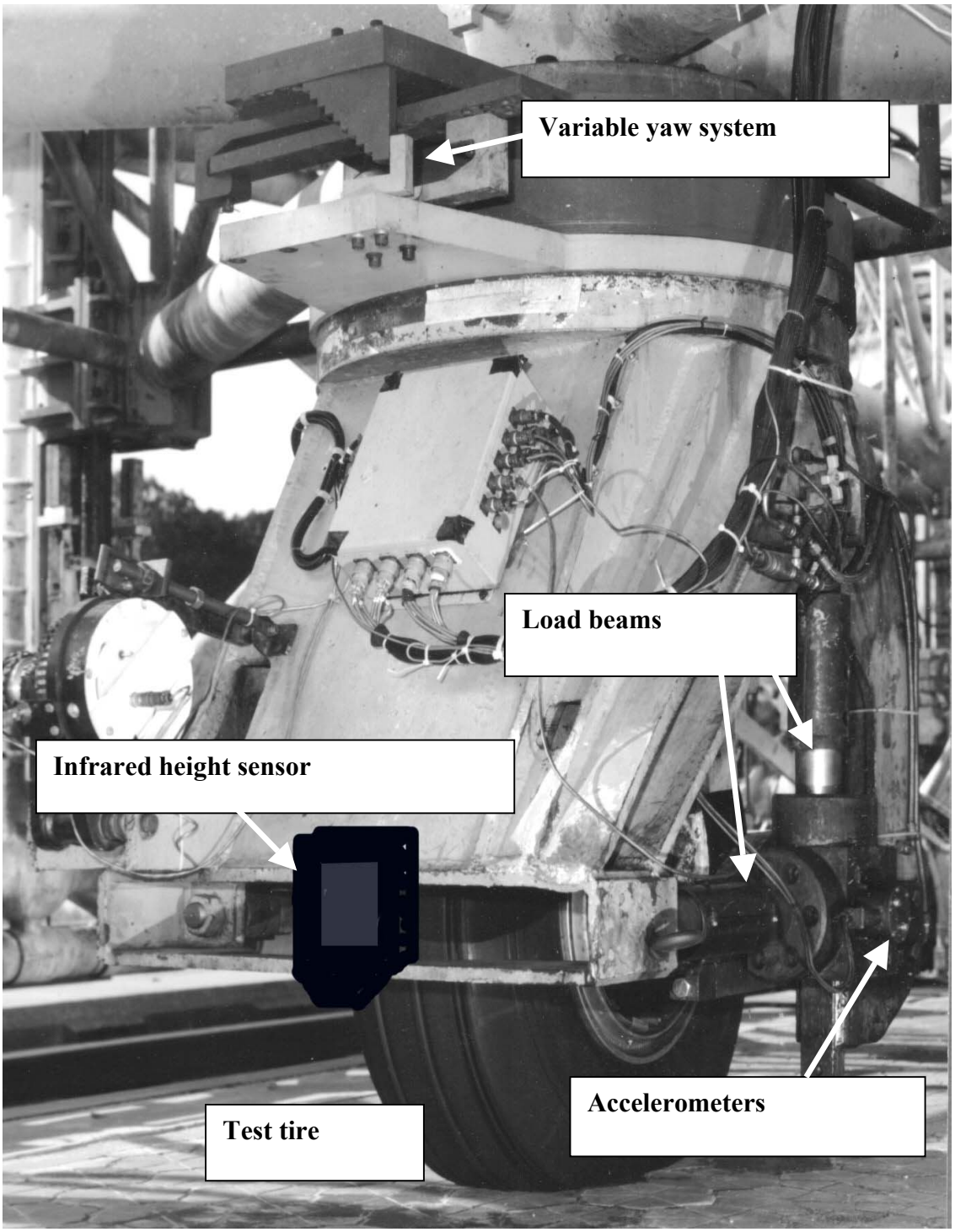


Figure 5. Photograph of the ALDF dynamometer.


Figure 6. Photograph of the frictionless platform.

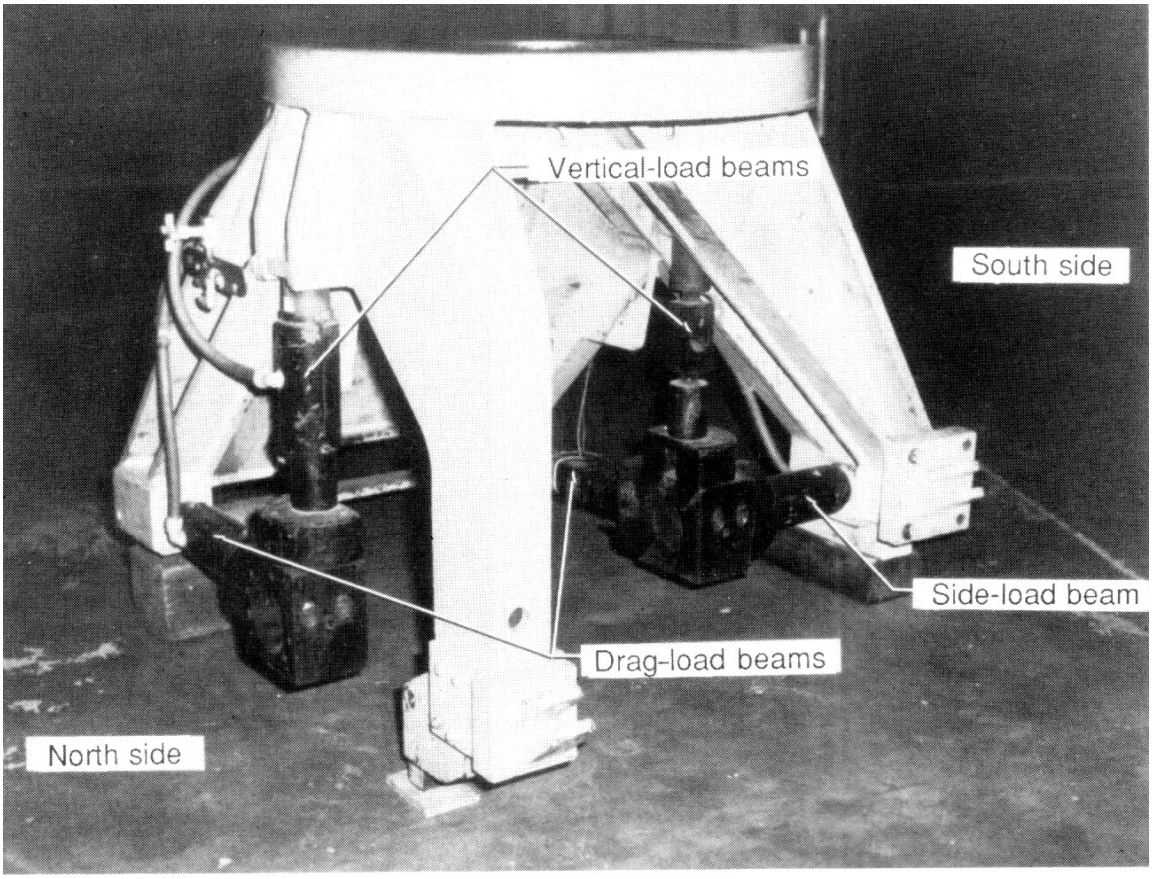


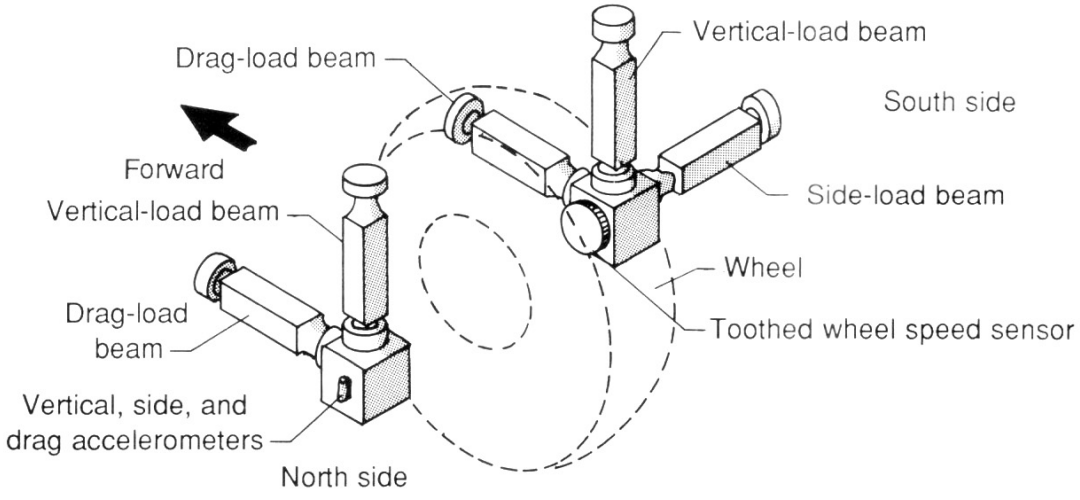


Figure 7. Layout of force measurement beams.

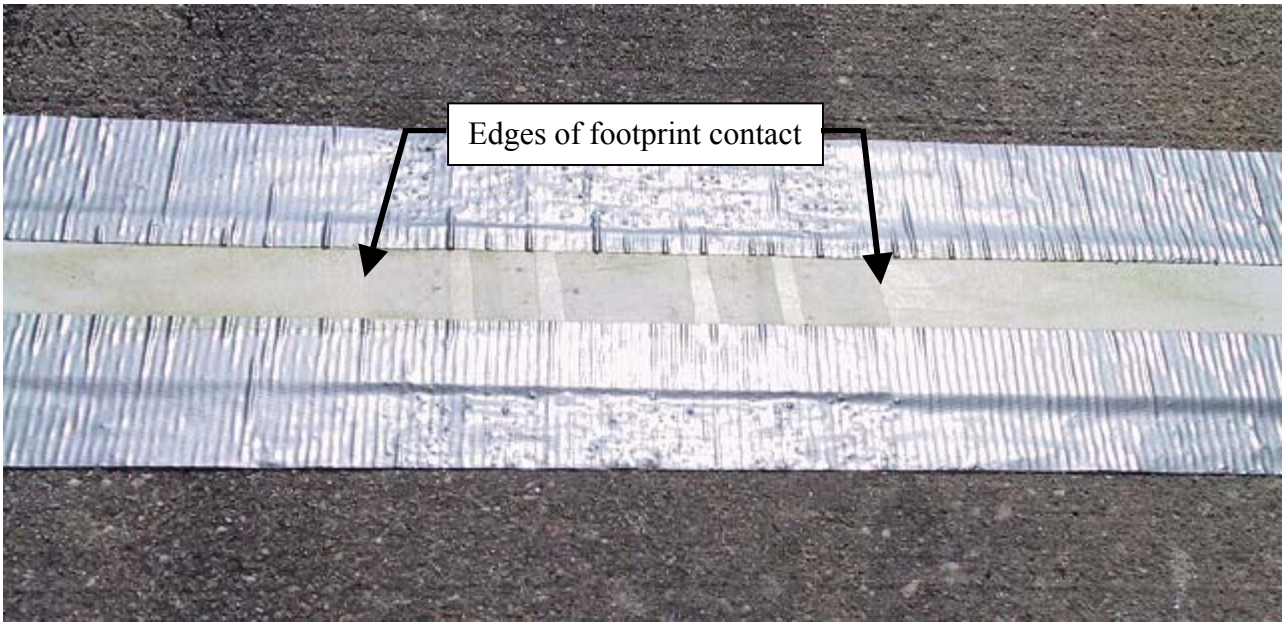


Figure 8. Footprint width indicator strip.

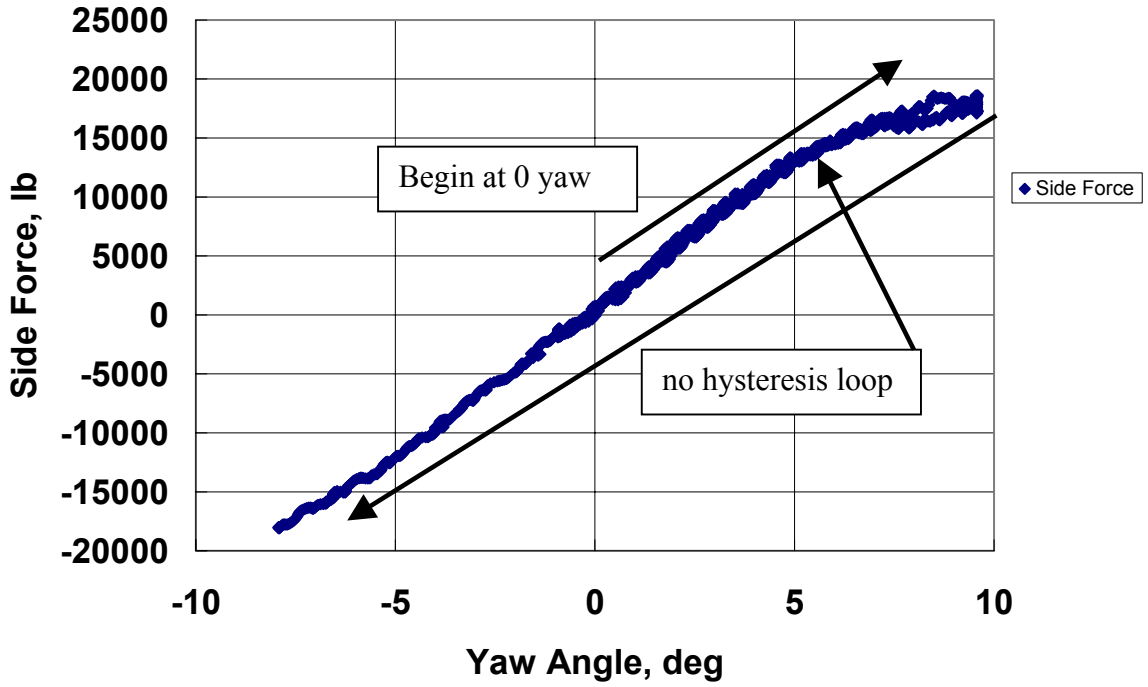


Figure 9. Plot of side force versus yaw angle demonstrating lack of hysteresis loop.

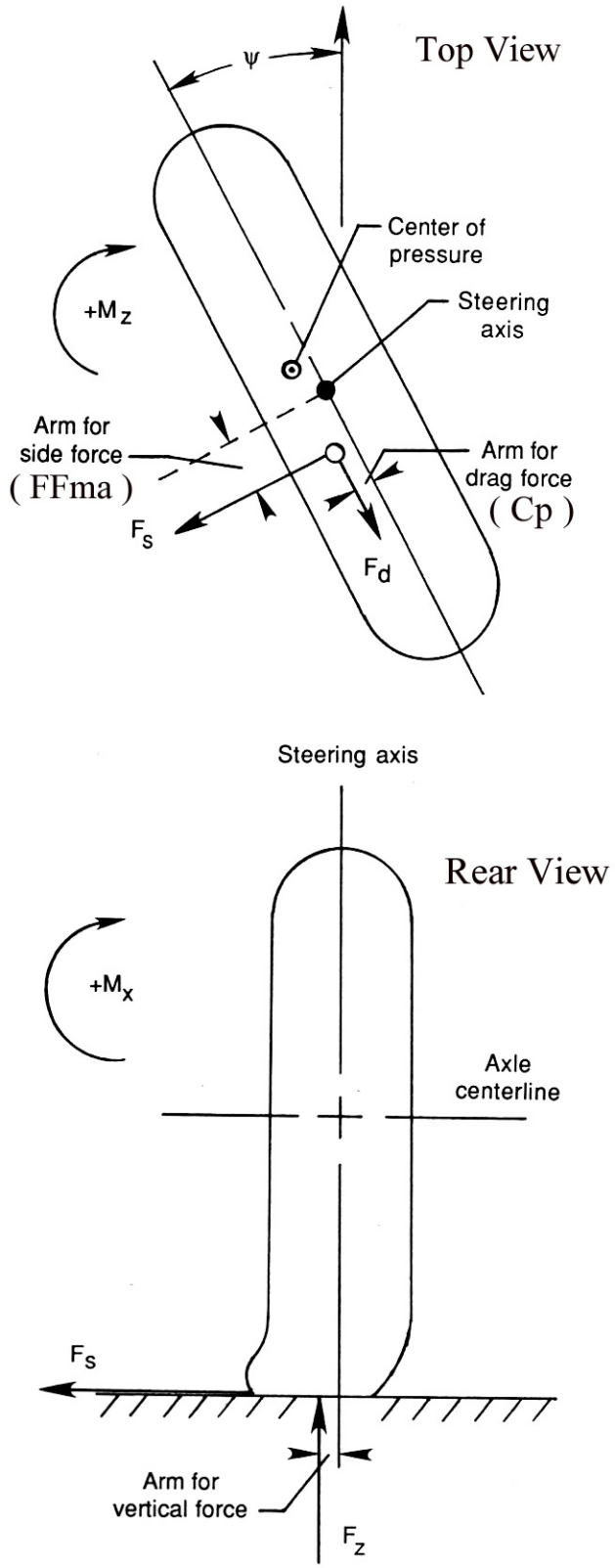


Figure 10. Forces and moments acting on a yawed, rolling tire.

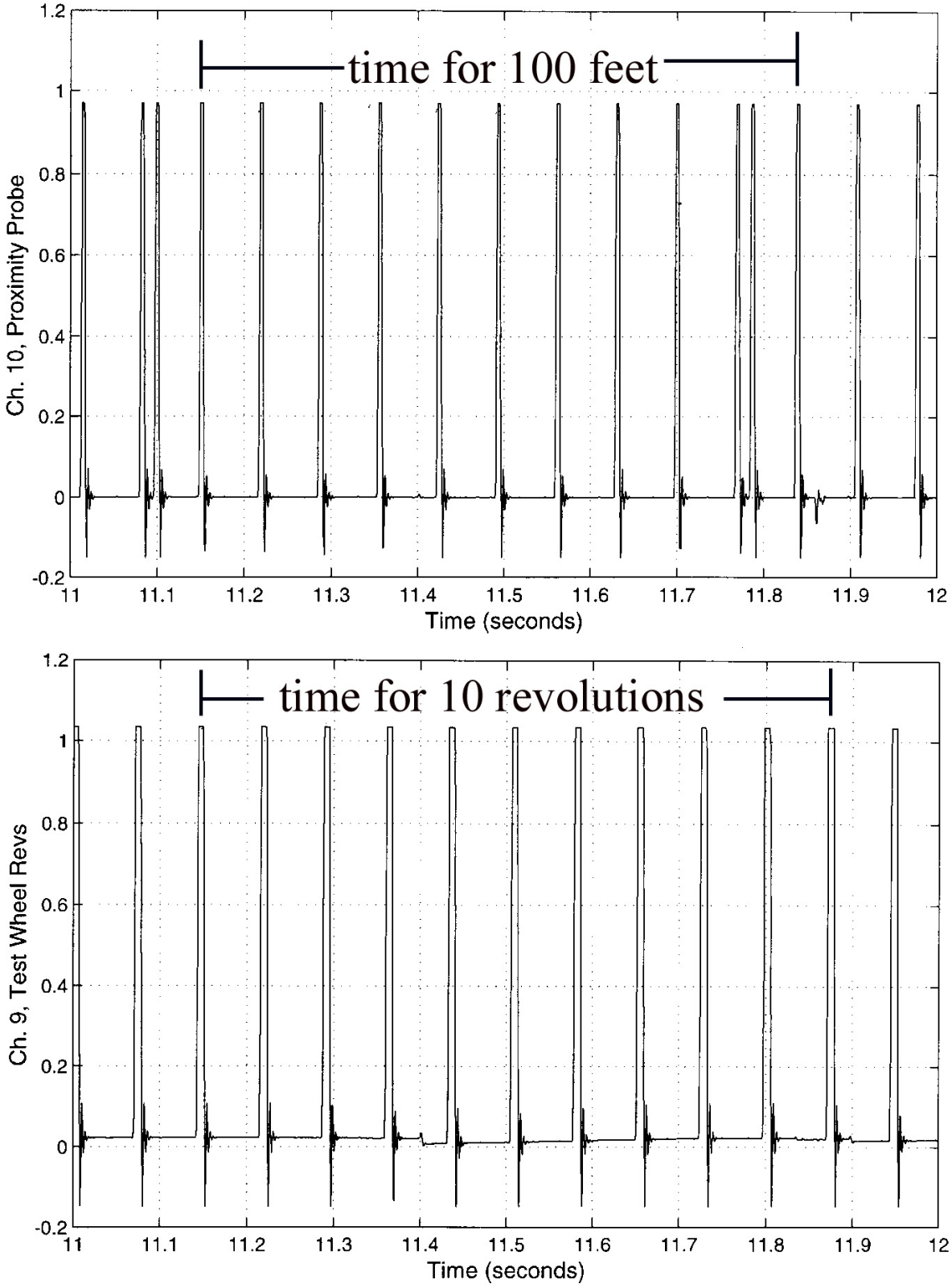


Figure 11. Typical time histories of carriage position and test wheel revolutions.

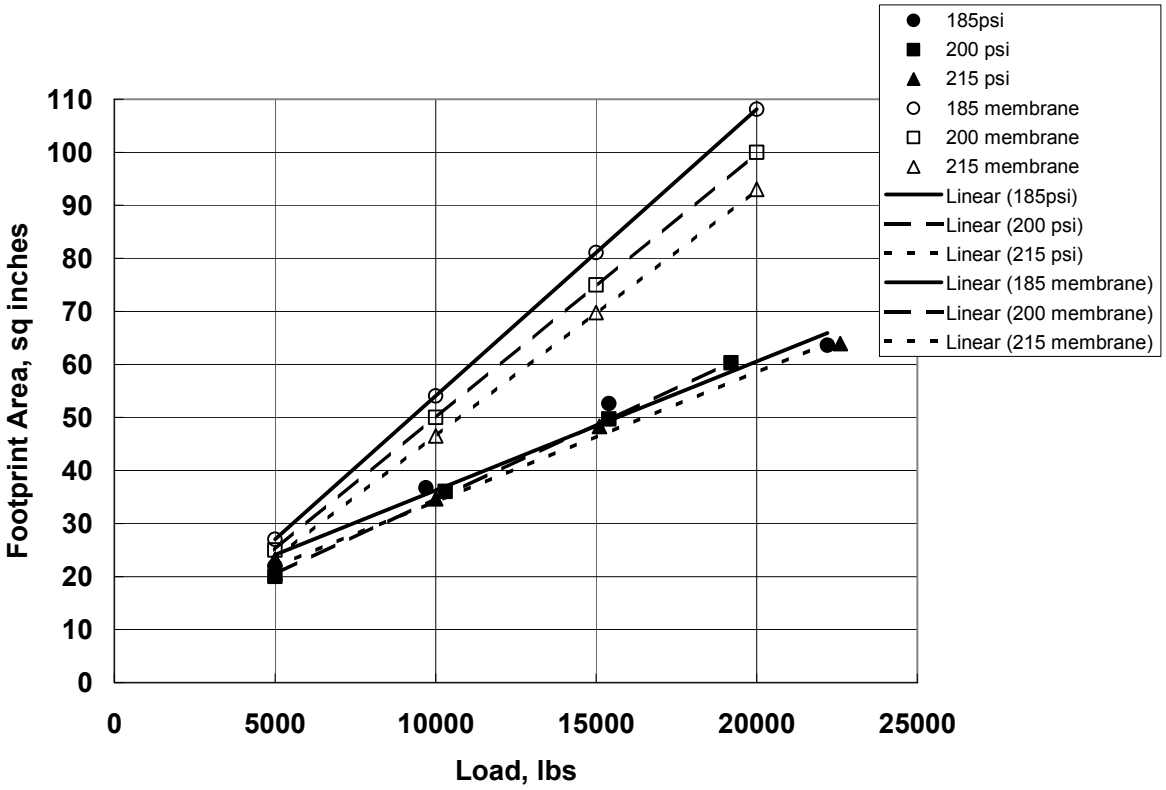


Figure 12. 737 nose tire footprint area.

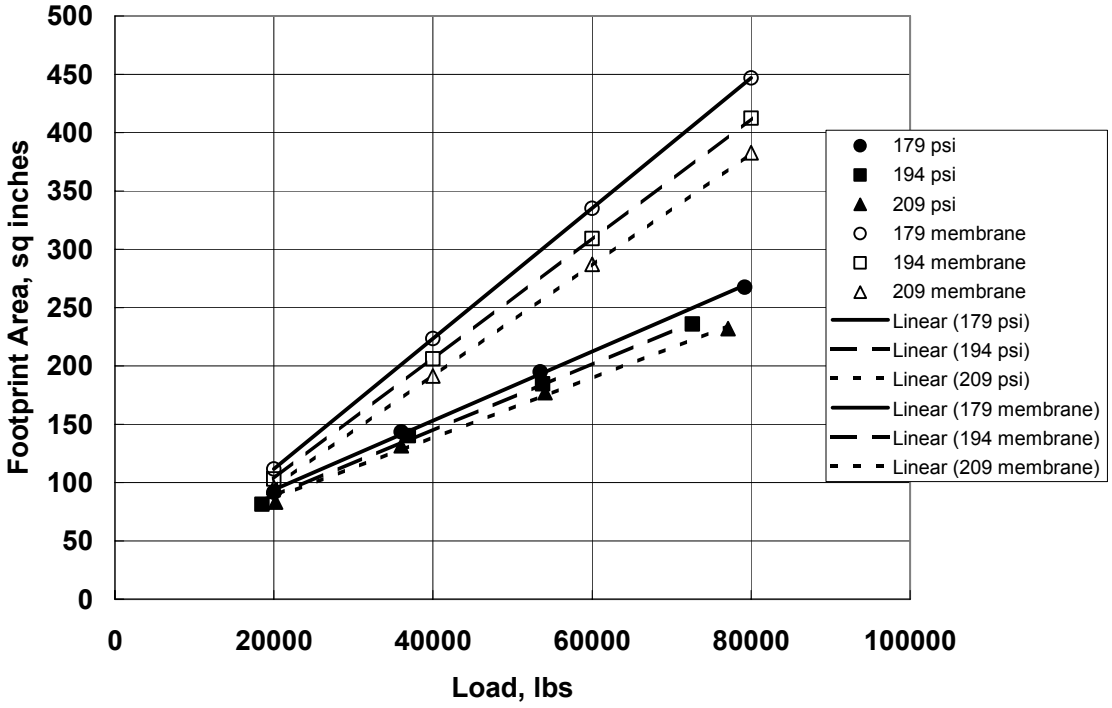


Figure 13. 777 nose tire footprint area.

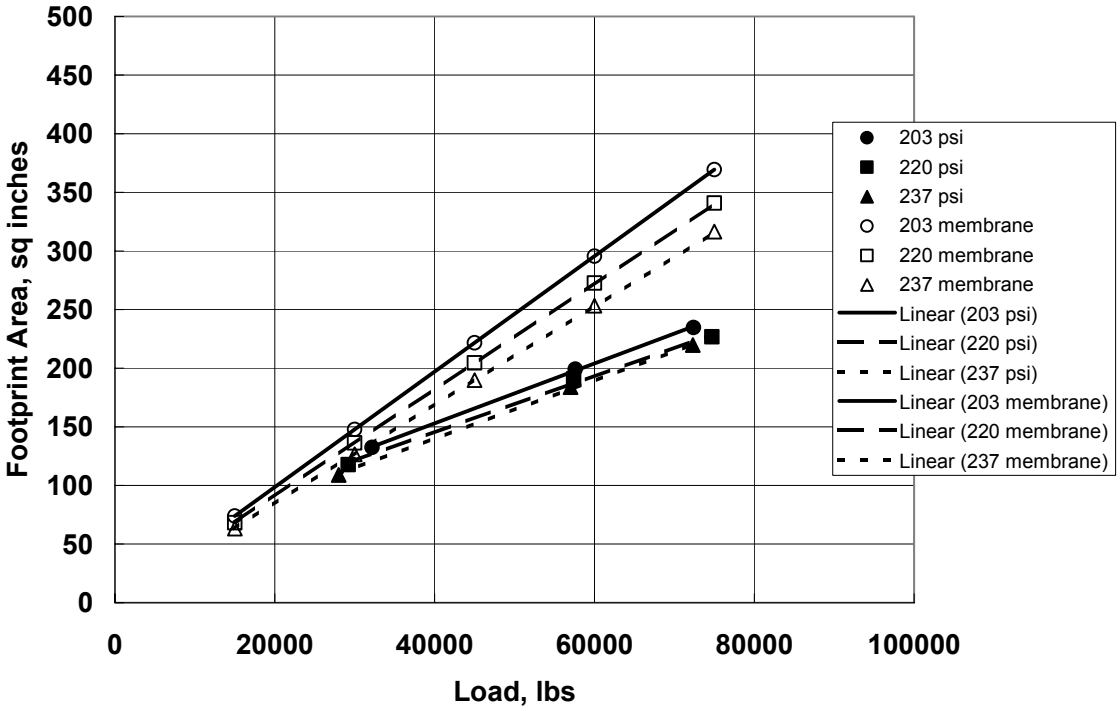


Figure 14. 777 main tire footprint area.

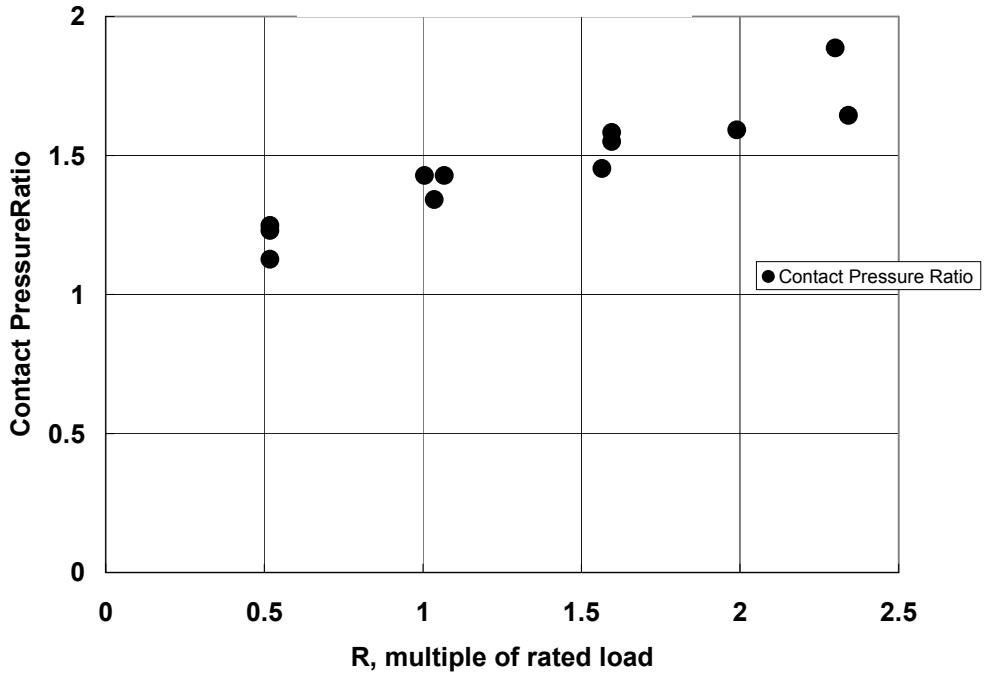


Figure 15. 737 nose tire contact pressure ratio.

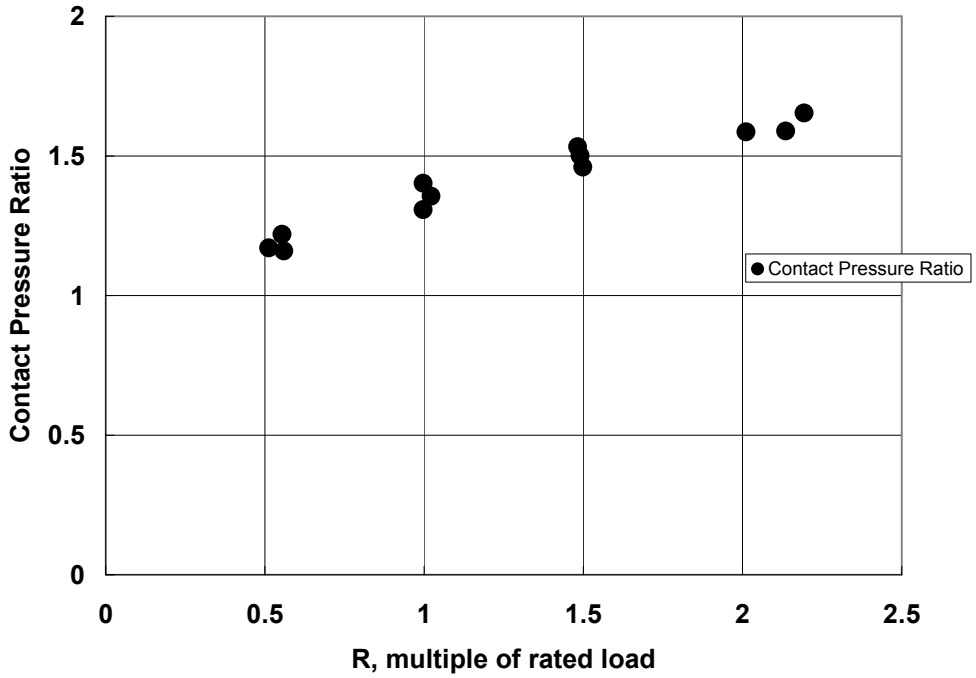


Figure 16. 777 nose tire contact pressure ratio.

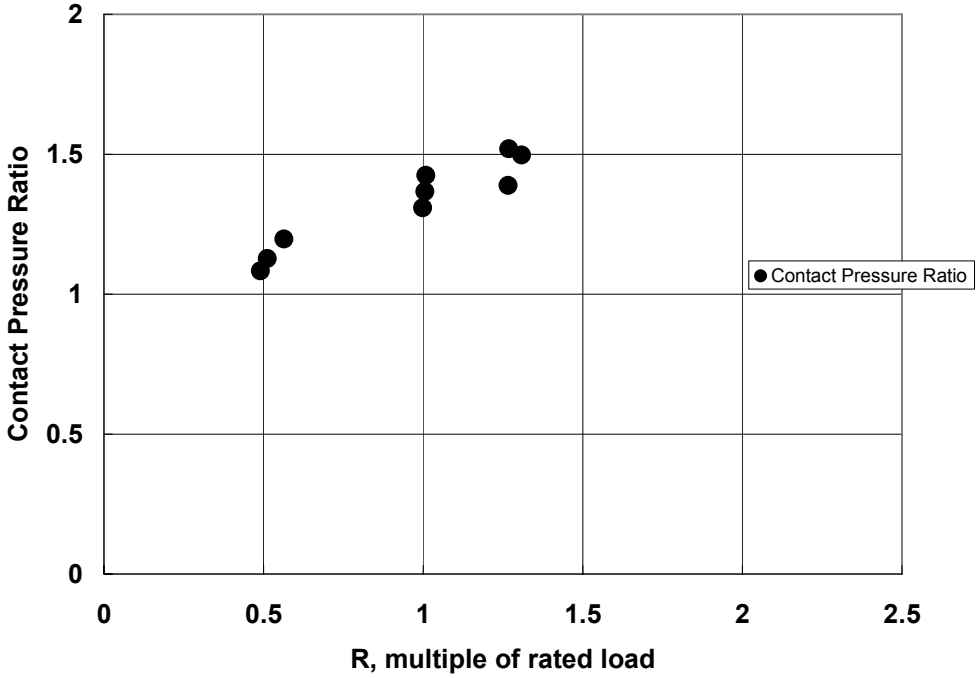


Figure 17. 777 main tire contact pressure ratio.

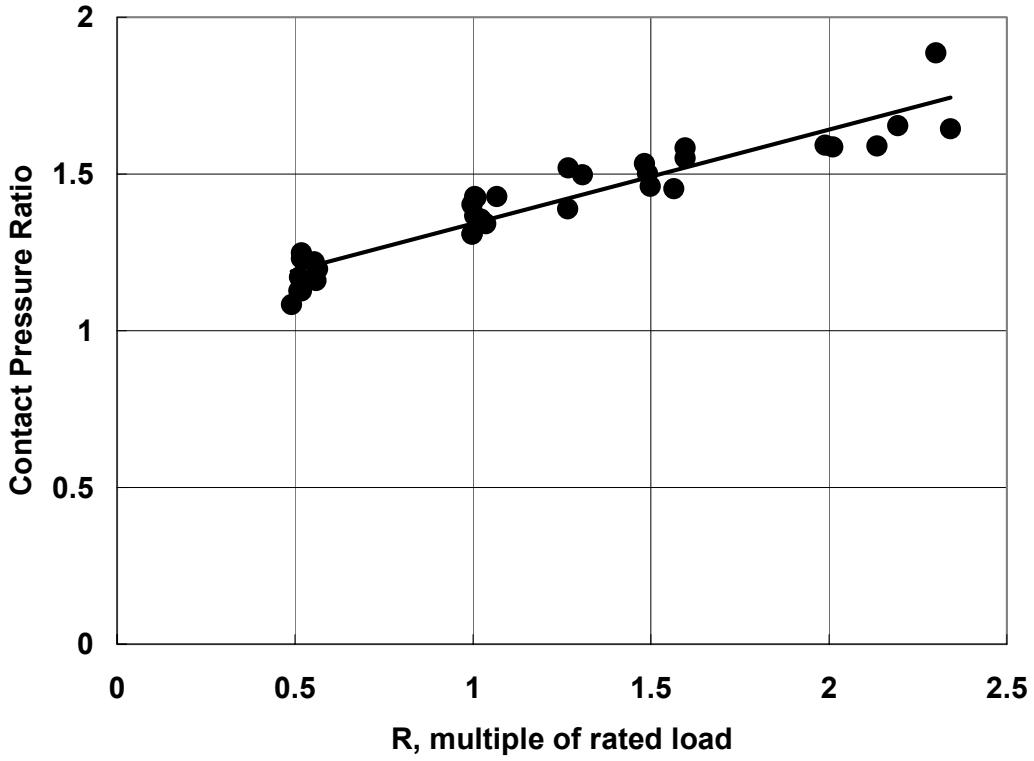


Figure 18. Contact pressure ratio model; all tire sizes, all pressures.

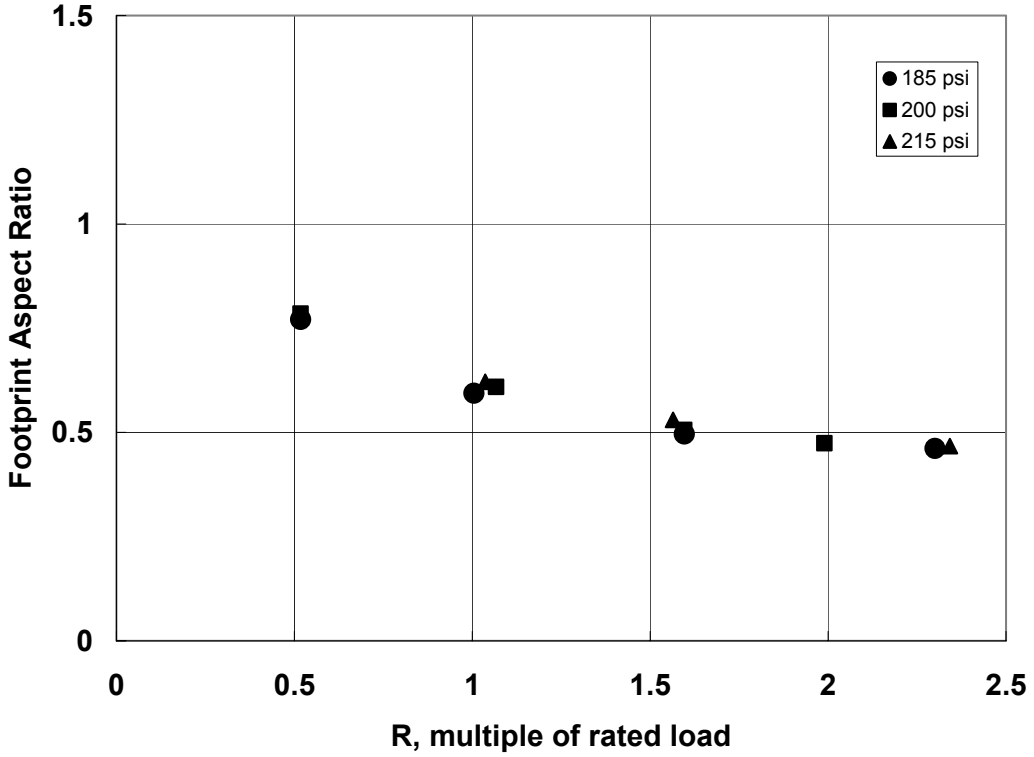


Figure 19. 737 nose tire footprint aspect ratio.

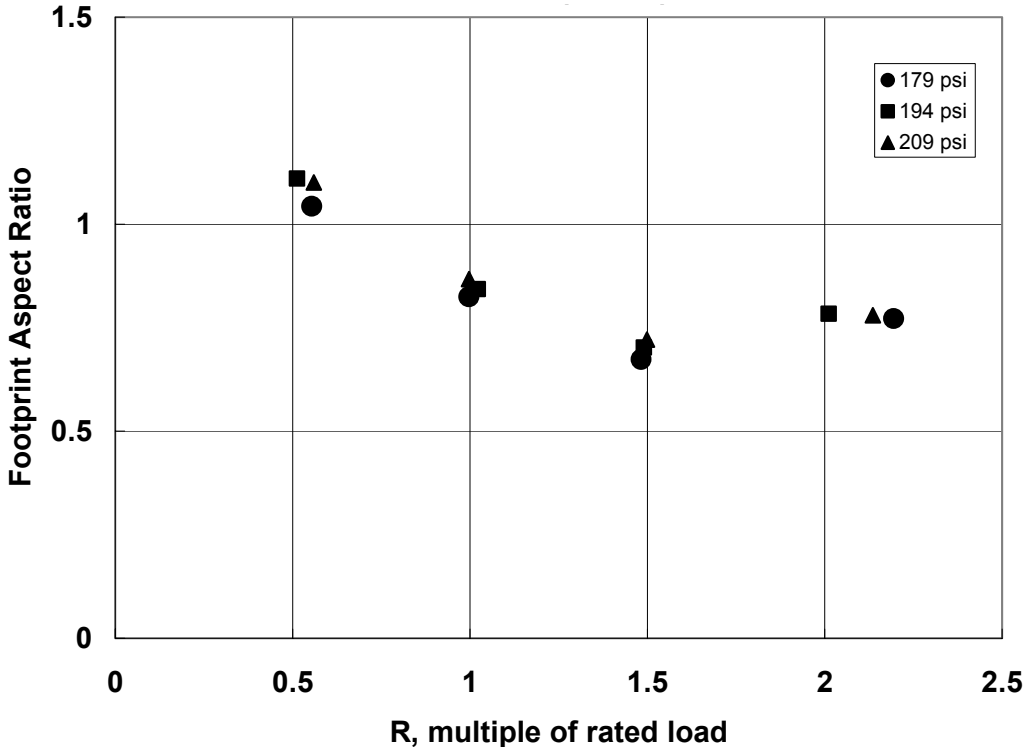


Figure 20. 777 nose tire footprint aspect ratio.

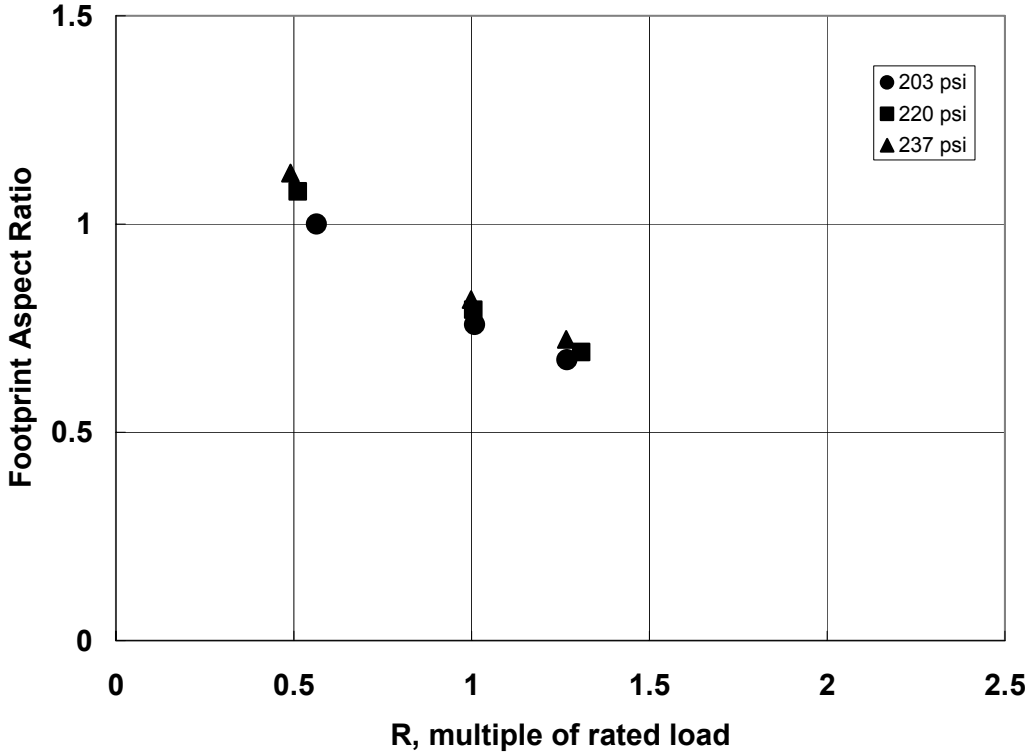


Figure 21. 777 main tire footprint aspect ratio.

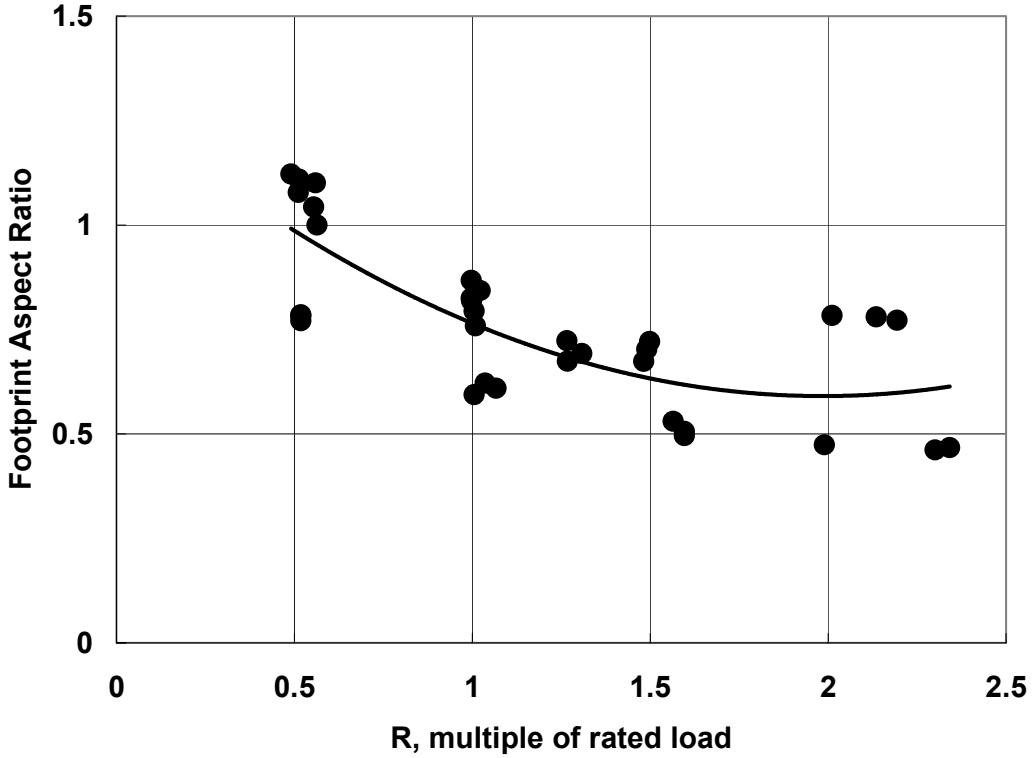


Figure 22. Footprint aspect ratio model; all tire sizes, all pressures.

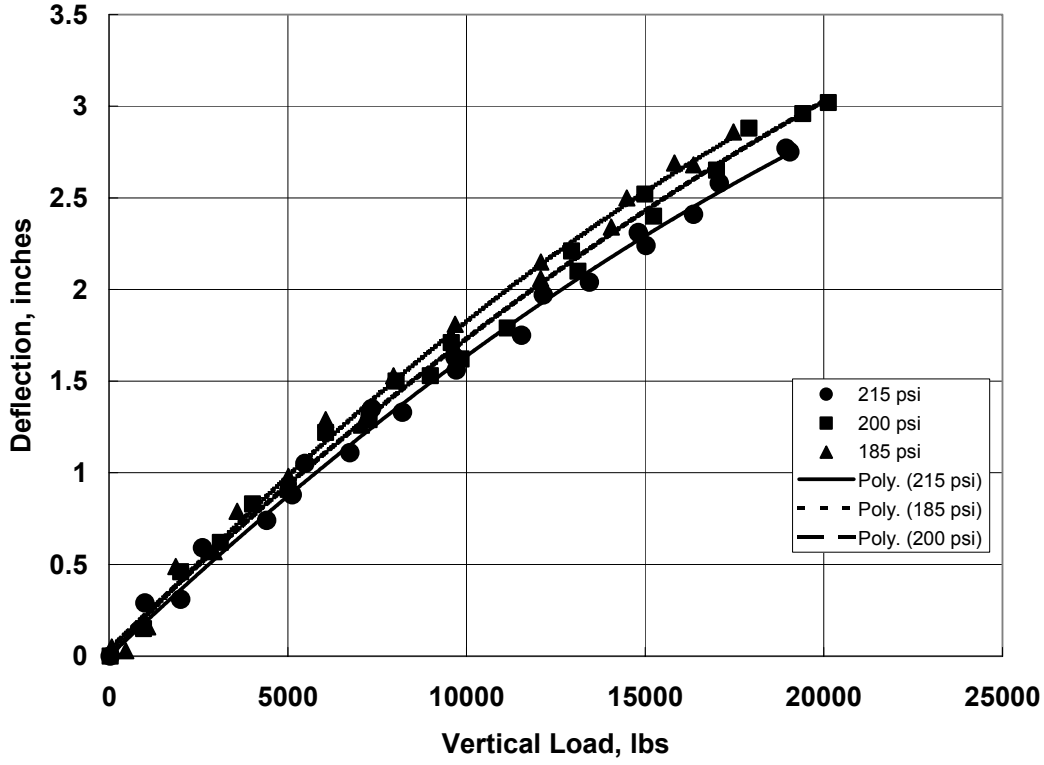


Figure 23. 737 nose tire load-deflection.

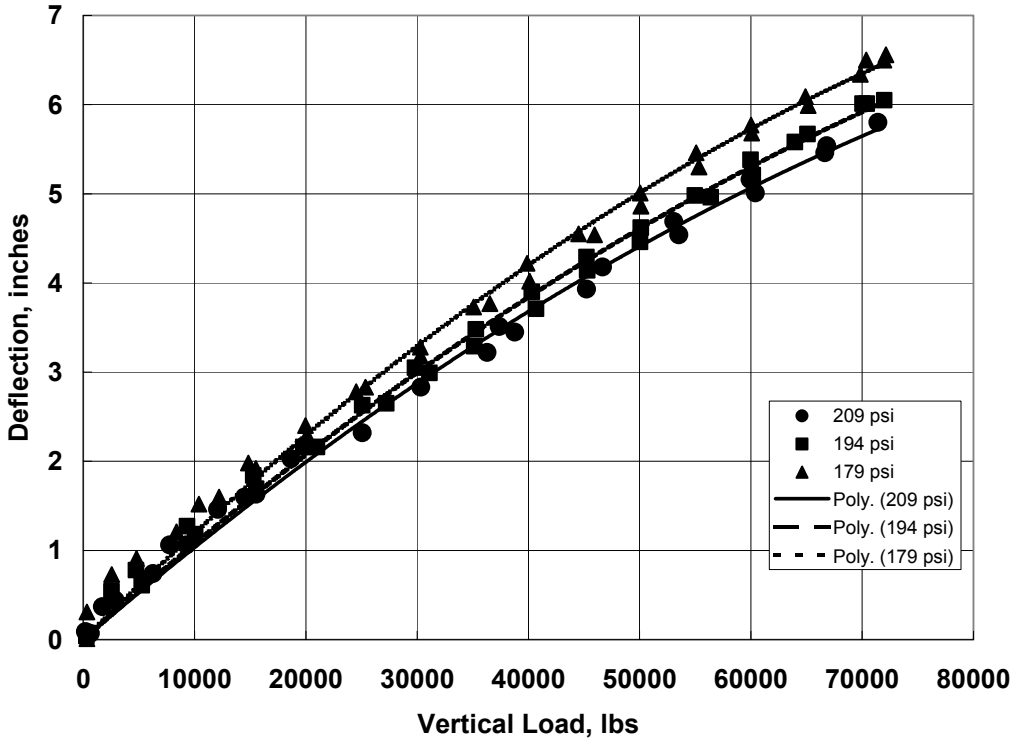


Figure 24. 777 nose tire load-deflection.

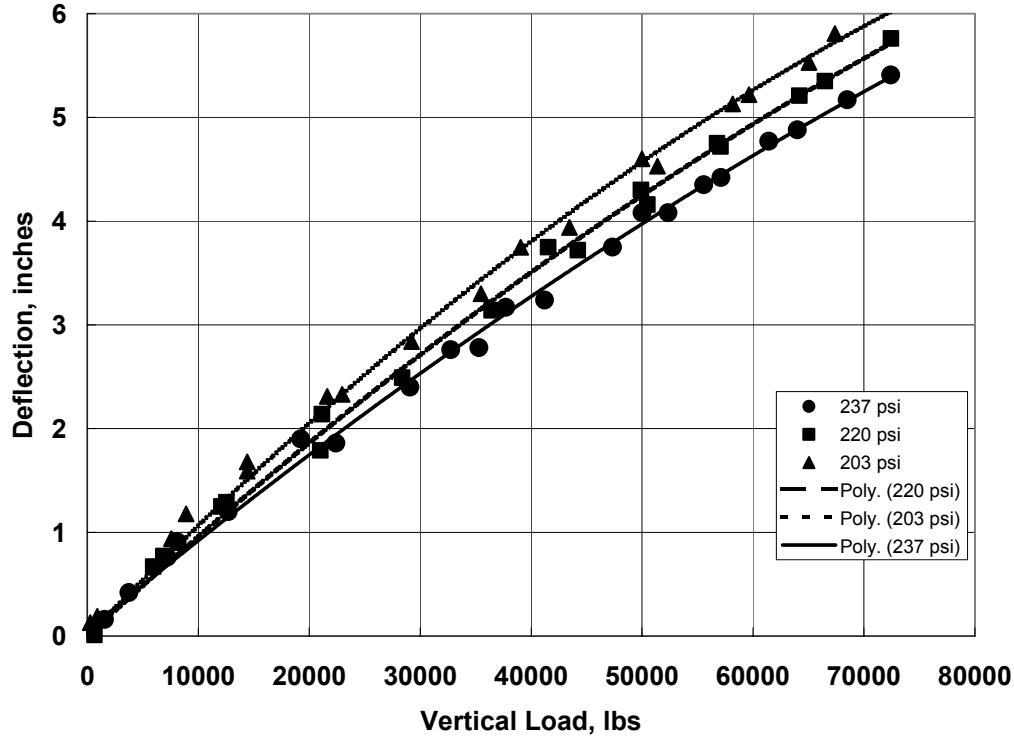


Figure 25. 777 main tire load-deflection.

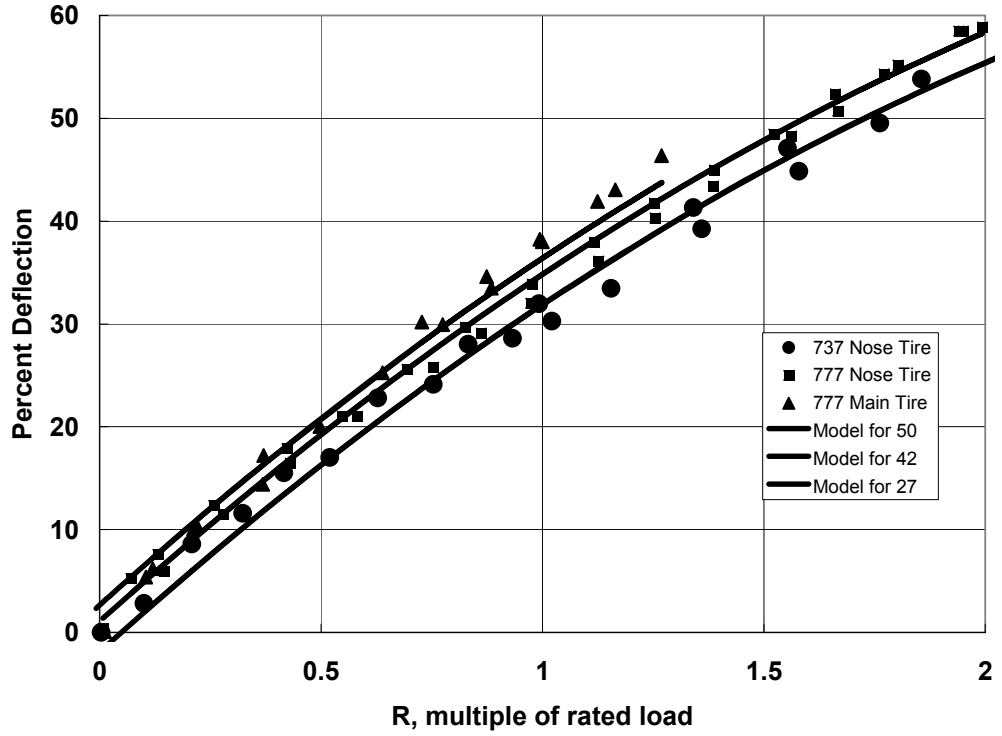


Figure 26. Nondimensionalized load-deflection.

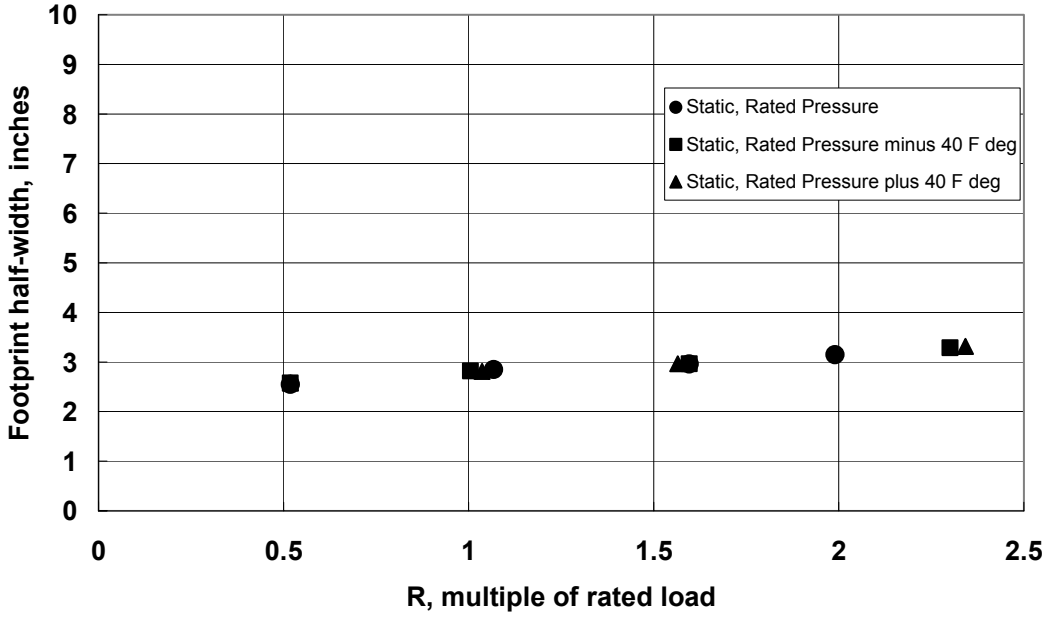


Figure 27. Effect of pressure on 737 nose tire footprint half-width.

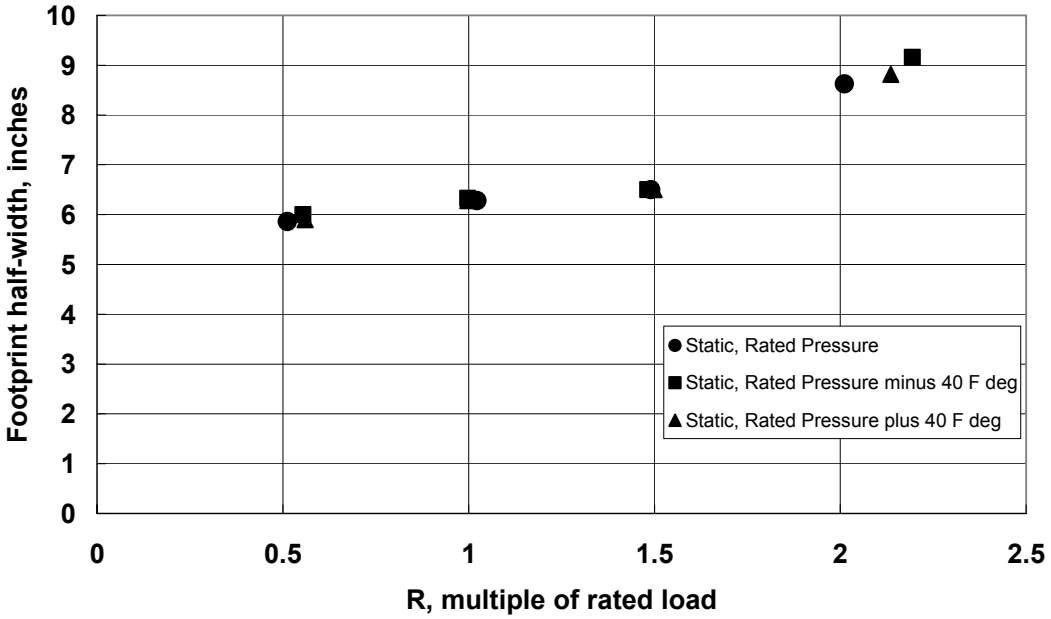


Figure 28. Effect of pressure on 777 nose tire footprint half-width.

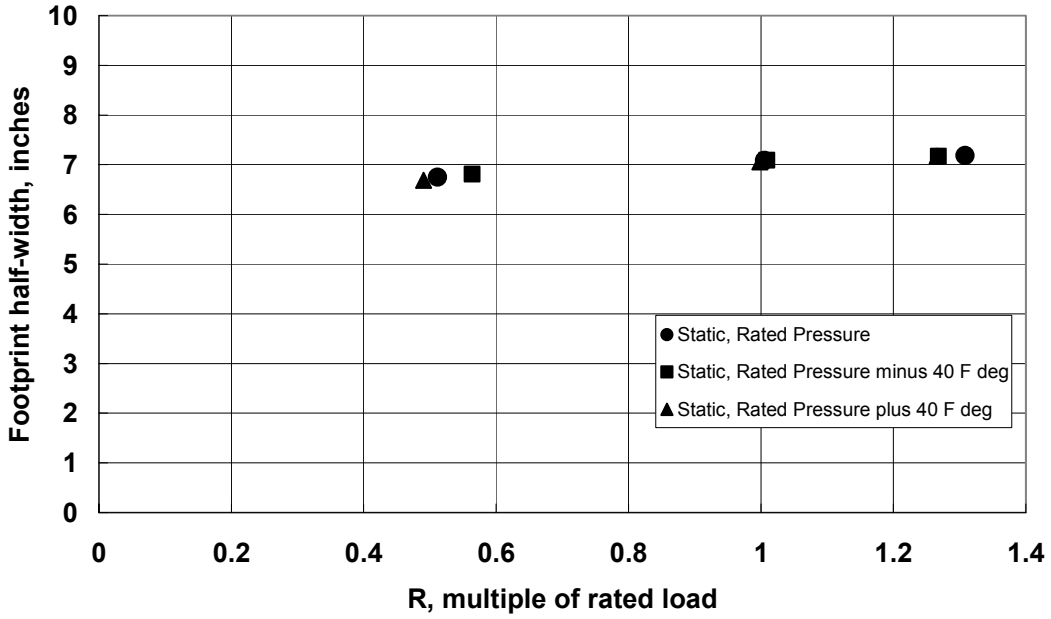


Figure 29. Effect of pressure on 777 main tire footprint half-width.

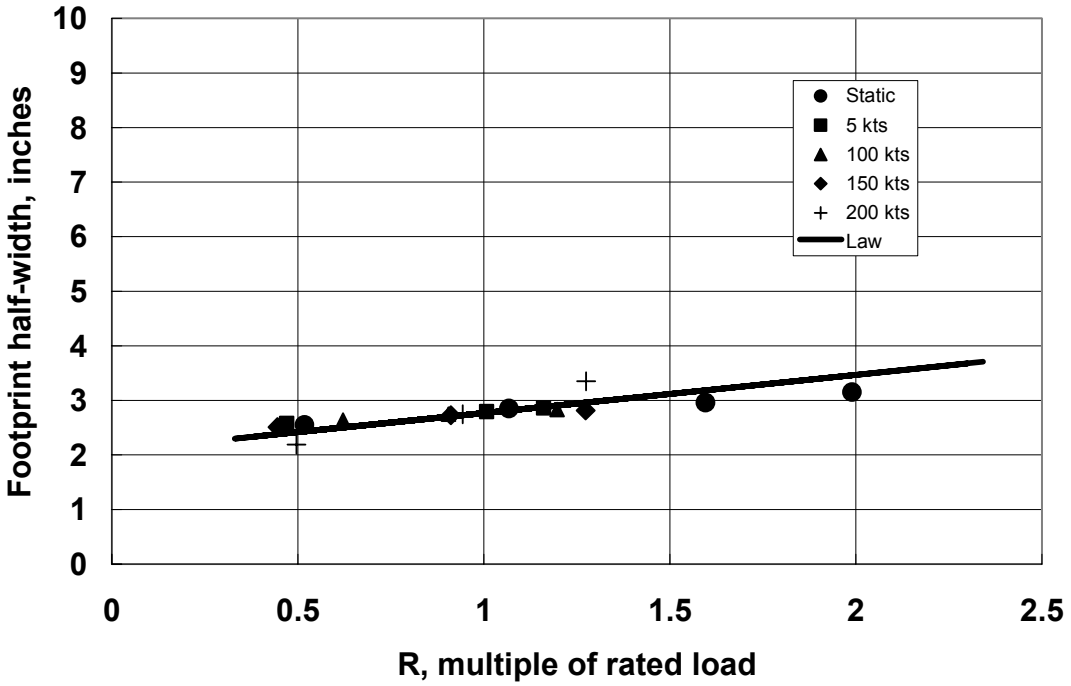


Figure 30. Effect of speed on 737 nose tire footprint half-width with prediction model.

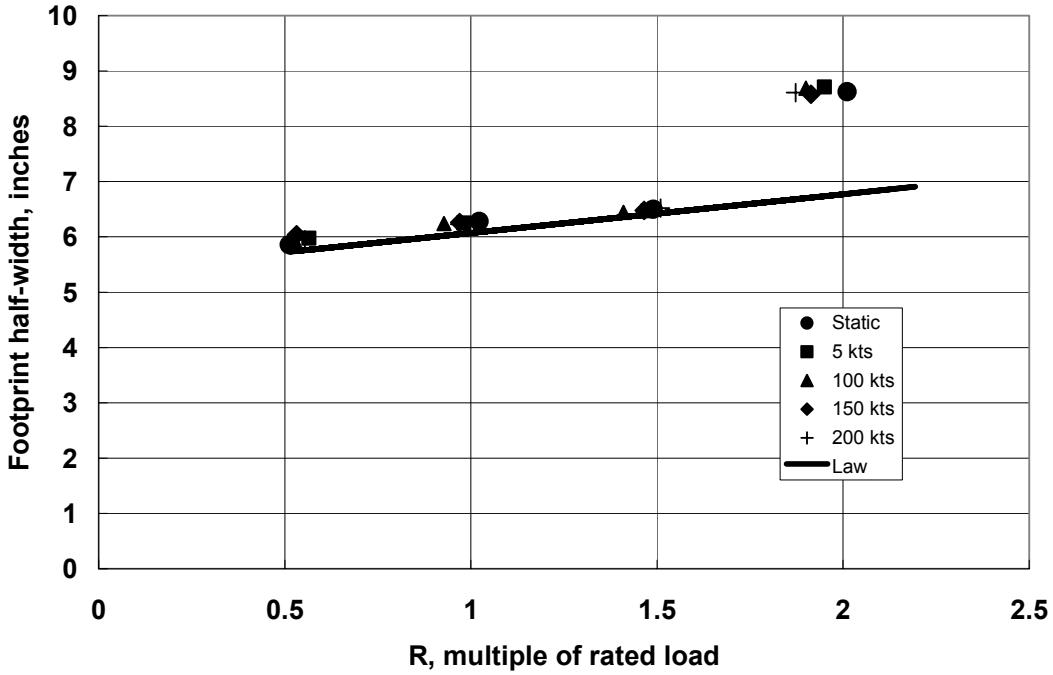


Figure 31. Effect of speed on 777 nose tire footprint half-width with prediction model.

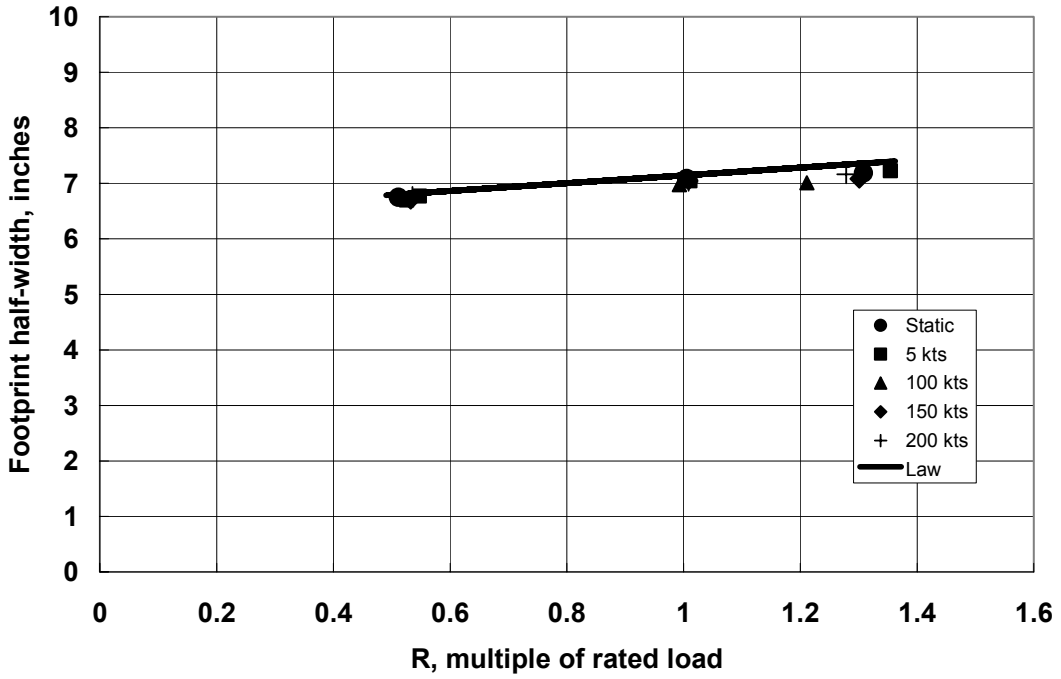


Figure 32. Effect of speed on 777 main tire footprint half-width with prediction model.

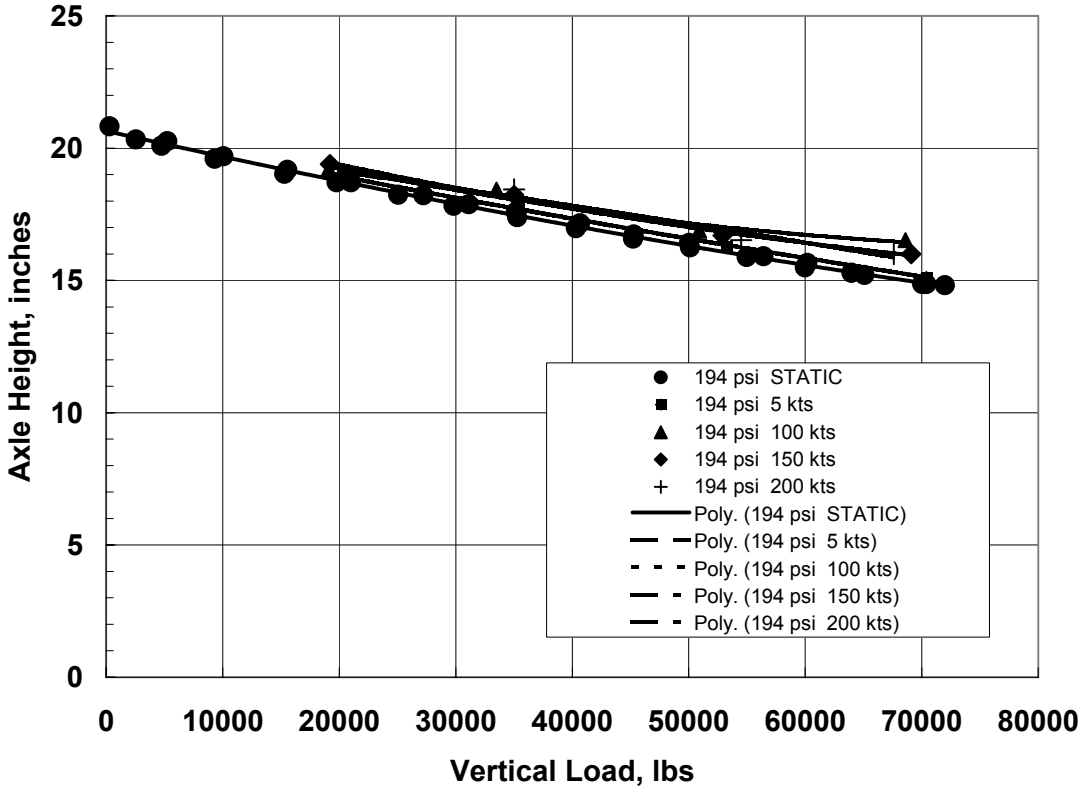


Figure 33. Effect of speed and vertical load on 777 nose tire axle height.

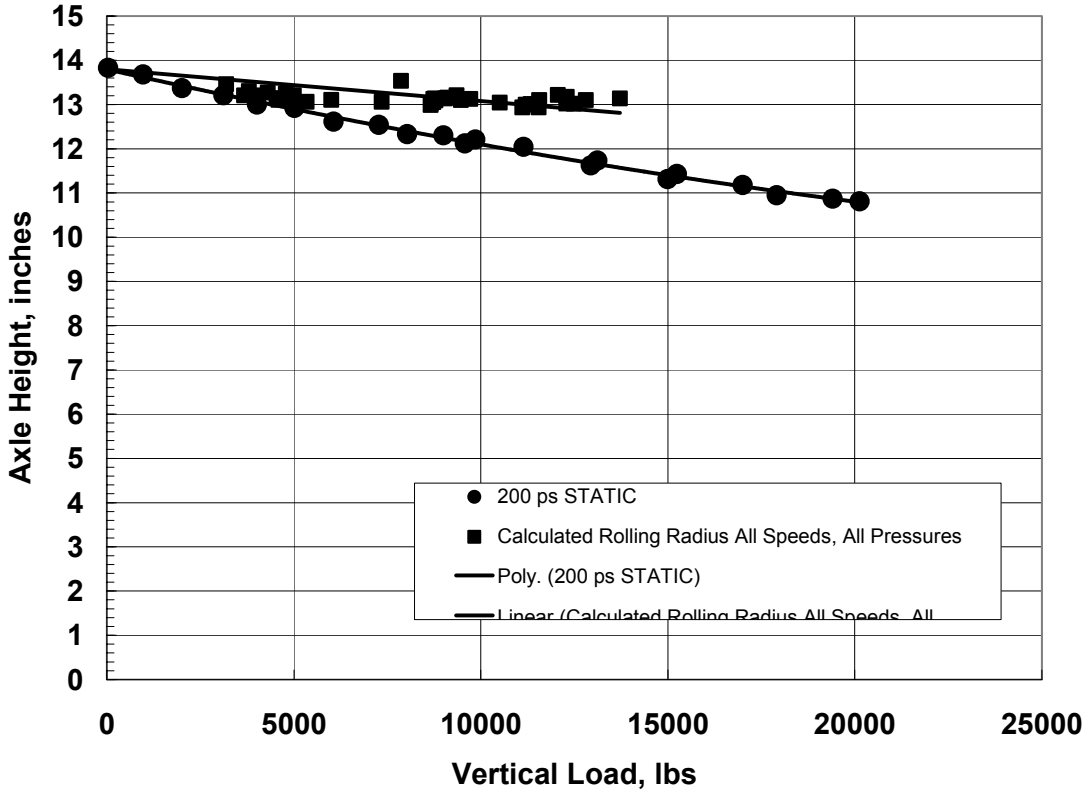


Figure 34. 737 nose tire rolling radius.

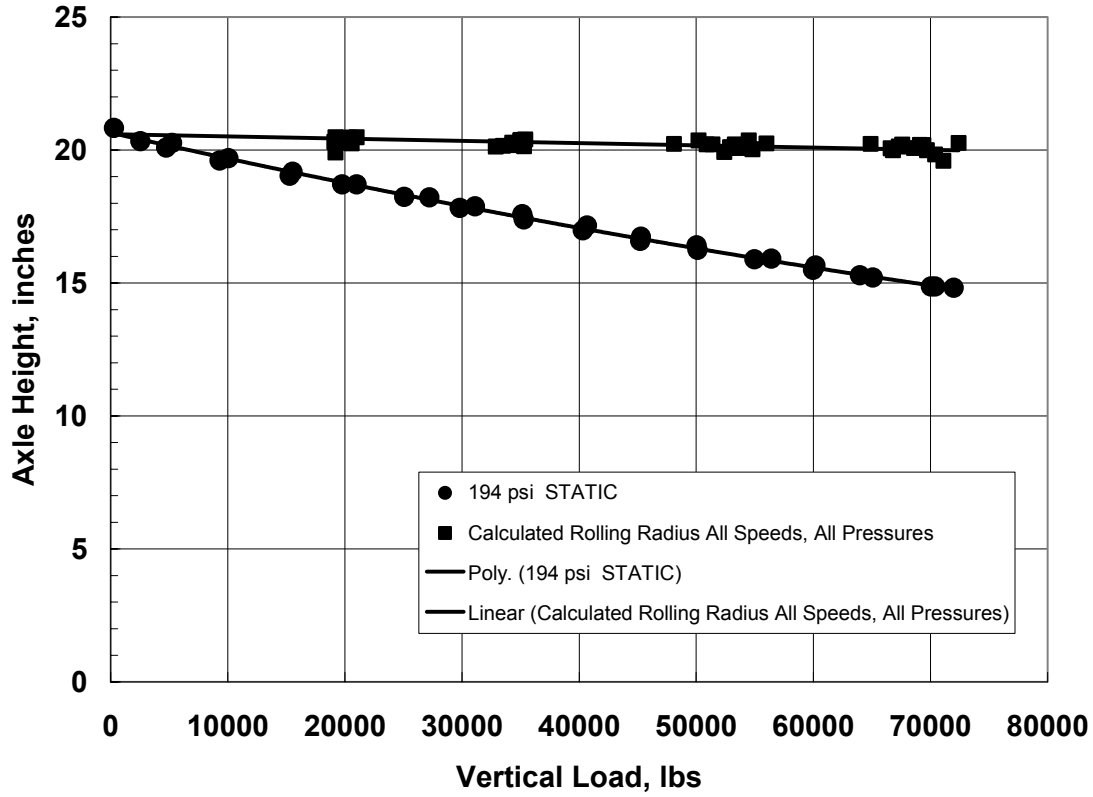


Figure 35. 777 nose tire rolling radius.

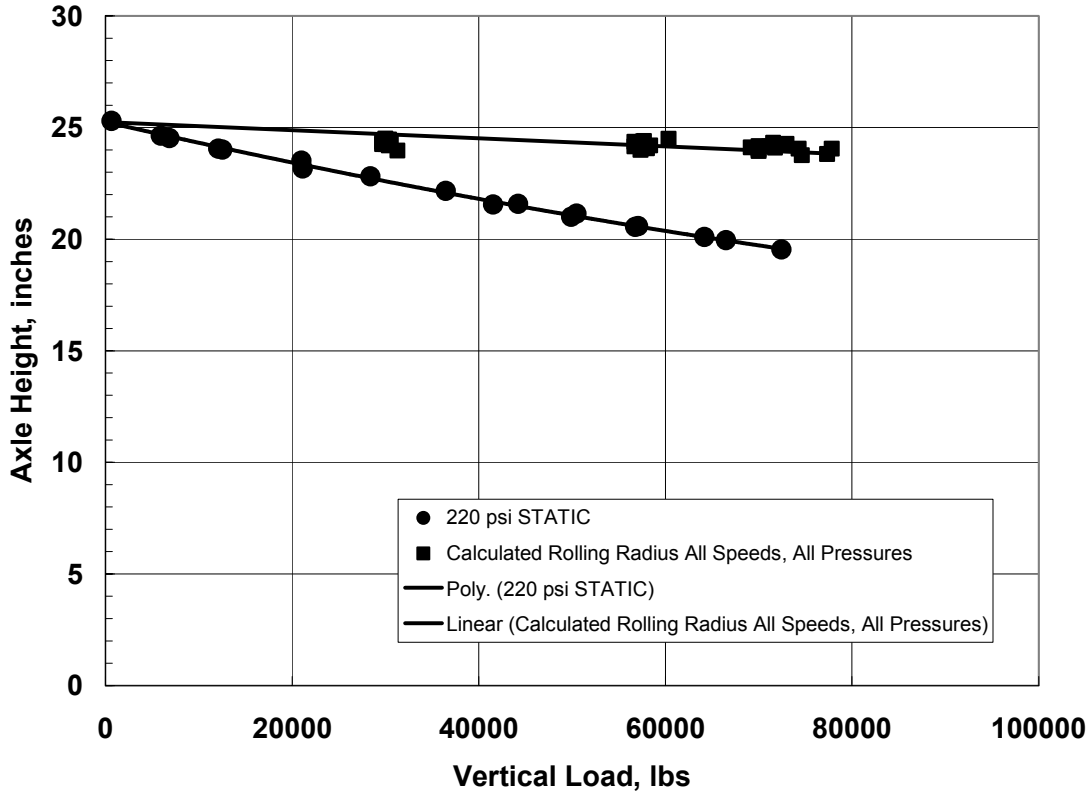


Figure 36. 777 main tire rolling radius.

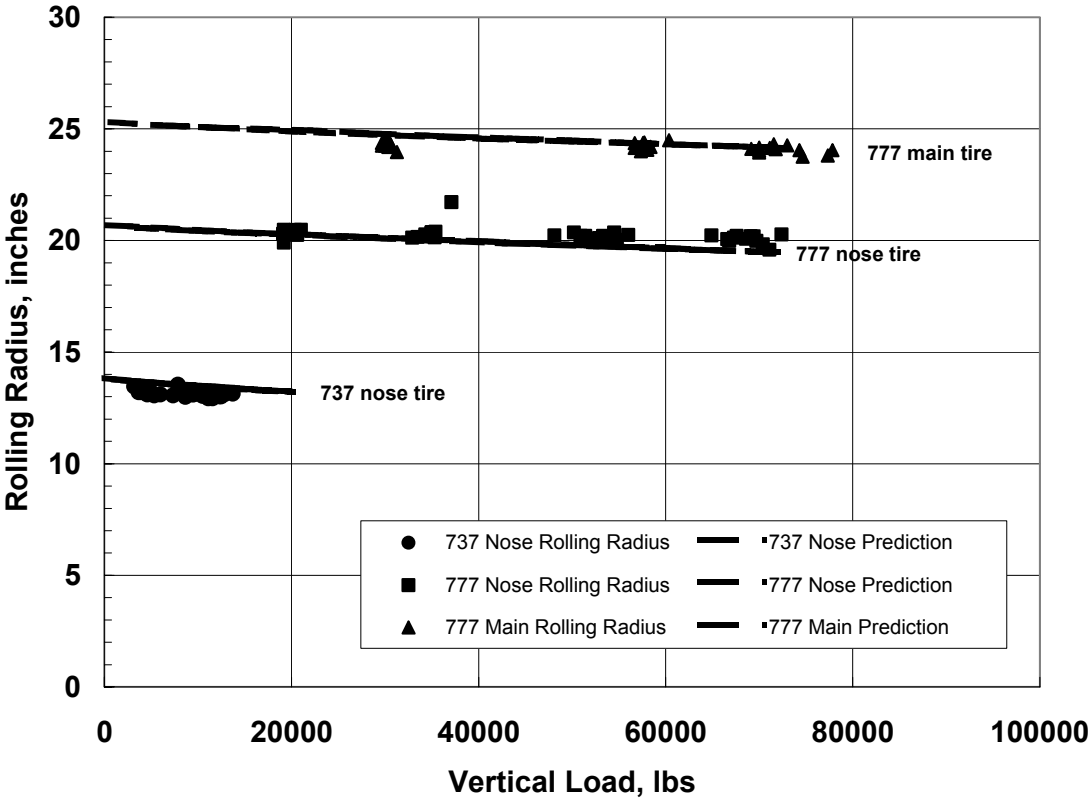


Figure 37. Rolling radius prediction for all tires.

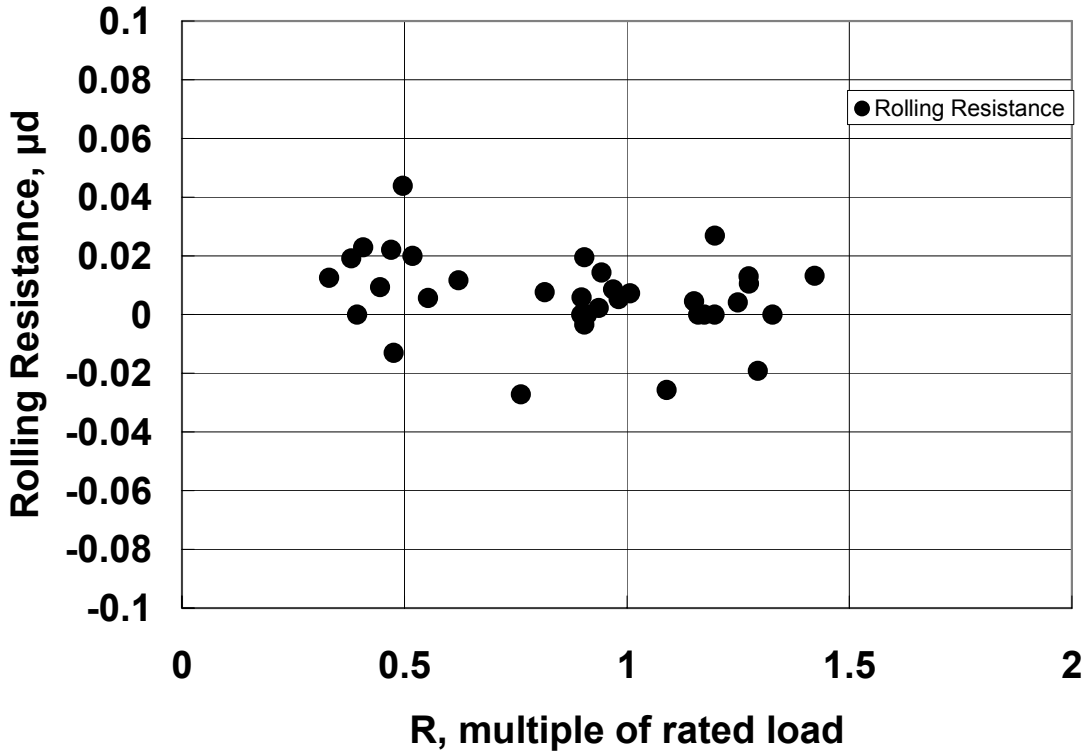


Figure 38. 737 nose tire rolling resistance.

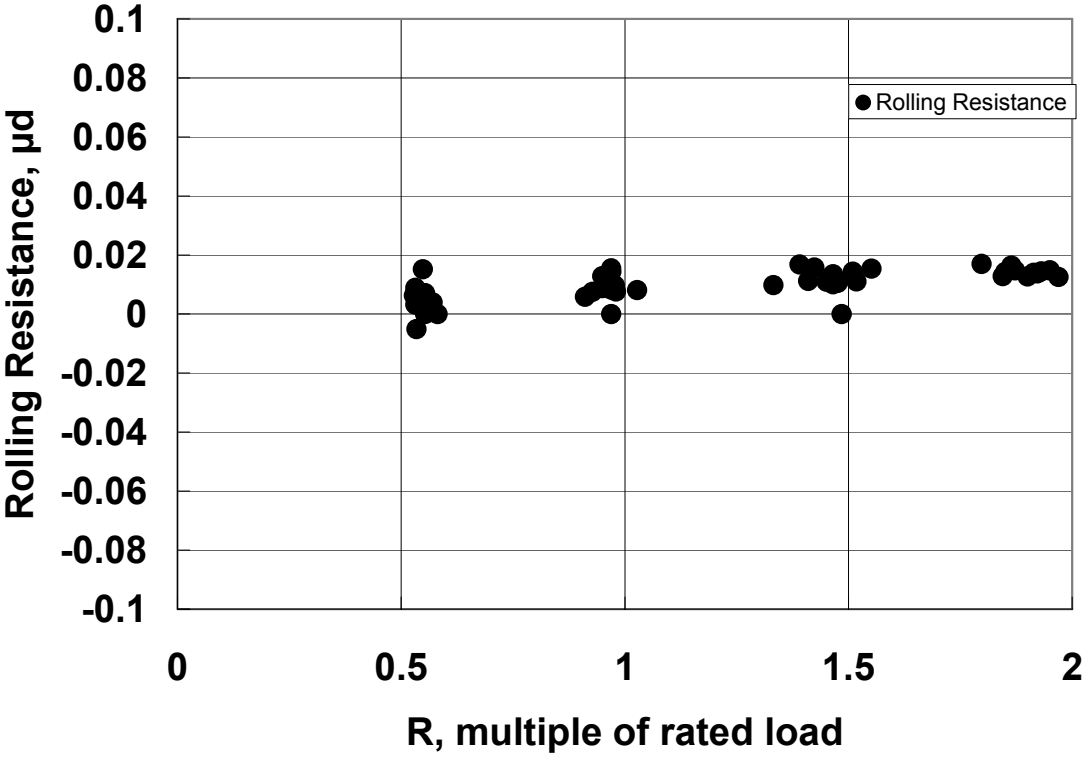


Figure 39. 777 nose tire rolling resistance.

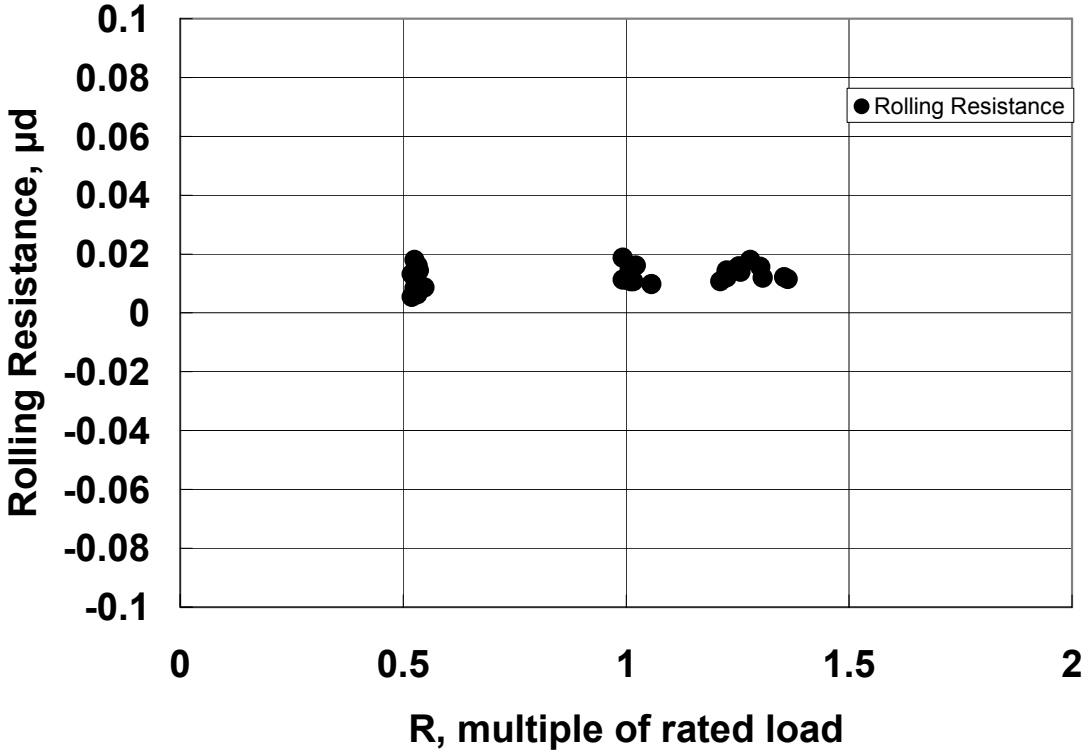


Figure 40. 777 main tire rolling resistance.

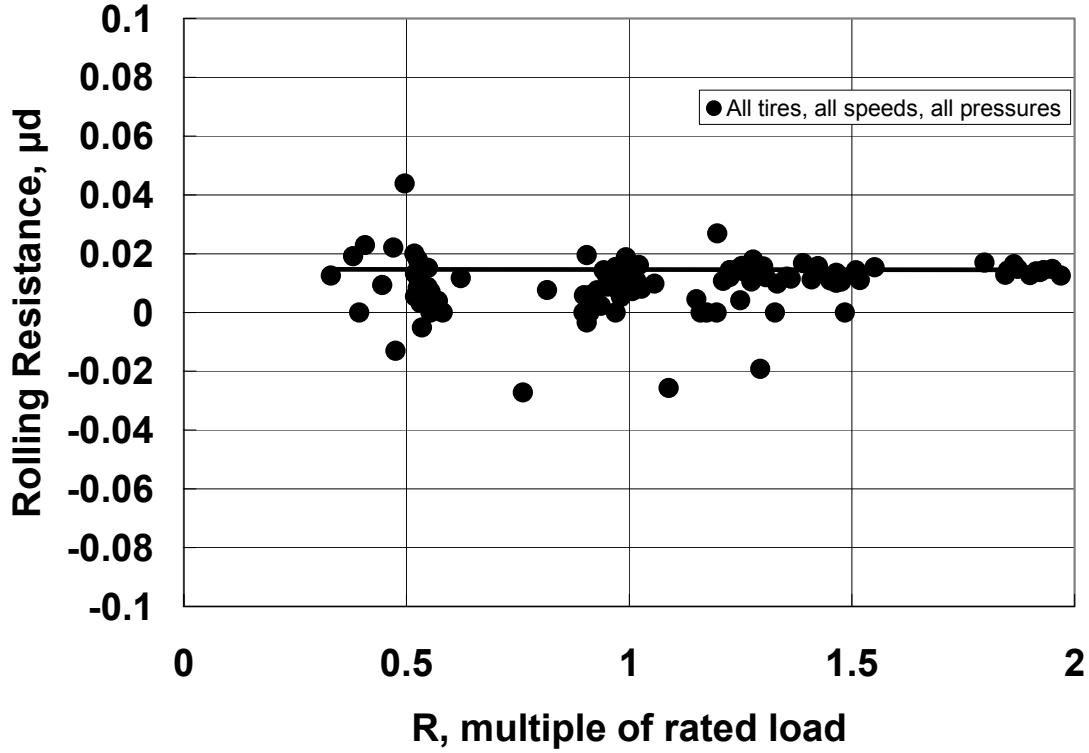


Figure 41. Rolling resistance prediction for all tires.

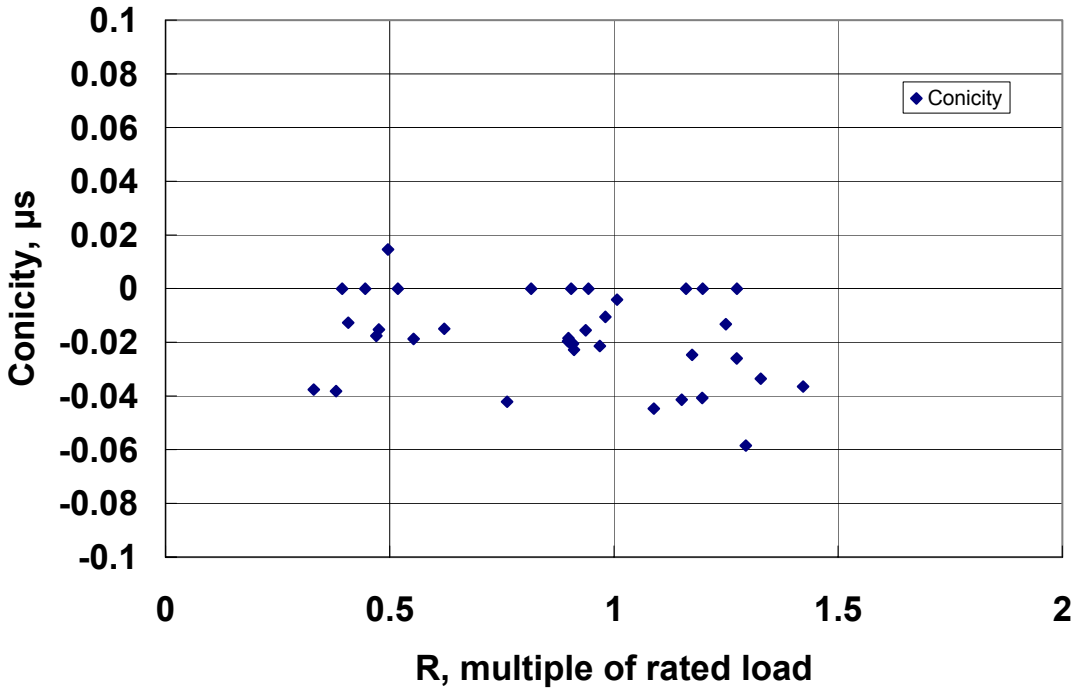


Figure 42. 737 nose tire conicity.

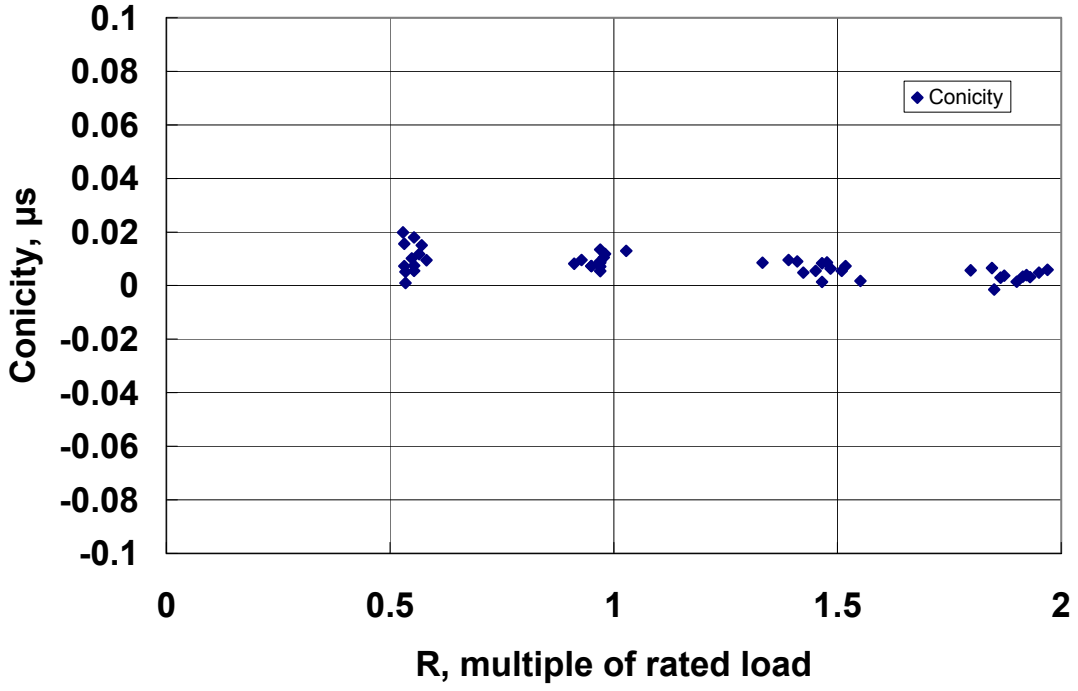


Figure 43. 777 nose tire conicity.

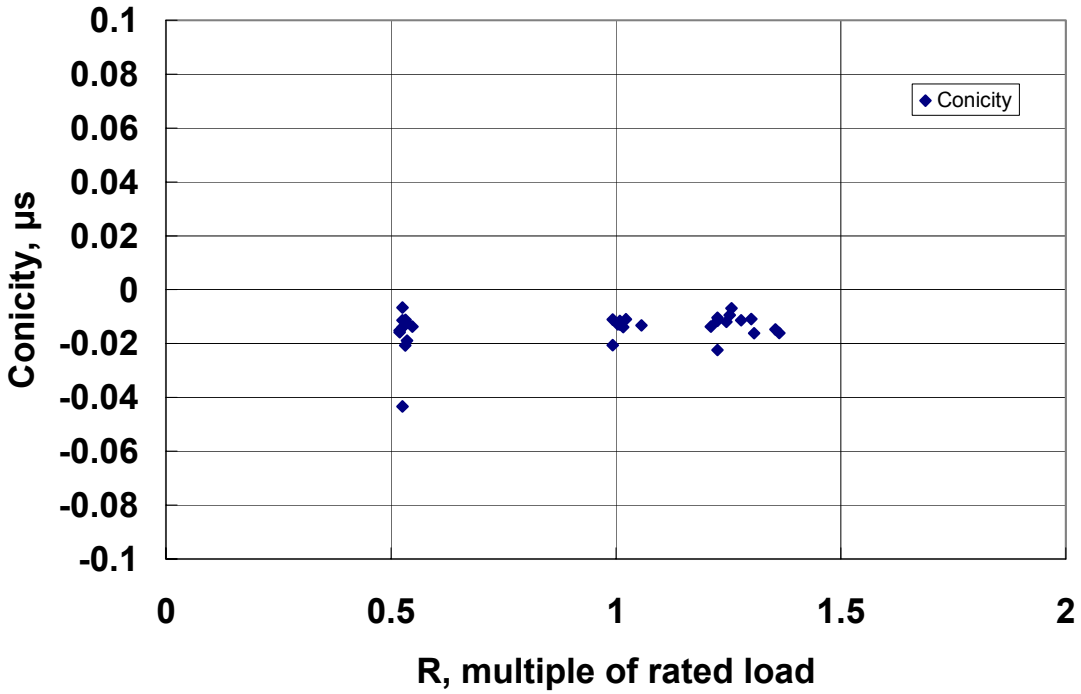


Figure 44. 777 main tire conicity.

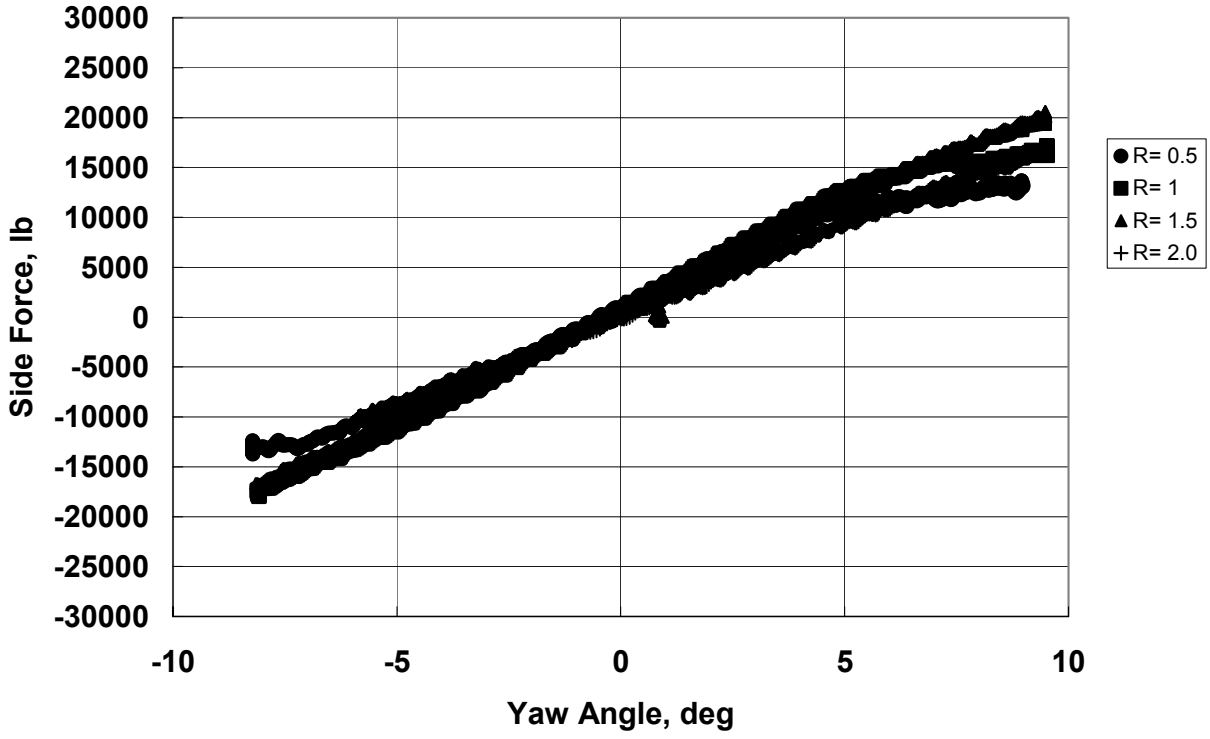


Figure 45. Effect of vertical force on side force for the 777 nose tire.

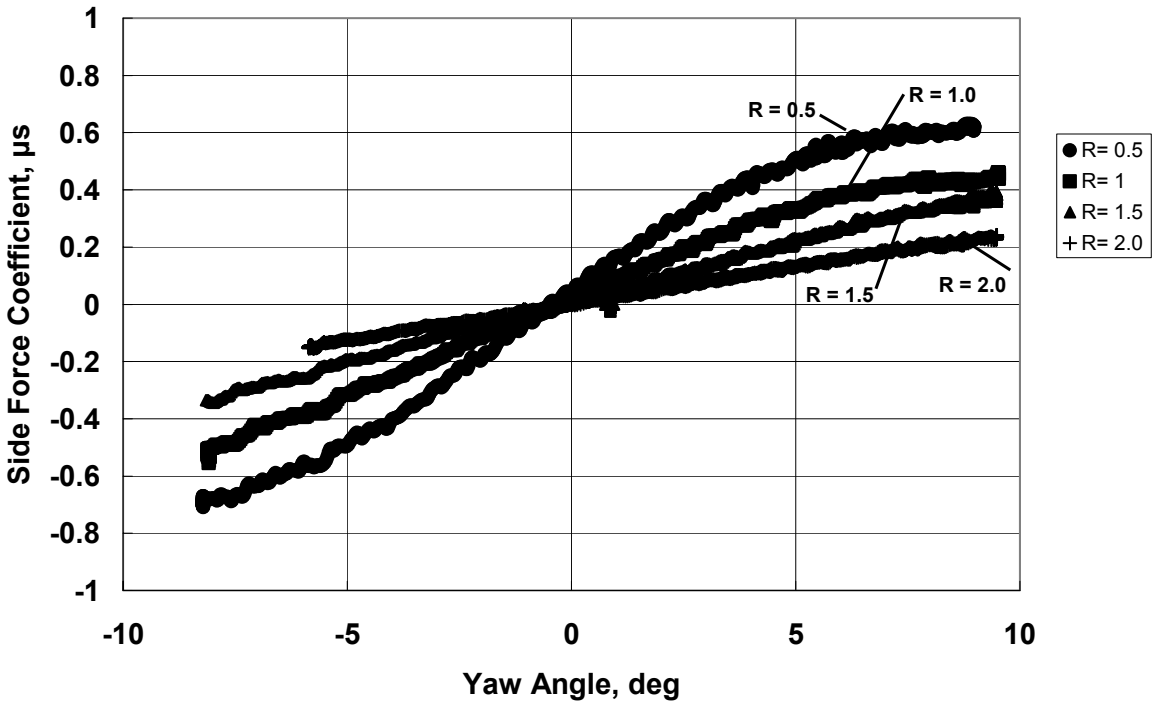


Figure 46. Effect of vertical force on side force coefficient for the 777 nose tire.

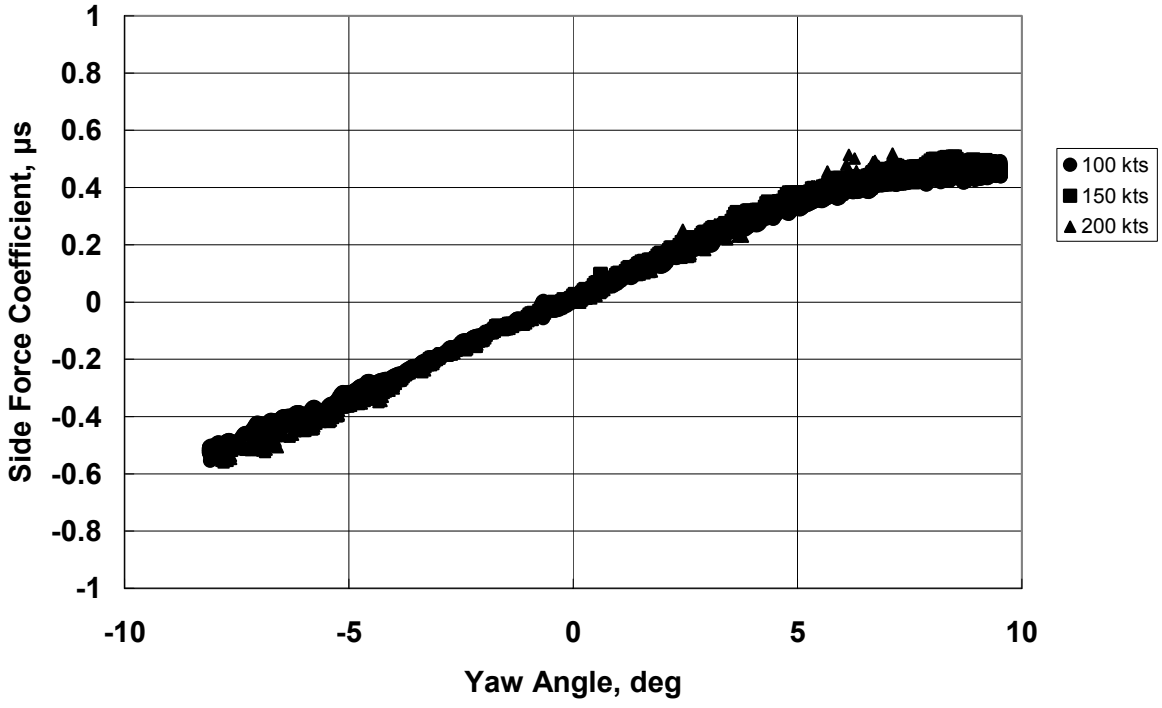


Figure 47. Effect of speed on side force coefficient for the 777 nose tire.

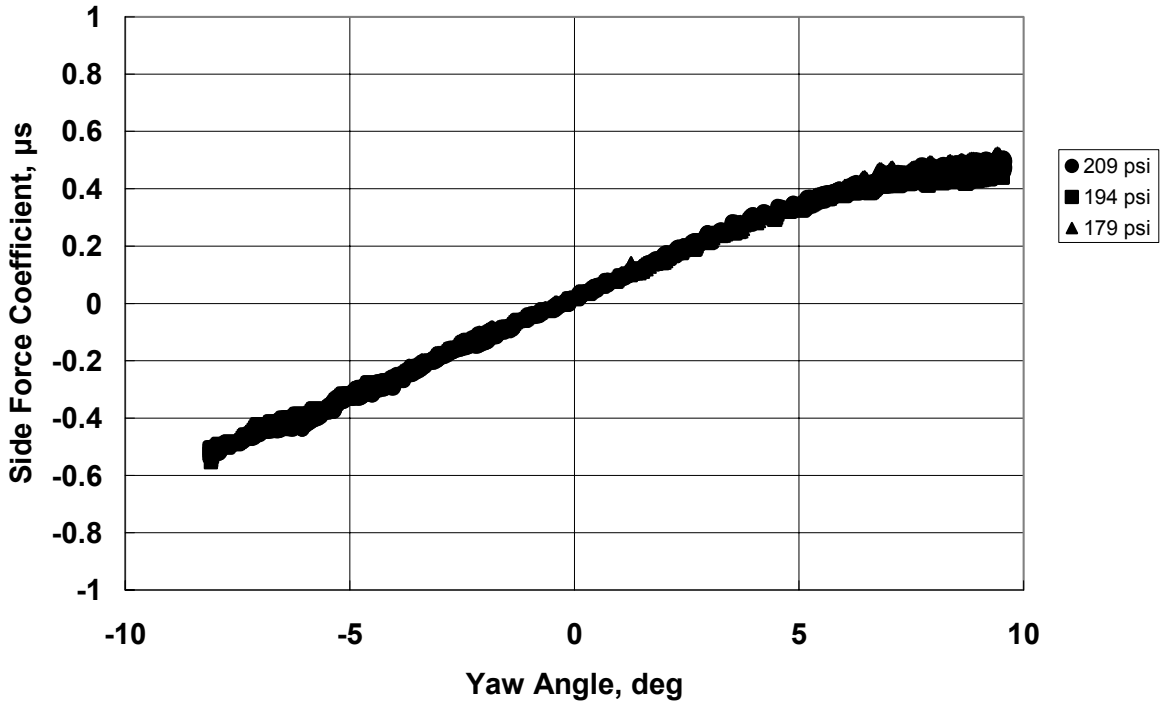


Figure 48. Effect of inflation pressure on side force coefficient for the 777 nose tire.


Figure 49. Effect of vertical force on side force coefficient for the 737 nose tire.


Figure 50. Side force coefficient for the 777 main tire at a single vertical force.

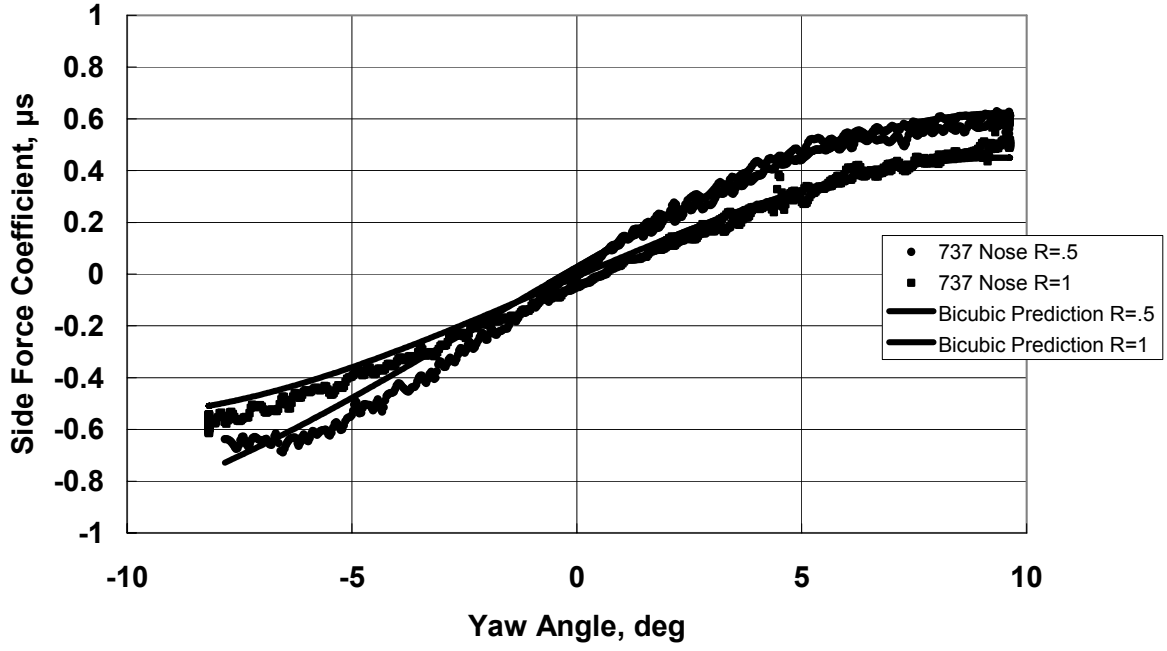


Figure 51. Side force coefficient prediction for the 737 nose tire.

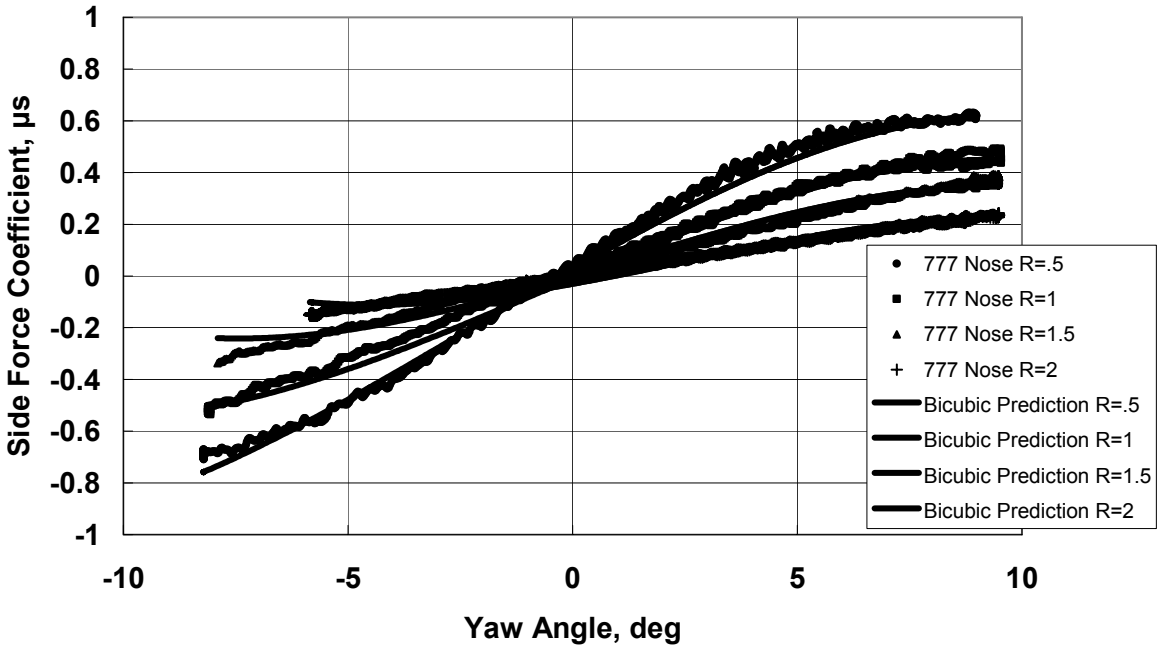


Figure 52. Side force coefficient prediction for the 777 nose tire.

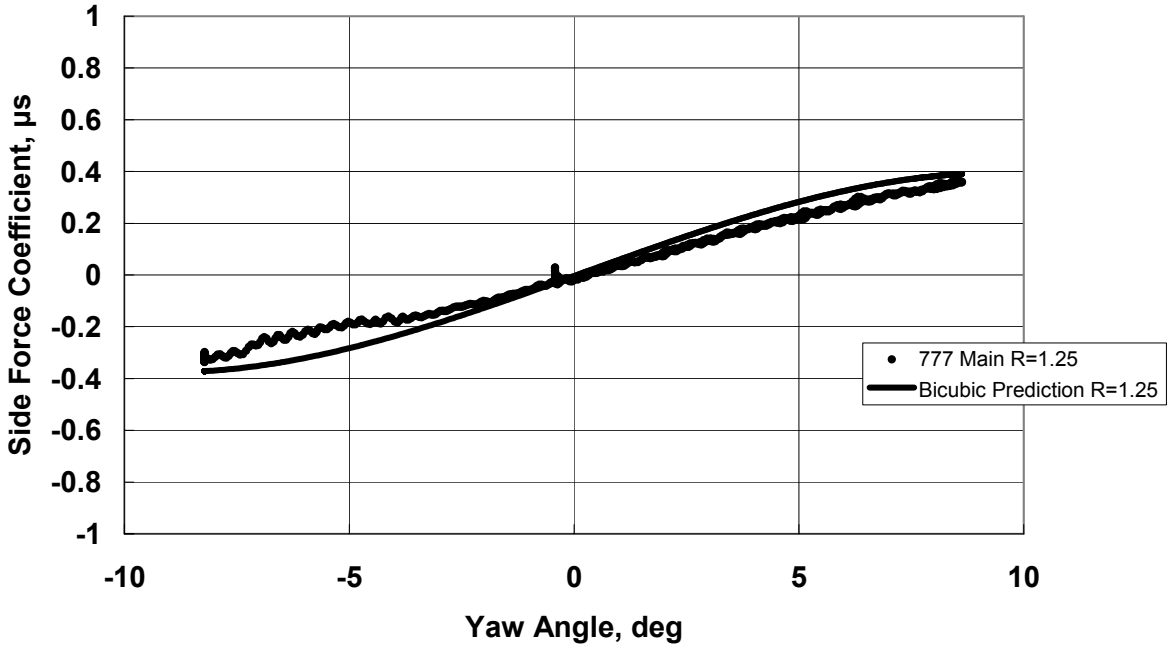


Figure 53. Side force coefficient prediction for the 777 main tire.

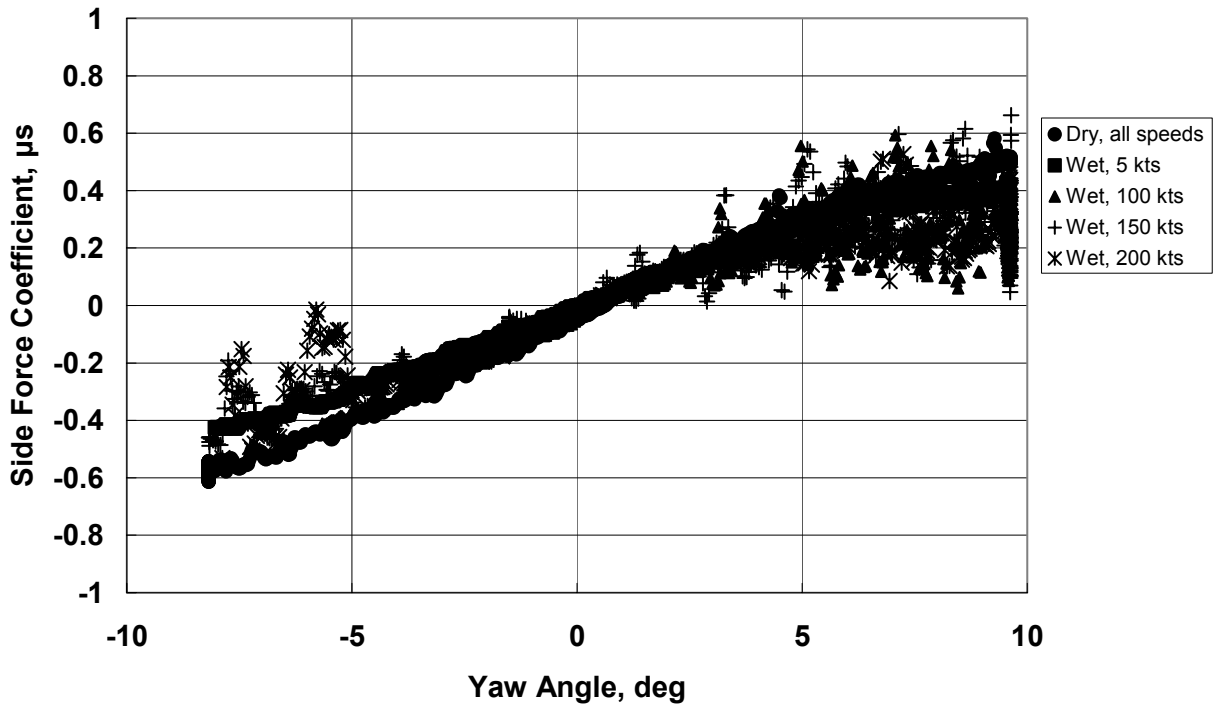


Figure 54. Effect of surface wetness on the side force coefficient for the 737 nose tire.

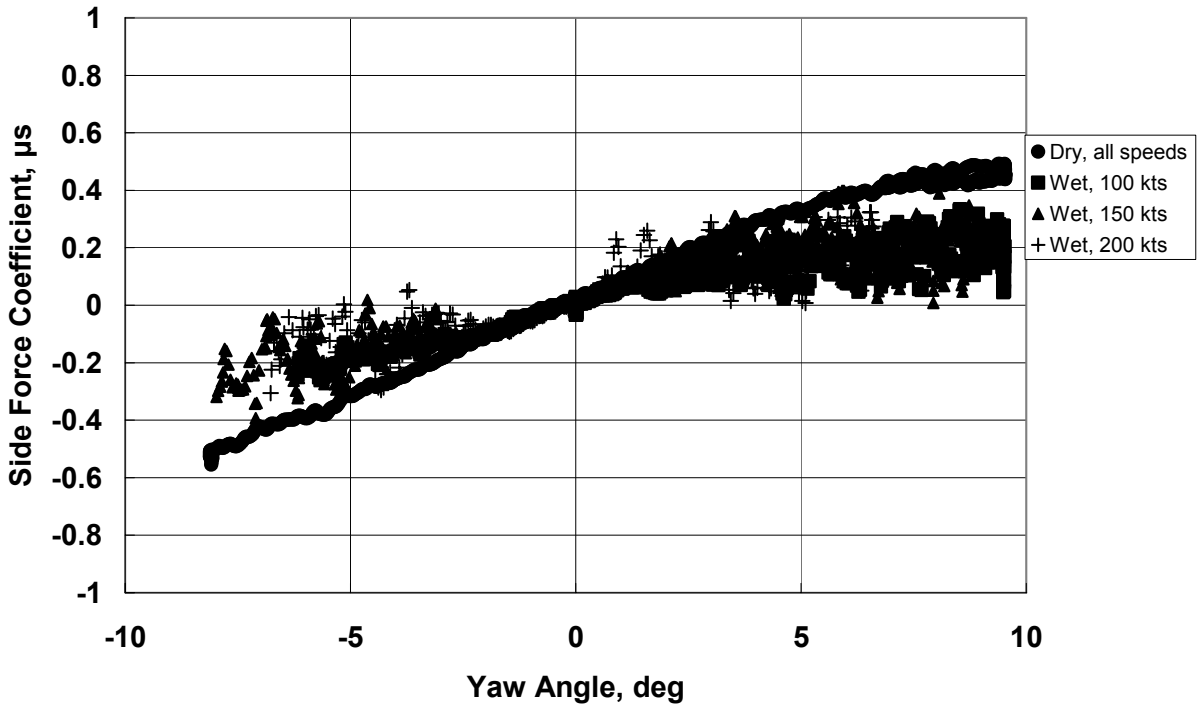


Figure 55. Effect of surface wetness on the side force coefficient for the 777 nose tire.

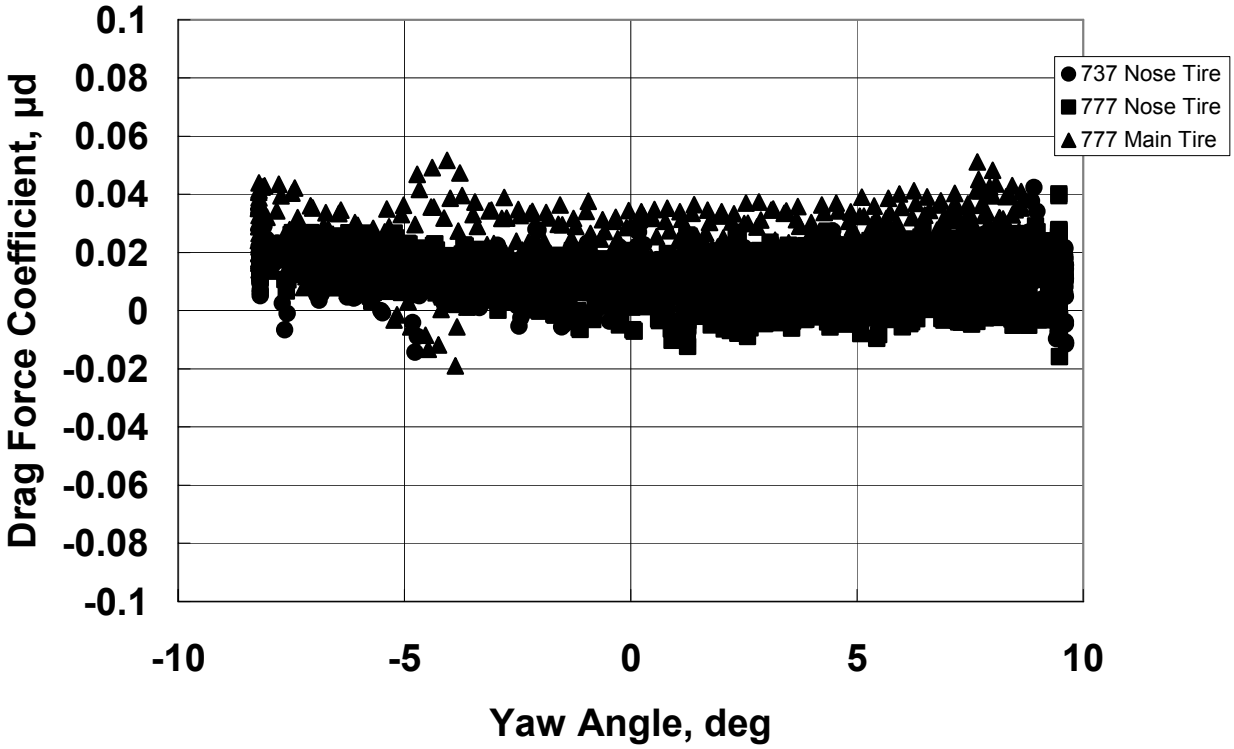


Figure 56. Effect of yaw angle on drag force coefficient for all tires.

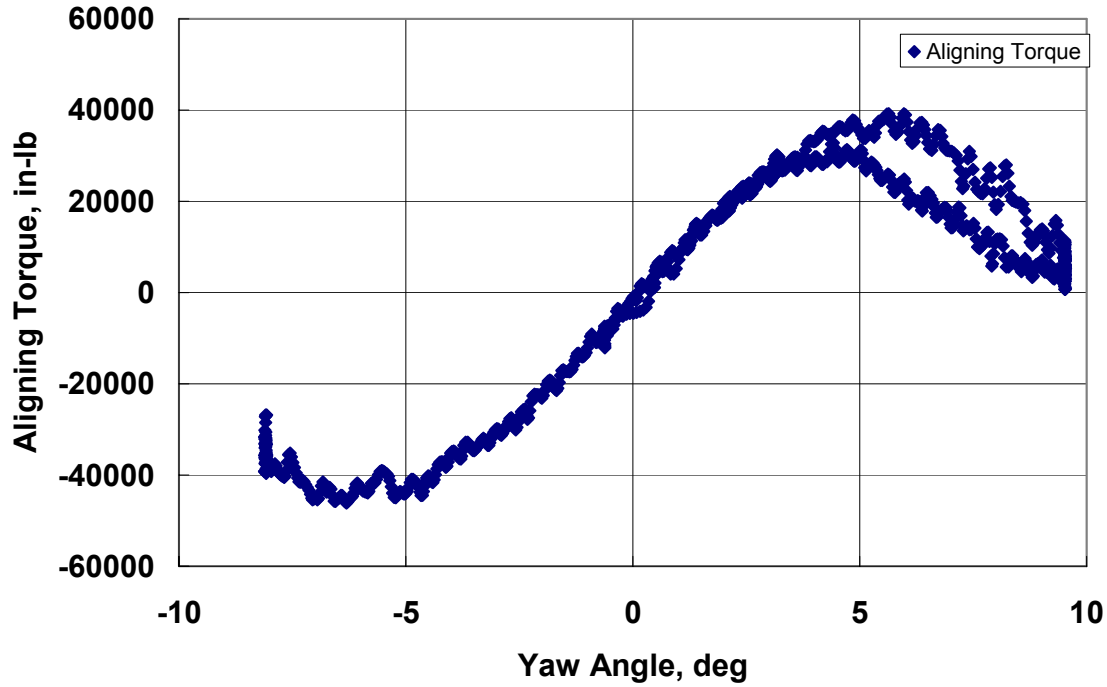


Figure 57. Typical behavior of aligning torque; 777 nose tire.

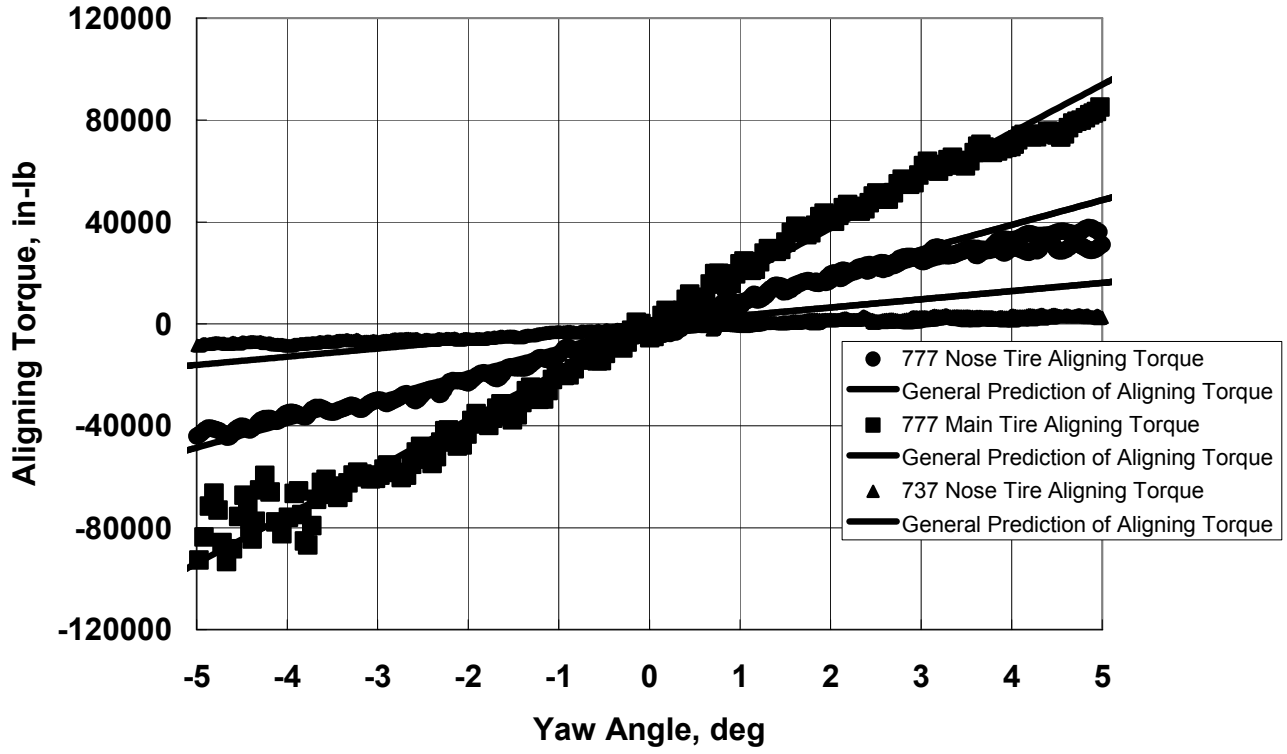


Figure 58. Aligning torque and prediction for all tires.

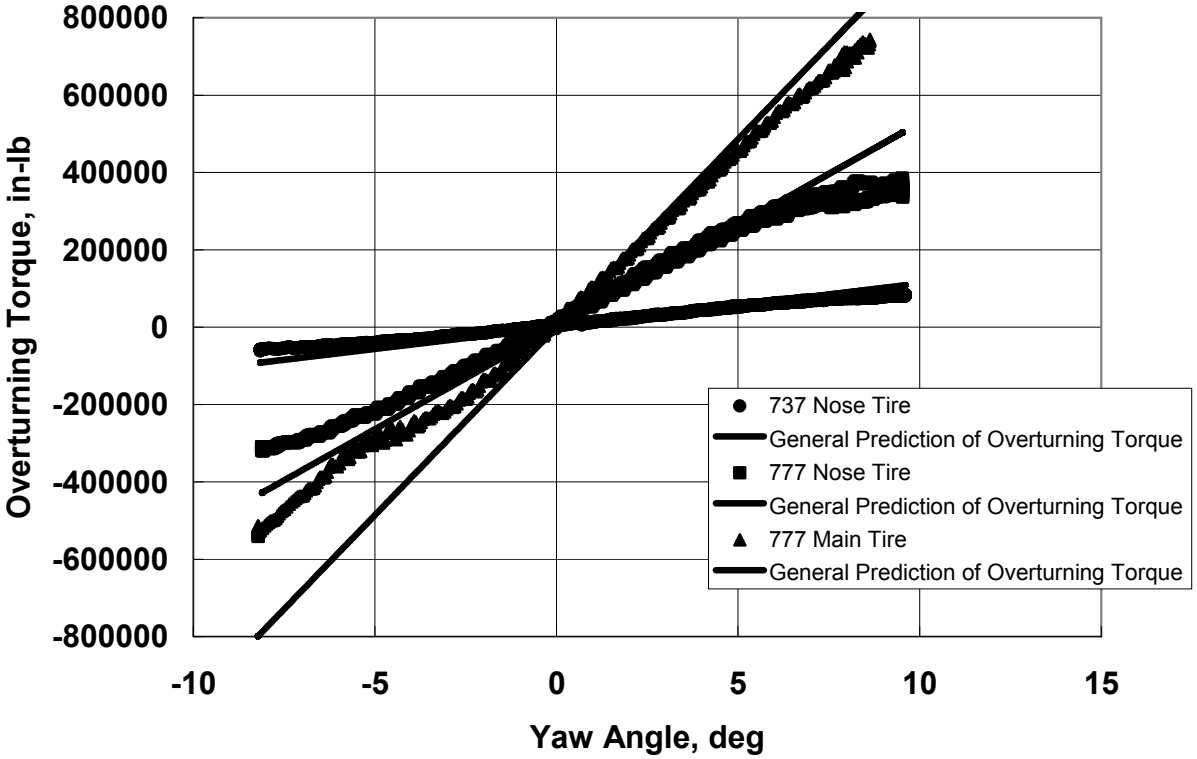


Figure 59. Overturning torque and prediction for all tires.

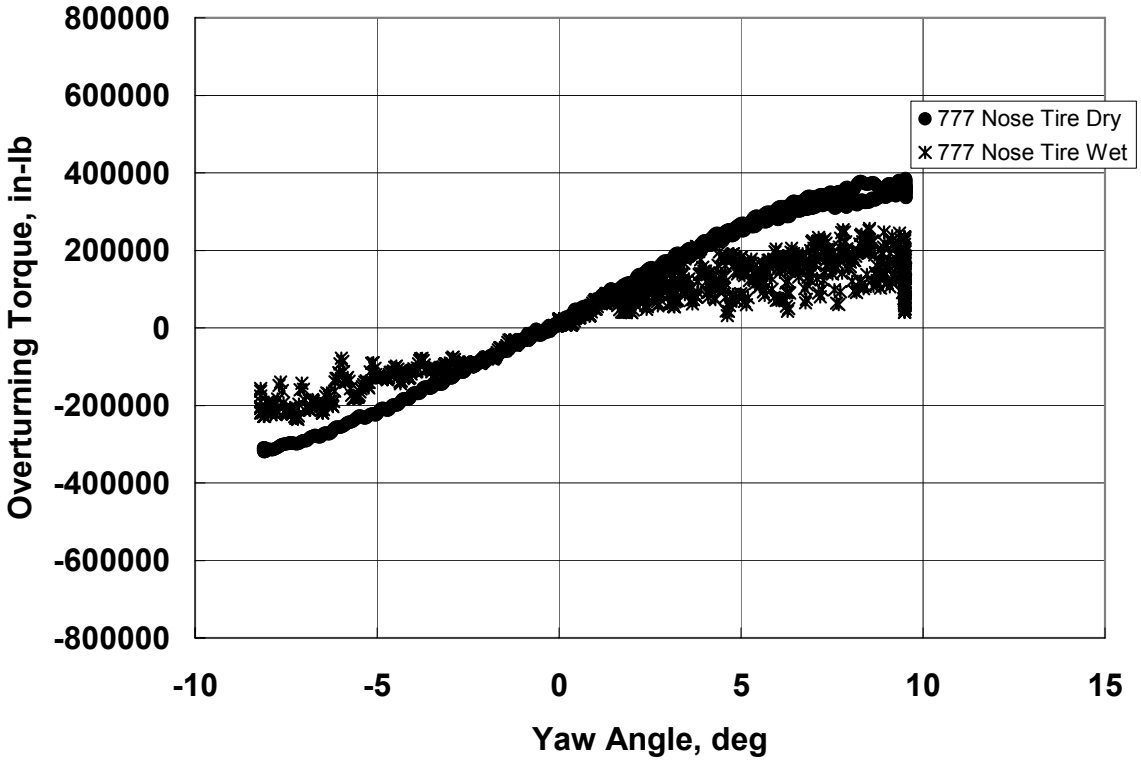


Figure 60. Effect of surface wetness on overturning torque.

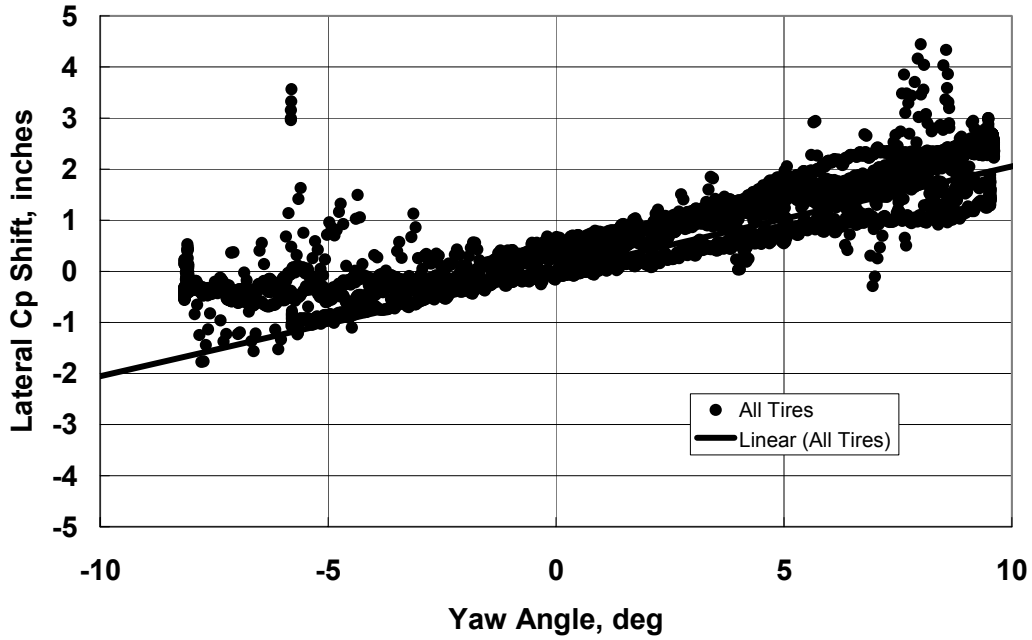


Figure 61. Lateral center of pressure shift and prediction for all tires.

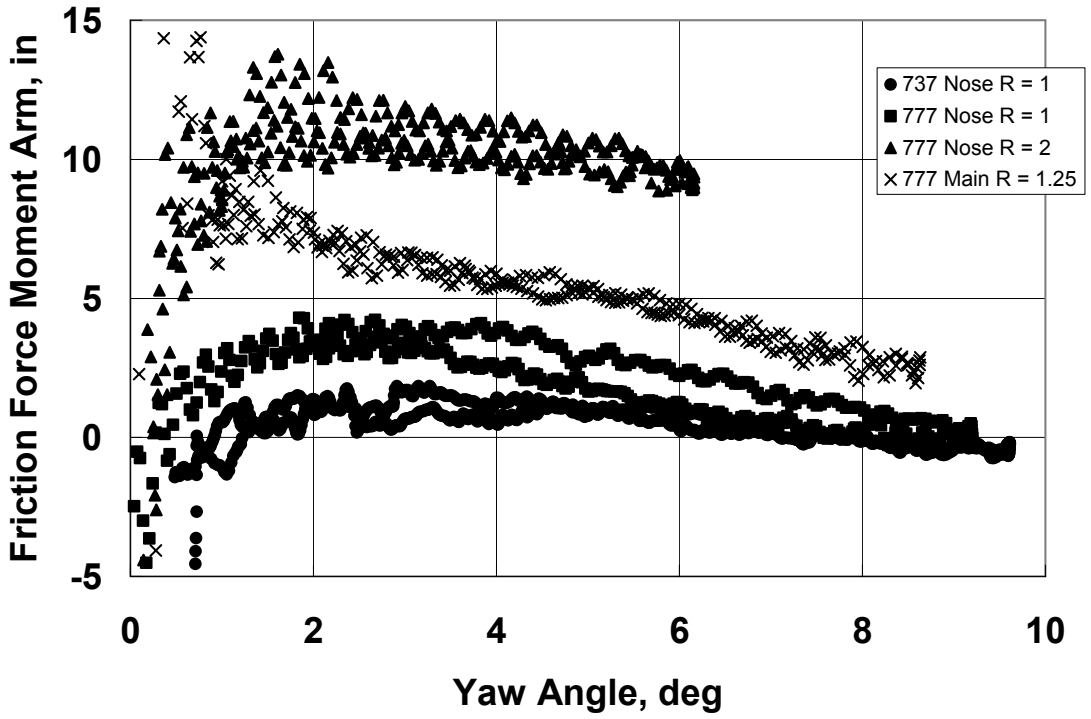


Figure 62. Friction force moment arm behavior for all tires.

# REPORT DOCUMENTATION PAGE

*Form Approved*
*OMB No. 0704-0188*



| 1. AGENCY USE ONLY (*Leave blank*) | 2. REPORT DATE | 3. REPORT TYPE AND DATES COVERED |
|---|---|---|
| | May 2003 | Technical Memorandum |

**4. TITLE AND SUBTITLE**
A Study of the Mechanical Properties of Modern Radial Aircraft Tires

**5. FUNDING NUMBERS**
762-10-33-03

**6. AUTHOR(S)**
Robert H. Daugherty

**7. PERFORMING ORGANIZATION NAME(S) AND ADDRESS(ES)**
NASA Langley Research Center
Hampton, VA 23681-2199

**8. PERFORMING ORGANIZATION REPORT NUMBER**
L-18286

**9. SPONSORING/MONITORING AGENCY NAME(S) AND ADDRESS(ES)**
National Aeronautics and Space Administration
Washington, DC 20546-0001

**10. SPONSORING/MONITORING AGENCY REPORT NUMBER**
NASA/TM-2003-212415

**11. SUPPLEMENTARY NOTES**

**12a. DISTRIBUTION/AVAILABILITY STATEMENT**
Unclassified-Unlimited
Subject Category 05 Distribution: Standard
Availability: NASA CASI (301) 621-0390

**12b. DISTRIBUTION CODE**

**13. ABSTRACT** *(Maximum 200 words)*

An experimental investigation was conducted at the NASA Langley Research Center to study the effects of various parameters on the mechanical properties of a number of modern radial aircraft tires such as would be found in the present commercial transport aircraft fleet. The range of tire sizes encompasses most of the tires that would be observed on both nose- and main-landing gear installations. Three radial tire sizes were tested and found to behave similarly in terms of static load-deflection when the results were non-dimensionalized. Footprint areas and rolling radii were found not to be very sensitive to either forward speed or variations in inflation pressure within a rather large range of pressures designed to simulate 80 Fahrenheit degrees of temperature change from origin to destination for a flight. The radial aircraft tires were found to behave like most other tires in response to variations in vertical load and yaw angle. The side-force coefficient, which is a measure of cornering efficiency, was found to increase with increases in yaw angle and decrease with increases in vertical load. A single model to provide a predictive capability for the side force coefficient, regardless of tire size, is presented.

**14. SUBJECT TERMS**
Aircraft tire, radial, vertical load, deflection, rolling radius, cornering, side force, rolling resistance, friction, yaw angle, inflation pressure

**15. NUMBER OF PAGES**
106

**16. PRICE CODE**

| 17. SECURITY CLASSIFICATION OF REPORT | 18. SECURITY CLASSIFICATION OF THIS PAGE | 19. SECURITY CLASSIFICATION OF ABSTRACT | 20. LIMITATION OF ABSTRACT |
|---|---|---|---|
| Unclassified | Unclassified | Unclassified | UL |